July 2016

Advanced Materials for Rapid Diagnostics in Food, Agriculture and Healthcare

Charmaine K.W. Koo
University of Massachusetts Amherst

ADVANCED MATERIALS FOR RAPID DIAGNOSTICS IN FOOD, AGRICULTURE AND HEALTHCARE

A Dissertation Presented

by

CHARMAINE K.W. KOO

Submitted to the Graduate School of the
University of Massachusetts Amherst in partial fulfillment
of the requirements for the degree of

DOCTOR OF PHILOSOPHY

May 2016

Food Science

ADVANCED MATERIALS FOR RAPID DIAGNOSTICS IN FOOD, AGRICULTURE AND HEALTHCARE

A Dissertation Presented

by

CHARMAINE K.W. KOO

Approved as to style and content by:

_____

Sam R. Nugen, Chair

_____

D. Julian McClements, Member

_____

Sarah L. Perry, Member

_____

Eric A. Decker, Department Head

Food Science

DEDICATION

To my parents for their unconditional love and support.

ACKNOWLEDGEMENTS

First and foremost, I would like to express my deepest gratitude to my advisor, Dr. Sam R. Nugen, for his teaching, guidance and support throughout the four years of my PhD. Getting a doctorate in Food Science would not have been made a reality if it was not for an opportunity given to me at IFT AMFE 2011. It was truly a privilege to work in his group. Thank you for inspiring me to become a better scientist and encouraging me to pursue my passions. And my most sincere appreciation to Dr. Julie M. Goddard for her thoughtful advice and patient support with my research and professional development. I would also like to extend my appreciation to my committee members, Drs. D. Julian McClements and Sarah L. Perry for being great mentors and providing constructive feedback and suggestions with my research.

My sincere appreciation to the past and present members of the BIOENG group for being great acquaintances and colleagues during my four years at UMass. Special thanks to Danhui, Ziyuan, Mindy, Sam, Juhong, Angelyca, Fei, Dana, Maxine, Stephanie, Luis and Fang for their selfless assistance with my research. Your friendship and comradery will never be forgotten and will forever be appreciated. Thank you to Cindy for managing our lab and keeping everything in order. I would also like to give my deepest gratitude to Cheryl, for being a great role model and mentor. Thank you for your patience - I am extremely grateful for your invaluable guidance. I would also like to thank Louis Raboin from the UMass Electron Microscopy Center for his assistance with obtaining micrographs for my projects.

Furthermore, I would also like to acknowledge my funding agencies for their financial support in my research, which include the USDA National Needs Graduate Fellowship Program and the U.S. Army Natick Soldier Research, Development and Engineering Center.

Last but not least, I would like to give my ultimate gratitude to my family, especially my parents, for their unconditional support over the years. Without their unwavering encouragement and upmost confidence in me, I would not have had the opportunity to further my education and complete my doctoral degree.

ABSTRACT

ADVANCED MATERIALS FOR RAPID DIAGNOSTICS IN FOOD, AGRICULTURE AND HEALTHCARE

MAY 2016

CHARMAINE K.W. KOO, B.Sc., UNIVERSITY OF BRITISH COLUMBIA

Ph.D., UNIVERSITY OF MASSACHUSETTS AMHERST

Directed by: Professor Sam R. Nugen

Paper based devices are an emerging trend for micro total analysis systems due to their rapid, sensitive and specific attributes. Lateral flow assays (LFAs), the predecessor of paper-fluidic devices, are developed for many applications which range from nucleic acid and antibody detection to commercial home pregnancy tests. With growing interest in replacing conventional detection methods, multistep assays are needed. These assays require multiple test reagents, therefore, there is a need to control fluid flow for the development of complex paper-based devices.

We were able fabricate paper-fluidic platforms where we used electrowetting-on-dielectrics to create valves on paper. With this method, we directly controlled the timing and flow of the fluid. However, the electrowetting valves required an external power source for actuation, thus we developed a passive fluid control method.

To do this, passive delay valves/barriers were inkjet-printed, by altering the drop spacing of the ink creating effective delay barriers, which decreases the rate of capillary

action of the throughput solution. The patterned devices were later used to create a paper based device where an amplified nucleic acid assay was performed.

After creating a paper based platform and understanding the properties that control fluid flow on paper, it is important to discover applications that are suitable for the devices. Phage amplified LFAs were developed, where a genetically engineered phage that overexpresses alkaline phosphatase was used, in combination with phage amplification kinetics to detect for low levels of *E. coli* in a sample. In the end, we were able to fabricate a barcode style LFA that had a visually quantitative colorimetric readout.

After understanding phage kinetics and amplification, their infectious and destructive mechanism was leveraged and applied to decontamination of agricultural rinse water. In general, bacteriophages are capable of infecting and lysing target bacteria and are kept viable by lyophilization, but freeze-drying is time consuming and requires large machinery. In our study, we dehydrated bacteriophages in electrospun nanofibers and studied the effects of excipients in polymeric solutions and different storage conditions on bacteriophage viability. Ultimately, electrospun nanofibers stored for eight weeks at ambient temperatures retained high phage viability which is sufficient for infection.

TABLE OF CONTENTS

Page

LIST OF TABLES

LIST OF FIGURES

CHAPTER 1

PAPER BASED MATERIALS FOR RAPID DIAGNOSTICS IN FOOD, AGRICULTURE AND HEALTHCARE

1.1 Introduction

The use of paper based materials as a platform for point-of-care devices have become increasingly popular for chemical and biochemical sensing. With growing number of foodborne illness and clinical related outbreaks, rapid detection and analytical methods have become a focus in recent years[1-3]. Other uses of these devices include medical diagnostics in low resource settings[4-5], chemical biology[6], electrochemical sensing in biological samples[7-8], drug analysis and development in the pharmaceutical industry[9-10]. Recently, there has been renewed interest in using lateral flow assays (LFAs) for rapid diagnostics due to its affordability and portability, yet still being sensitive enough for accurate detection[11-13]. The home pregnancy test kit is a product that exemplifies the benefits of using LFAs for detection. Most currently, paper-fluidics, which evolved from LFAs, is a hybrid of microfluidics and LFAs, where it uses the advanced patterning techniques of microfluidics to fabricate and develop more complex assays than the basic LFA. The goals of paper-fluidics are to retain the same principles of the conventional microfluidic device, which are to provide rapid, cost-effective, specific and sensitive methods of analysis, but at the same time provide a more affordable, portable and easier to use format[14-16].

1.2 Lateral flow assay

1.2.1 Components of a lateral flow assay

A lateral flow assay test strip is made of several simple components. In its most common form, the LFA consists of a nitrocellulose membrane, where the test and control lines are immobilized; a sample pad, where the sample is dispensed; a conjugate pad, where the reporter molecules are immobilized; and an absorbent pad, where it is used to wick up excess solution. In a typical LFA, a sample is first dispensed onto the sample pad, where the sample is treated so that it is compatible with the assay and release the analyte with high efficiency[14]. In most instances, the composition of the sample is diverse and complex, which can range from whole blood samples, sputum samples to ground beef samples, which all require separation before the target analyte could be extracted[17]. Thus, sample pads are usually made of cellulose, glass fiber, rayon, and other filtration media, which are further treated with assay buffer and dried.

The sample analyte then travels onto the conjugate pad where the reporter is immobilized. The role of the conjugate pad is to store the conjugate reporter, hold it stable during storage, allow hybridization of the analyte, and the successful release of the conjugate complex. The conjugate pad is commonly made of glass fibers, polyester or rayons and the conjugate labels range from colloidal nanoparticles made of gold and latex, visual or fluorescent dye[18-19], as well as enzymatic reporters[20-22].

After conjugation with the analyte, the complex will then flow onto the membrane towards the detection zone. The role of the paper membrane is to bind proteins at the test and control area and to maintain stability and activity over the shelf life of the product.

Some common materials used are nitrocellulose, nylon and polyvinylidene fluoride (PVDF)[14]. After immobilization of the test and control lines, the paper membrane is treated and blocked with proteins and surfactants to prevent non-specific binding of analyte.

Once sample has flowed past the detection zone, excess will be wicked up by the absorbent pad, which is usually made of high density cellulose. The flow rate of the LFA is governed by the wicking ability of the absorbent pad. The pad should effectively pull excess fluid from the membrane and should not release fluid back into the assay, which can cause false positives.

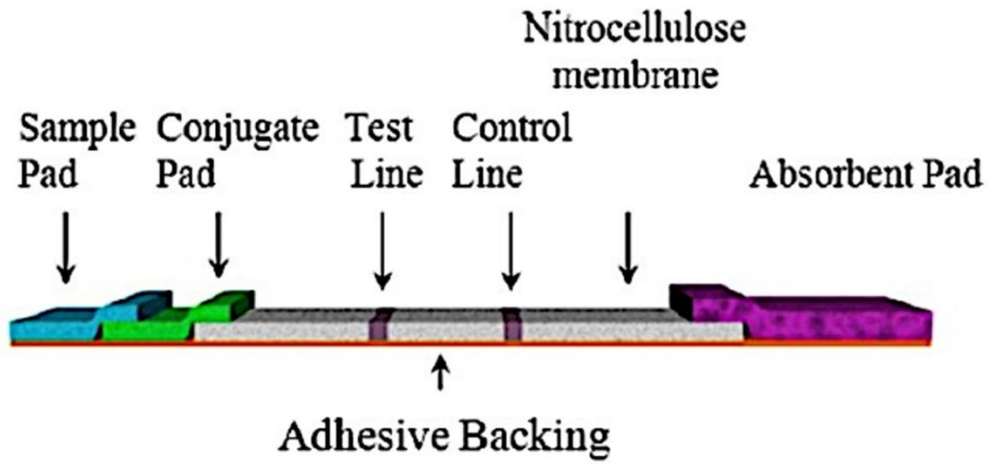

Fig. 1.1. Schematic diagram of a simple lateral flow assay.

1.3 Paper-fluidics

The convenience and benefits of performing analytical assays on small-scale portable devices has been materialized with the invention of microfluidics. Miniaturized medical diagnostic devices on small chip-size platform (e.g., blood-type determination, DNA separation[17]) have since been fabricated and utilized to perform analytical assays on

the go (lab on a chip) or for point-of-care use (POC), for use in low-resource settings and above all only small sample size is needed. Microfluidics, in brief, is the science and technology of a system to process and manipulate small amount of fluids within microchannels[9]. The manipulation and control of fluid flow is enabled by the microcomponents built in the chip e.g., microchannels, valves, mixers, and pumps. The flow of fluid in microchannels is different from large-scale systems, where the mixing of two or more fluids in microchannels occurs as a result of diffusion of molecules across the interface between the fluids – termed as laminar flow[9]. In large-scale systems, mixing of two fluids occurs by convection.

The shift from microfluidic to paper-fluidic devices is mainly to produce low-cost, portable and disposable microTAS to perform analytical assays especially in low-resource environment[11-13]. Paper-fluidic development has been on the rise since 2007, which largely is attributed to the Whitesides Group of Harvard University[3, 23]. Nevertheless, history of patterning paper can be dated back to 1949 where Müller and co-worker patterned filter paper using paraffin to form barriers for preferential elusion of a mixture of pigments within the channel[24]. Paper-fluidic devices are able to retain the sensitivity and specificity of microfluidic devices but subsequently are easier to use and often do not require additional instrumentation. Lateral flow test strips, the predecessor of paper-fluidic devices, have been developed for many applications which range from nucleic acid and antibody detection for diseases in developing countries to commercially available home pregnancy tests.

With the growing interest in replacing LFAs with paper-fluidic devices, multistep assays and tests are performed on these devices. These assays require more than one type

of reagent being passed through, therefore, there is a need to control fluid flow for the development of more complex paper-based devices.

1.3.1 Patterning physical barriers and channels

With the advancement of technology, barriers and channels of paper-fluidic devices can be fabricated using several different techniques, *e.g.*, photolithography, plotting with analogue plotter, plasma treatment, inkjet printing, wax printing as well as laser treatment.

- **Photolithography**

One of the earliest methods in developing two-dimensional paper networks is a method called fast lithographic activation of sheets (FLASH)[25]. Microchannels in the paper-based device were created by using a modified photolithographic method without the need of a cleanroom and with the use of an inkjet printer, UV lamp and hot plate. This results in hydrophobic photoresist barriers that can be as small as 200 μm. However, this method can be inconvenient as they require a cleanroom photolithography environment to create patterns and photoresist can be costly.

- **Plotting**

Poly(dimethylsiloxane) (PDMS) dissolved in hexanes can be patterned into channels onto filtered paper using a modified desktop plotter[26]. This method allows the ability to easily create channels that can be folded, without destroying the integrity of the barrier. However, the accuracy and precision of the modified plotter, which uses a series of eight altered felt tip pens, is much lower than a materials inkjet printer, where it is designed to print different types of customizable inks in a very exact and accurate manner.

- **Screen printing**

Screen printing barriers on paper involves passing ink through a fine screen onto the paper substrate. The advantage with this method is the high throughput of devices using a simple process[27]. However, the channels that are created are not well defined (rough edges) and requires different masks for creating different patterns.

- **Laser treatment**

Another method in creating channels in paper involves cutting the paper into strips with different inlets with different dimensions[28-30]. This method relies on the capillary flow and wet-out of the paper, which changes as the dimensions of the paper changes. The disadvantage with this method is that the edges of the paper tend to singe when being cut, which can affect the resolution of the channels.

- **Wax printing**

A significant breakthrough in the fabrication of paper fluidic devices was seen when wax printing was used to create hydrophobic barriers to make channels. This method involves using a relatively inexpensive and commercially available wax printer, to create barriers[23, 27, 31]. The method is simple, cost efficient and rapid, but the main disadvantage is the precision, feature size and temperature stability.

- **Inkjet printing**

Inkjet printing has become a popular method for patterning in the recent years for creating channel and barriers on paper. Many have successfully printed polymer inks on paper by modifying office printers and also using by using research based piezoelectric

printers[22]. The ability to easily print micron sized patterns using computer aided design software and the potential for inkjet printing to be applied in a roll-to-roll high throughput setting are the main advantages. However, developing a suitable ink for jetting is difficult to optimize, thus, extensive studies on print quality is required for consistent results.

- **Valves on paper**

The ability to manipulate the fluid flow on a paper-fluidic chip is important in creating more developed and complex devices and assays[15]. With the use of different patterning techniques, as mentioned above, researchers have successfully controlled fluid flow on paper by application of different valving techniques. One method that was used in the early stages of development was creating varying geometries and topologies on the paper itself[28]. This method not only was a passive method, but was also unable to achieve adequate control for complex assays. Some researchers have also tried to create heat sensitive monolith valves that would actuate at certain temperatures[16]. The advantage with this type of valve was that it could be used numerous of times without an observed decrease in its function. However, downfall disadvantage of these methods was the need to be performed in a certain temperature range, which would be ineffective in low resource settings as most are located in areas where extreme climates occur. Another type of approach was to use hydrophobic materials to create channels and valves on paper[17-19]. Some researchers have printed paraffin wax on paper to create "fluidic timers", which are partially hydrophobic barriers that slow down the fluid flow[32]. In this case, the wax physically blocked the membrane, which allowed it to direct flow, but not actively control the rate of the flow. A similar concept using surfactants to create a barrier that would restrict fluid flow by the use of trigger and delay valves was also developed by Chen et

al[22]. Similarly, this method was unable to directly control the rate of the fluid flow. Recently, we have fabricated an active valve where we were able to directly control the fluid flow[33]. These valves were based on a phenomenon called electrowetting on dielectric (EWOD) where a dielectric, such as polytetrafluoroethylene (PTFE), which naturally is hydrophobic, could be polarized with an applied potential and become hydrophilic. This was done by creating a self-assembled fluorinated monolayer within the hydrophobic electrode that was sufficient to stop the fluid flow[23] on a nitrocellulose membrane. We fabricated the valves with the combination of inkjet-printing and spraying directly on the substrate surface. To actuate the valve, the hydrophobic monolayer was rendered hydrophilic by an applied potential which was achieved with the negative terminal attached to an already hydrophilic electrode that acted as a conductive surface. With this method, we were able to directly control the timing and flow of the fluid, which is a more active approach compared to the other types of valves discussed previously.

1.4 Methods of detection

There are several methods that have been used for detection and even quantification of analytes in paper-based devices: a) colorimetric detection, b) electrochemical detection, c) chemiluminescence and electrochemiluminescence detection, d) fluorescence detection and e) electrical conductivity. In the following sub-section section, we will discuss on the more commonly used methods for detection and quantification of analytes.

1.4.1 Colorimetric detection

This detection method is widely used in paper-based devices, where a color change indicates that an enzymatic or chemical interaction takes place. This simple method is

usually used to signify the presence or absence of a specific analyte, *i.e.*, "Yes/No". The color change can often be visualized with unaided eye[34-36]. The sensitive and accuracy of the detection method can be improved by using an external photography device *e.g.*, camera or scanner or image processing software[5]. A recent study[37] demonstrated the limit of detection colorimetric assay using a simple chromatographic paper-based for analysis of selected food compounds. Dark purple colored reaction product developed on the surface of chromatography paper when a reaction occurs between the food compounds (*e.g.*, (L)-glutamate, (L-)-lactate, or ethanol) and the enzymes from dehydrogenase family coupled with diaphorase in the presence of tetrazolium dye MTT (thiazolyl blue tetrazolium bromide) and NAD^+. The colored reaction could either be qualitatively analyzed by naked eye or quantitatively analyzed using a smartphone camera or evaluated in freeware ImageJ. The limit of detection for (L)-glutamate by naked eye was 0.05 mmol L^{-1} and 0.028 mmol L^{-1} by digital imagine[37].

1.4.2 Fluorescent detection

When compared to colorimetric detection, it has been reported that fluorescent detection have lower limits of detection (LOD). Fluorescent detection on LFAs rely on the use of fluorescent dyes, fluorescent label antibodies and fluorescent doped reporters[38]. In our group, we were able to develop a LFA for nucleic acid detection through the use of novel fluorescent doped silica nanoparticles. We were able to obtain a limit of detection of 66 amols compared to the LOD of colloidal gold, which was 15 fmols[19]. Another study has also reported that they were able to perform multiplex analysis on nucleic acids, which used human papillomavirus (HPV) as a model analyte[18]. The fluorescent signal was read by a robust, portable and cost efficient fluorescent LFA reader. With the low LOD of

fluorescent detection and the use of handheld readers on the market, fluorescent based LFAs are great tools for rapid quantification detection.

1.4.3 Electrochemical detection

This method is found to be more sensitive and selective than colorimetric detection in detecting and quantifying analytes[36, 39-40]. This detection method requires three electrode systems, *i.e.*, working electrode, counter electrode and reference electrode and a low power source and potentiostat to conduct electrochemical measurements. The electrodes are deposited on the paper source using conductive inks. Paper-based analytical devices using electrochemical detection is often termed as ePADs. Some examples of conductive inks used include carbon, silver/silver chloride, and some noble metals[39-45]. The power source applies a small potential difference to the electrode pair and cause the analytes in the samples to undergo redox reaction. Some of the commonly used electrochemical techniques to detect and quantify the analytes in microfluidic devices include amperometric detection (AD) coupled to capillary electrophoresis (CE), conductivity-based detection (CD), potentiometric techniques (*e.g.*, cyclic voltammetry), and electrochemical impedance spectroscopy (EIS) – more information on each technique can be found in the cited reference[40].

1.4.4 Chemiluminescence and electrochemiluminescence detection

Chemiluminescence detection is also another method that has been used in paper-based devices[46]. This method has higher sensitivity than colorimetric detection method. This method detects and quantifies the light intensity (electromagnetic radiation (ultraviolet UV), visible or infrared) generated from a photochemical reaction that yields

electrically excited intermediate or product that luminesces. Inexpensive reagents are required in the system for generating the luminescence[47-48]. Electrogenerated chemiluminescence or known as electrochemilumiscence uses electrochemical reactions to generate luminescence at an electrode[49].

1.4.5. Bacteriophage based detection

Bacteriophages, a type of virus that infect bacterial cells and hijack their metabolic mechanism through genetic transfer, have a range of specificity for hosts, and would be a great alternative to be used as a detection component in paper based devices. There are many advantages in using phage as a detection probe, as they are relatively easy to culture, are host specific and have the ability to differentiate between viable and non-viable cells[50-51]. Most importantly, they are able to infect bacterial cells and release more phage after replication, which is termed as phage amplification or signal amplification. Microphage (Longmont, CO) developed a phage amplification-based LFA for clinical settings that detected for *Staphylococcus aureus* and antibiotic resistance determination on methicillin-resistant *S. aureus* (MRSA) in blood[52]. The total analysis time for the LFA, including amplification, was 5.5 hours compared to a conventional MRSA test of 48 hours. Phage amplification-based LFA is a promising technique for low bacterial count samples and can also be applied to detect for other pathogens, such as *E. coli*[51, 53]. Studies have shown that not only have phages been applied to paper based detection but have also been detected through electrochemical, surface plasmon resonance, bioluminescent and fluorescent detection[51].

1.5 Potential application of paper-based devices

Paper-based devices have found practical applications in food safety and quality control, healthcare, and environmental monitoring in recent decades[35, 54-55]. Of food safety and quality control, it is vital that tests be performed on food products during the whole process line and up to shelving. Taking example of the recent foodborne illness outbreak in America, *e.g., Salmonella Poona* in cucumbers and Shiga toxin-producing *E. coli* O157:H7 in chicken salad containing celery (U.S. Food and Drug Administration, 2015), it is crucial to perform safety control tests, particularly on fresh produce during the whole preparation process and even prior to consumption. Therefore, paper-based devices would be ideal kits to provide convenient, simple and quick tests at a minimal cost, with little external equipment needed on site.

1.5.1 Food safety and quality control

Some paper-based devices fabricated thus far detect common pathogenic strains of foodborne bacteria like *Escherichia coli*, *Salmonella spp.*, and *Listeria monocytogenes*. Some studies have developed paper-based analytical device (μPAD) for screening detection of *E. coli* O157:H7, *Salmonella* Typhimurium, and *L. monocytogenes* in food samples[56] and agricultural water[57]. In both studies the detection of pathogen was measured by color change (colorimetric detection) when an enzyme associated with the pathogen of interest reacts with a chromogenic substrate. In combination with enrichment procedures, the assay was capable of detecting bacteria in concentrations in inoculated ready-to-eat (RTE) meat as low as 10^1 CFU/cm^2 within 8 to 12 h[56] or in filtered agricultural water as low as 0.1 CFU/mL detection limit within 24 h[57].

Besides testing for pathogenic bacteria that cause foodborne illness, paper-based devices may also have use in determining quality of food products, for example, antioxidant content in food products[58-59]. One study[59] fabricated paper-based platforms to determine ferulic acid (a superior antioxidant) content in simple food matrix (corn milk and corn cider) and in complicated cosmetic matrix (preceded with thin-liquid chromatography separation to minimize interference). For detecting the antioxidant in simple food systems, a paper-based electrochemical device was developed using photolithographic method. The working electrode and counter electrode were made of carbon ink while the reference electrode and conductive pads of Ag/Ag/Cl ink. A colorimetric device was instead created for detection in complicated cosmetic serum. Both devices were able to determine the amount of ferulic acid, with a limit of detection (LOD) and limit of quantization (LOQ) of 1 ppm and 3 ppm, respectively for the electrochemical device and 7 and 20 ppm, respectively for the colorimetric device.

1.5.2 Healthcare and environmental monitoring

Paper-based devices have wide applications in healthcare and environmental monitoring. Some examples of healthcare application includes detection, diagnosis or monitoring of hepatitis C virus infection[60], serotype-2 dengue fever in human serum[61], influence A H1N1 and H3N2 viruses[62], and protein and glucose content[63]. Paper-based devices have also found application in dental care. One recent study[64] has developed a paper-fluidic device used for monitoring dental caries (tooth decay), which is a debilitating irreversible disease that can ultimately lead to loss of tooth structure. The paper-fluidic device measures pH and reductase of saliva to estimate its buffering capacity and susceptibility of caries, respectively. The device was fabricated by inkjet printing olive oil

on paper and then heated the paper to render it hydrophobic in oil-covered regions. The reagents (mixture of bromothymol blue and bromocresol green in isopropanol for pH estimation and diazoresorcinal in ethanol for caries susceptibility test) for the dental assay were then inkjet-printed on the paper. The paper-fluidic devices produced results that are closely correlated to the results from standard tube-based assay performed in dental clinics[64].

Paper-based devices have also used in environmental monitoring. For example, one study[65] used multiplexed paper for quantification of nickel(II) (Ni), copper(II) (Cu) and iron(II) (Fe) metals from aerosolized particulate matter using distance-based detection. The device was fabricated by using commercial inkjet printer for printing hydrophobic barriers and colorimetric reagents in concentration gradients. The analyte was quantified visually with distance-based detection of a colorimetric reaction. The detection limit in single-channel device was as low as 0.1 μg (6.7 ppm), 0.1 μg (6.7 ppm) and 0.05 μg (3.3 ppm) for Ni, Cu and Fe, respectively while the detection limit in multiplexed (multi-channel) device for all three metals were 5 μg (100 ppm), 5 μg (100 ppm) and 1 μg (20 ppm), respectively. With printing of concentration gradients, the dynamic range of distance-based detection was improved by 50% and 41.2% for Ni and Cu, respectively[65].

1.6 Challenges in fabricating paper-based devices and future outlooks

Despite the immense research on fabrication of paper-based devices, much studies and improvements are still needed for better precision, sensitivity and reliability to match the gold standard of conventional laboratory methods and techniques. One of the limitations of paper-based device is the sensitivity of detection level. With the small

amount of sample applied, the analyte concentration decreases at the detection zone after traveling from the loading zone due to spreading and evaporation[35-36, 66-67]. Pre-concentration of analytes, amplification of signals (*e.g.*, using gold or graphene nanoparticles) or coat printing toner on the channels could overcome the low efficiency of sample delivery and low limit of detection problems[66-69].

Another limitation in paper-based devices is fabrication techniques and material properties. It is important that the materials used are able to build strong barriers on the paper to form channels for fluid flow. For example, strong hydrophobic barriers are needed to direct low surface tension samples within the channels[36].

In multiplexed devices, cross talk of signals from adjacent channels may be a problem. To overcome this, more careful consideration in the design of the fluid pathways and the location for analysis is needed[35]. Some studies have overcome this problem with small sample volume and/or proper washing steps[70-71].

1.6.1 Future outlooks

With paper based devices becoming more sophisticated and multiplexed, there are huge opportunities for scientists to develop more practical and user friendly devices that are capable of performing sensitive and rapid assays. It is evident that if scientists tackle the limitations (discussed above) and develop tests that can be robust and work on the field, then there definitely will be huge advances in diagnostics, from clinical settings to even the household. However, it is important to remember the underlying criteria of paper based devices, where simplicity and cost should not be sacrificed in order to achieve such devices.

CHAPTER 2

AN INKJET-PRINTED ELECTROWETTING VALVE FOR PAPER-FLUIDIC SENSORS

2.1 Introduction

The use of microfluidics in a device for chemical and biochemical sensing have become increasingly popular in the bioengineering field and have also been applied to point-of-care (POC) diagnostics[7], such as in the safety of foods by the detection of foodborne pathogens[72]. Other uses of these devices include medical diagnostics in low resource settings[4-5], chemical biology[6], electrochemical sensing in biological samples[7-8], drug analysis and development in the pharmaceutical industry[9-10]. A re-emerging trend in using paper based materials as a platform for point-of-care devices has generated a great amount of interest in the field, thus creating a new area called paper-fluidics[12, 73]. The goals of paper-fluidics are to retain the same principles of the conventional microfluidic device, which are to provide rapid, cost-effective, specific and sensitive methods of analysis, but at the same time provide a more affordable, portable and easier to use format[14-16]. Nitrocellulose, a porous material, is now commonly used to develop POC devices due to their ability to customize the pore size and porosity, their application in adsorbing proteins, their use in dry reagent storage and their lower limit of detection for analyte detection[15]. These properties have led to increasing interest in the use of paper-fluidics for low-resource settings[3]. Currently, there are many approaches in the fabrication of paper-fluidics, but a common challenge is the control of fluid flow on the paper device.

The ability to manipulate the fluid flow on a paper-fluidic chip is important in creating more developed and complex devices and assays[28]. One method that was used in the early stages of development was creating varying geometries and topologies on the paper itself. This method not only was a passive method, but was also unable to achieve adequate control for complex assays. Some researchers have also tried to create heat sensitive monolith valves that would actuate at certain temperatures[74]. The advantage with this type of valve was that it could be used numerous of times without an observed decrease in its function. However, downfall disadvantage of these methods was the need to be performed in a certain temperature range, which would be ineffective in low resource settings as most are located in areas where extreme climates occur. Another type of approach was to use hydrophobic materials to create channels and valves on paper[26, 75-76]. Some researchers have printed wax on paper to create a hydrophobic barrier[23, 31]. In this case, the wax physically blocked the membrane, which allowed it to direct flow, but not actively control the rate of the flow. A similar concept using surfactants to create a barrier that would restrict fluid flow by the use of trigger and delay valves was also developed by Chen *et al.*[77]. Similarly, this method was unable to directly control the rate of the fluid flow.

In a previous study, we fabricated and surface characterised electrowetting valves for capillary-driven microfluidics on a PET device[78]. These valves were based on a phenomenon called electrowetting on dielectric (EWOD) where a dielectric, such as polytetrafluoroethylene (PTFE), which naturally is hydrophobic, could be polarized with an applied potential and become hydrophilic. We successfully applied these valves in PET channels in a microfluidic device to control the fluid flow without the application of an

external pumping mechanism. Therefore, in this project, our goal was to apply EWOD to control fluid flow on a paper-fluidic device. This was done by creating a self-assembled fluorinated monolayer within the hydrophobic electrode that was sufficient to stop the fluid flow[78] on a nitrocellulose membrane. We fabricated the valves with the combination of inkjet-printing and spraying directly on the substrate surface. To actuate the valve, the hydrophobic monolayer was rendered hydrophilic by an applied potential, which was achieved with the negative terminal attached to an already hydrophilic electrode that acted as a conductive surface. With this method, we were able to directly control the timing and flow of the fluid, which is a more active approach compared to the other types of valves discussed previously. This method will also allow for subsequent loading of buffers and solution, eliminating the waiting time for loading after incubation, which can decrease the amount of labor used performing an assay and therefore reduces user error. Furthermore, we used the valves in conjunction with a lateral flow assay for the detection of nucleic acids – in our case, an rRNA sequence for *Saccharomyces cerevisiae*, to show the possibility of our valves being applied in a micro total analysis system. Our study showed that we can effectively and directly control the fluid flow in a paper-fluidic device and assay, which could be used as a new technique for the further development of fluid control in paper-based microfluidics.

2.2 Materials and Methods

2.2.1 Materials

All chemicals and reagents were of analytical-reagent grade. Silver acetate (99% pure) and ethyl alcohol (absolute, 200 proof, 99.5+%, ACS reagent) were obtained from

Arcos Organics. 1H, 1H, 2H, 2H-perfluorodecanethiol (PFDT) and 2, 3-butanediol was obtained from Sigma-Aldrich. All other chemicals and reagents were obtained from Fisher Scientific.

- **Oligonucleotides**

The oligonucleotides used for the lateral flow assays were ordered from Eurofins MWG Operon.

- **Solutions**

Phosphate buffered saline (PBS) solution consisted of 40mM sodium chloride, 50mM sodium phosphate, dibasic and was titrated to pH 6.8.

2.2.2 Assembly of test strips

The plastic backing (Highland Transparency Film, 901) was cut into 75 x 215 mm rectangular sheets. Double sided tape (3M, St. Paul, MN) with the dimensions of 38 x 215 mm was adhered 10 mm from the bottom edge of the backing. A pre-cut 38 x 215 mm nitrocellulose membrane (AE 98 Fast, Whatman®) was gently pressed onto the double the sided tape. The assembled test strip was stored in a desiccator at room temperature until further use.

2.2.3 Synthesis of reactive silver ink

An inkjet-printable silver ink with high conductivity and a low sintering temperature was used for the electrodes[79]. The silver ink was synthesized by mixing 0.5 g of silver acetate with 1.25 mL of aqueous ammonium hydroxide and vortexing at room temperature for 15 seconds. Formic acid (0.1 mL) was titrated into the solution dropwise

within 60 seconds, while vortexing after each drop. After titration, the solution should be translucent with the presence of dispersed dark grey silver particles. The silver ink was left undisturbed at room temperature for 20 to 24 hours for the large particles to settle out. The clear supernatant was then removed and filtered through a 0.22 μm syringe filter (25mm, MCE, Sterile, Fisherbrand) to remove any large particles. The filtered ink was stored away from light at 4°C.

- **Preparation of hydrophilic silver ink for printing**

The hydrophilic silver ink solution was made by mixing 10% (v/v) deoxygenated absolute ethanol in silver ink. The absolute ethanol was deoxygenated with nitrogen for 10 minutes.

- **Preparation of hydrophobic silver ink for printing**[78]

A volume of 0.57μL of 3.33M PFDT was added into 1 mL of deoxygenated absolute ethanol and was mixed by vortexing. The hydrophobic ink was then prepared by adding 45% silver ink, 45% PFDT/ethanol and 10% of 2,3-butanediol. The final concentration of PFDT in the hydrophobic silver ink was 1.55 mM. The ink was then vortexed to ensure homogeneity.

2.2.4 Printing of silver electrodes

The assembled test trips were placed on the printing area of the Linomat IV (Linomat IV, CAMAG, Wilmington, NC, USA) and held down by magnets. 38μL of the prepared hydrophilic ink was deposited in a 180 mm line, which results in a total concentration of 0.05μL/mm. Subsequently, 38μL of the prepared hydrophobic ink was

printed with a length of 190 mm, which results in a total concentration of 0.2µL/mm. The hydrophobic electrode was air dried at room temperature for 10 minutes and 19µL of hydrophobic ink was sprayed on top of the electrode with a length of 190 mm and a total concentration of 0.1µL/mm. The test strip was then incubated in an oven at 95°C (Thermo Isotemp Oven) for 45 minutes and was then additionally incubated in a vacuum oven at 95°C at -20 mmHg for 45 minutes to remove excess 2,3-butanediol.

2.2.5 Assembly and testing of silver electrodes/valves

After incubation, the test strips were cut into 75 x 4 mm pieces. A buffer pad (CF5, Whatman International Ltd., Piscataway, NJ, USA), measuring 30 x 4 mm, was placed 8 mm away from the hydrophobic line. Two thin wires were attached to each electrode with tape, which was attached to an 80W switching D/C power supply (Extech Instruments). 200 µL of 1 x PBS was pipetted onto the buffer pad and the PBS flowed past the hydrophilic electrode and stopping at the hydrophobic electrode/valve. To investigate the opening of the valves, five different voltages were tested – 0 V, 4 V, 9 V, 12 V and 16 V. Potential was applied to disrupt the PFDT monolayer with a cycle of 3 seconds on and 1 second off. The valve was also characterized by observing the effect of the distance (1.36 mm, 4.15 mm and 7.31 mm) between the two electrodes at each of the five different voltages.

2.2.6 SEM imaging

The surfaces of the hydrophilic and hydrophobic electrodes were captured by the FEI Magellan 400 field emission scanning electron microscope using a magnification of

5µm. All of the images were captured at 1kV and a horizontal field width (HFW) of 29.8 mm.

2.2.7 Application of silver valves in nucleic acid detection with gold nanoparticles in lateral flow assays

2.2.7.1 Inkjet printing silver electrodes with Dimatix Materials Printer

The silver electrodes were inkjet printed with a Dimatix Materials Printer (Fujifilm DMP-2800) with a 1 picoliter cartridge on the pre-assembled test strips. The hydrophilic line was printed with the prepared hydrophilic ink with a drop spacing of 10µm, a line width of 200µm, a line height of 0.7µm and was printed with a total of 20 layers. The hydrophobic line was printed with the prepared hydrophobic ink with a drop spacing of 5µm, a line width of 200µm, a line height of 0.7µm and was printed with a total of 12 layers. The ink and plate temperature was set at 30°C. The distances between the two electrodes were 5.98 mm.

2.2.7.2 Lateral flow assay test strip preparation

- **Immobilization of oligonucleotides for test and control lines**[46]

10µL of 300µM biotin capped oligonucleotide (Table 2.1), 10µL of streptavidin and 30µL of 0.4M $NaHCO_3/Na_2CO_3$, pH 9.0, containing 5% methanol were incubated for 20 minutes. Using the Linomat IV, the test and control lines at 30mm and 38mm, respectively, were sprayed onto another pre-assembled nitrocellulose test strip, each measuring 190mm in length and 0.2µL/mm in concentration. The test strip was then placed into a vacuum oven to dry at 40°C and -15mmHg for 1.5 hours. The membrane was then blocked with 35mL of blocking solution (0.015% sodium caseinate, 0.3%

polyvinylpyrrolidone (MW 8000), 0.001% Tween 20 brought to volume with 10 x TBS), agitating for one minute. The test strip was then dried in a vacuum oven at 25°C and -15 mmHg for 2 hours.

Table 2.1. Nucleic acid sequences for the oligonucleotides used in the lateral flow assay.

NAME	**SEQUENCE**
Test line	[Biotin]GGGCATCACAGACCTG
Control line	GGAGGGCAAGTCTGGT[Biotin]
Reporter (gold nanoparticle)	ACCAGACTTGCCCTCC[Biotin]
Target	GGAGGGCAAGTCTGGTACCATCCGCTGGATT ATGGCTGAACGCCTCTAAGTCAGAATCCATG CTAGAACGCGGTGATTTCTTTGCAGGTCTGTG ATGCCC

- **Immobilization of nucleic acid-gold reporter nanoparticle complex on a conjugate pad**[46]

A conjugate pad treatment solution (CPTS) was made by combining 23.75µL of 12% sucrose buffer (pH 7.4), 15µL of stock conjugate and 56µL of dilution buffer (50mM Na_2HPO_4, 1% BSA, pH 7.4). The stock conjugate was prepared by incubating 62.5µL of 23.8µM DNA in PBS, 1.6mL of streptavidin linked gold nanoparticles in HPLC grade water (OD_{520}=1.0) and 170µL of 10% BSA (pH 9.0) at room temperature, shaking for one hour. The stock conjugate was then centrifuged at 3000 x g at 4°C for 20 minutes and re-suspended in 2mM borax (pH 9.0) to OD_{520}=3.0. A 10 x 16 mm conjugate pad (Conjugate Pad Grade 8975, Life Science-PALL Corp.) was submerged into the CPTS and was air-dried at room temperature.

2.2.7.3 Lateral flow assay assembly and testing

The inkjet-printed membranes and lateral flow test strips were cut into 75 x 4 mm pieces. The dried conjugate pad was cut into 10 x 4 mm and was fixed onto the lateral flow test strip. A sample pad (CF5, Whatman International Ltd., Piscataway, NJ, USA), measuring 7 x 4 mm, was fixed on the test strip overlapping the conjugate pad by 2mm. A buffer pad (CF5, Whatman International Ltd., Piscataway, NJ, USA), measuring 30 x 4 mm, was placed 8 mm away from the hydrophobic valve on the silver electrode test strip. The test strips were then perpendicularly taped to the lateral flow test strips with double-sided tape ensuring that the membranes were touching each other. Two thin wires were attached to each electrode with tape, which was attached to a D/C power supply (Extech Instruments). 50µL of *Saccharomyces cerevisiae* target (200 fmol/µL) was dispensed on the sample pad and was allowed to flow to the conjugate pad. 200 µL of 1 x PBS was then pipetted onto the buffer pad and the PBS flowed past the hydrophilic electrode and stopping at the hydrophobic electrode (valve). After the sample flowed passed the control line, 16V of potential was applied until the valve was actuated, allowing the buffer to flow onto the lateral flow test strip.

2.3 Results and Discussion

2.3.1 Printing of silver electrodes on nitrocellulose test strips

The Linomat IV was used to spray two silver electrodes on each of the pre-assembled test strips – hydrophilic and hydrophobic. After printing, the hydrophilic electrode measured 180 x 0.86 mm. The hydrophobic electrode measured 190 x 1.60 mm. Due to the hydrophilic nature of the nitrocellulose, absolute ethanol and 2,3-butanediol was

used in the hydrophobic silver ink to keep PFDT immiscible in solution, which allowed for better homogeneity throughout the membrane during printing of the electrode. 2,3-butanediol was also used to increase viscosity of the hydrophobic ink to create thinner lines during printing because of a decrease in lateral diffusion of ink within the membrane. A higher concentration of silver ink was also used in the hydrophobic valve in order for the self-assembled monolayer (SAM) to be more easily distributed throughout the 5µm thickness of the nitrocellulose membrane. In a previous study, we used X-ray photoelectron spectroscopy (XPS) to confirm that the PFDT monolayer was formed[78]. Results show that there was a presence of fluorine and sulfur, which proves that a PFDT SAM was successfully achieved. A lower concentration of silver ink was used in the hydrophilic valve so that only a conductive surface was created. The hydrophilic electrode is used to provide a conductive surface for the valve to be actuated. The electrodes were then annealed at 95°C to evaporate excess ethanol. A vacuum oven set at 95°C at -20 mmHg was used to evaporate 2,3-butanediol due to its higher boiling point than ethanol.

2.3.2 Design of the test strip

The hydrophilic electrode was printed preceding the hydrophobic electrode to act as a conductive substrate for the actuation of the valve (Fig. 2.1). There are four main components in EWOD – an ionized solution that serves as a medium, a conductive material that act as electrodes and the dielectric which provides capacitance between the electrodes and the medium and also act as a hydrophobic barrier[80]. PBS, the ionized solution, was dispensed onto the buffer pad and was wicked up the nitrocellulose membrane by capillary action towards the electrodes. PBS first flowed past the hydrophilic electrode (the conductive material) and the fluid front was stopped at the hydrophobic valve (the

dielectric) due to the PFDT monolayer (Fig. 2.2). To actuate the valve, potential was applied to the electrodes to destroy the fluorinated monolayer[78].

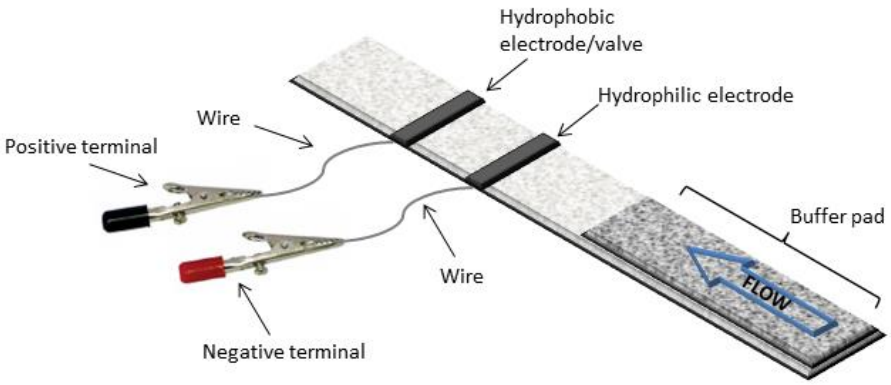

Fig. 2.1. Schematic diagram of the test strip with a hydrophobic and hydrophilic electrode.

The positive terminal (black wire) was connected to the hydrophobic electrode/valve and the negative terminal (red wire) was connected to the hydrophilic electrode. It is important that the negative terminal is in contact with the liquid medium, where the applied potential (the threshold voltage) creates charges on the liquid and electrode interface and change the wettability of the hydrophobic electrode (dielectric)[81]. At this point, the wettability of the hydrophobic valve is still reversible and can be detected by a change in the contact angle. However, due to the uneven surface of the nitrocellulose membrane and our final application of the valve, we did not measure the contact angle. Instead, we allowed the applied potential to run until the contact angle is irreversible which allows a permanent change in the wettability of the hydrophobic valve (dielectric)[81] and opens the valve indefinitely. This type of applied potential is termed as the breakdown voltage[81] or the phenomenon is called the dielectric breakdown in dielectrics[80].

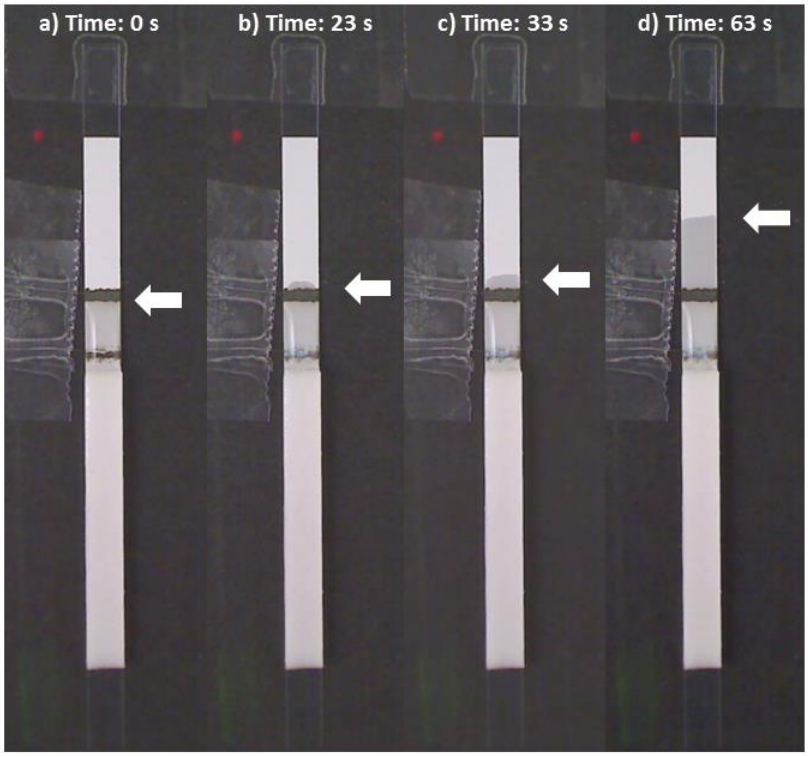

Fig. 2.2. Photograph of the valves. a) Fluid front has flowed past the hydrophilic electrode and stopped at the hydrophobic valve. A potential of 16 V has been applied to the electrodes with a cycle of 3 seconds on and 1 second off. b) Hydrophobic monolayer has been destroyed by the applied potential and fluid front has flowed past the valve. c) Flow of fluid front after passing valve for 10 seconds. d) Flow of fluid front after passing valve for 40 seconds.

2.3.3 Understanding the relationship between valve actuation and applied potential

To have a better understanding of how the valves work, they were actuated at different voltages and were also tested with different distances between each electrode (Fig. 2.3). The different voltages tested were 0, 4, 9, 12 and 16 V with a square alternating current cycle of 3 seconds on and 1 second off and with electrode distances of 1.36, 4.15, and 7.31 mm. In Fig. 2.3, we observe that as voltage was increased, the time for the valves to open decreased. The more electricity was applied to the valve, the faster the PFDT monolayer

was disrupted which decreased the time for the fluid front to flow past the valve. When a voltage of 12V or higher was applied, electrolysis in the PBS was observed. Furthermore, we find that there is no significant difference in the time required to open the valves as the distance between the hydrophilic and hydrophobic electrode was increased. The porosity of the nitrocellulose membrane seems to decrease the effect of resistance between the two electrodes. This allows us to have more flexibility in designing paper-fluidic devices since the distance between the two electrodes can be changed without having much effect on the actuation of the valves.

Furthermore, by using a square voltage cycle of 3 seconds on and 1 second off, it further enhanced the fluid front to be pulled away and pushed towards the hydrophobic valve, respectively. When the voltage was applied, bubbles due to electrolysis would appear and form an interface between the electrodes and PBS. The bubbles act as an insulator, which increases the resistance between the valves. When the voltage was removed, the bubbles would disappear, which would allow the PBS to come in contact with the edge of the electrode. This decreases the resistance between the electrodes, allowing the valves to be actuated faster. The square voltage cycle can easily be controlled with the use of a relay, which can be incorporated within the applied potential source, thus allowing it to be used in low resource settings.

In our previous study where electrodes were printed on PET, we found that we were able to actuate the valves at 2V and 4V with shorter times[82]. Here, printing was conducted on nitrocellulose, which has a more porous structure and more surface area than PET. Because the wettability of EWOD depends on the surface roughness and heterogeneity, we observe that the valves required more time and higher applied potentials to actuate[81]. As

the surface roughness increases, a higher voltage is needed to open the valves. In addition, studies also show that the thickness of the dielectric layer affects the voltage needed to observe wettability changes in the valve[81]. The electrode thickness on PET was 54.9 ± 13.5 µm whereas the electrode thickness on the nitrocellulose membrane was 200µm, which is approximately a fourfold increase[78].

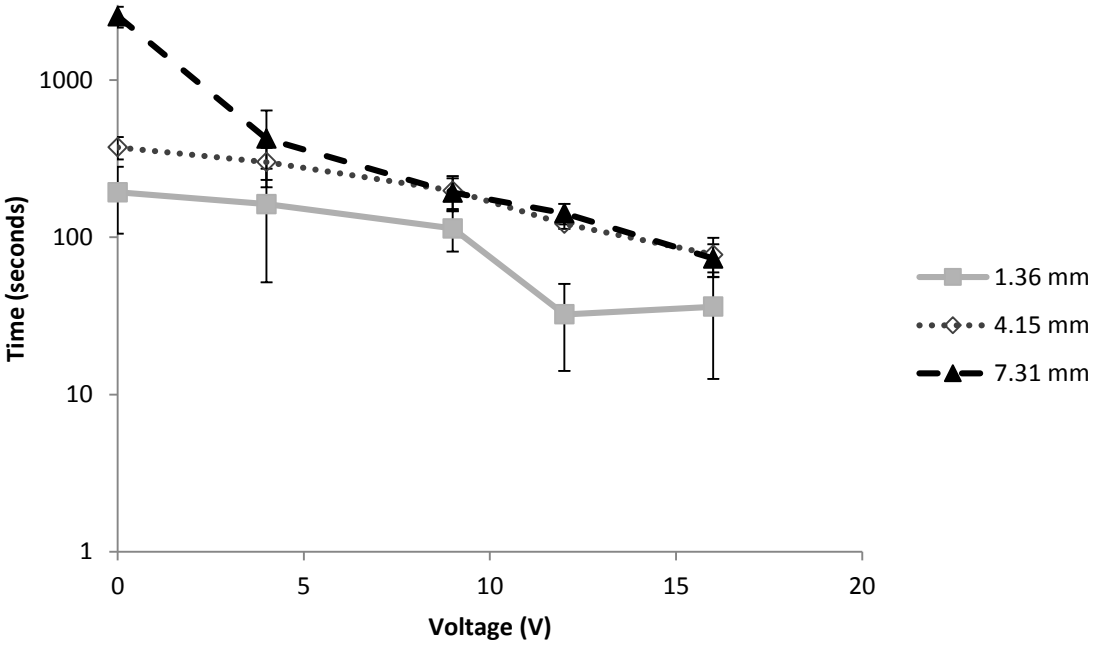

Fig. 2.3. Amount of time (seconds) for fluid front to pass valve vs. amount of voltage applied to valve for a cycle of 3 seconds on and 1 second off.

2.3.4 Surface characteristics of the valves due to different types of printing and the effect of fluid flow

Both the hydrophilic and hydrophobic electrodes were surface characterized underimaged with a scanning electron microscope. In Fig. 2.4a and 2.4b, which showed the electrodes inkjet printed by the Dimatix, the surface of the nitrocellulose membrane of the hydrophobic electrode (Fig. 2.4a) was interwoven with the silver ink. When compared

to the hydrophilic electrode (Fig. 2.4b), the membrane contained less silver ink, which was expected due to a lower ink concentration that was printed. This can be confirmed by observing the underside of the membrane, where a significantly darker and thicker line is present for the hydrophobic electrode when compared to the hydrophilic electrode. Because the hydrophilic electrode was only used as a conductive element, it only needed to be conductive on the surface of the membrane, which meant that only a minimal amount of ink was needed. This allowed the fluid to flow with no obstructions through and over the electrode.

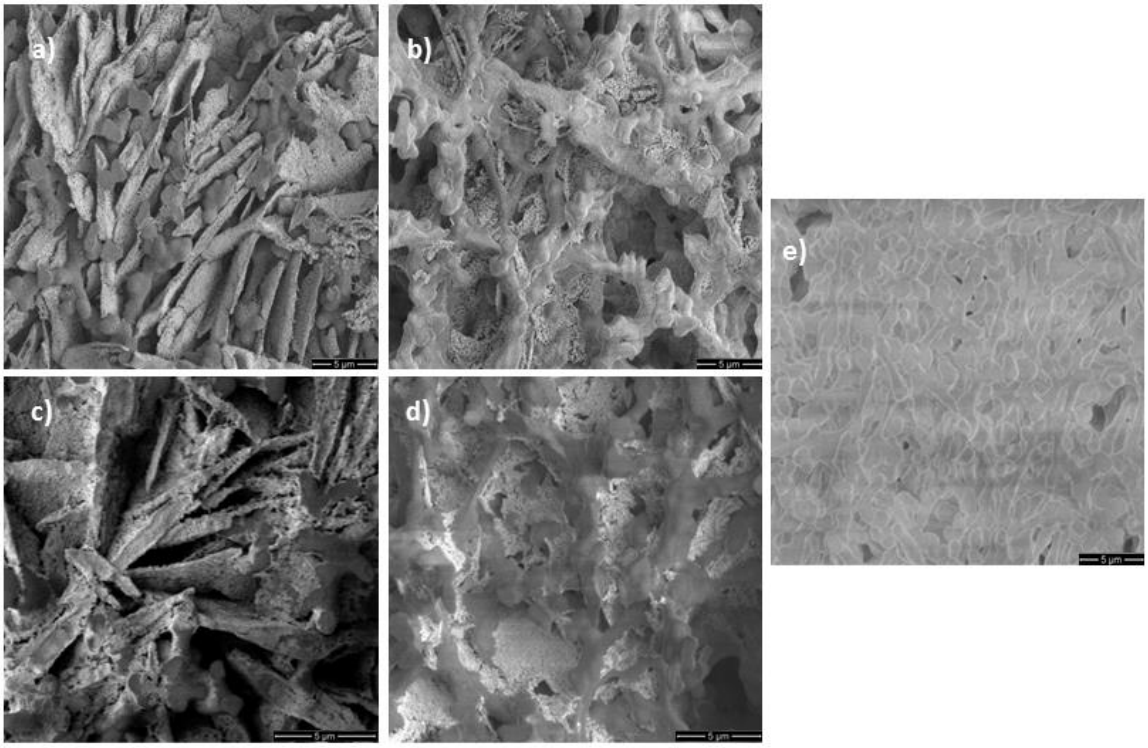

Fig. 2.4. Scanning electron microscope images of the hydrophobic and hydrophilic electrodes on a nitrocellulose membrane. a) Hydrophobic electrode printed by Dimatix piezoelectric printer b) Hydrophilic electrode printed by Dimatix piezoelectric printer c) Hydrophobic electrode sprayed by Linomat IV d) Hydrophilic electrode sprayed by Linomat IV e) Nitrocellulose membrane.

In Fig. 2.4c and 2.4d, which showed the electrodes sprayed by the Linomat IV, the surface of the nitrocellulose membrane of the hydrophobic electrode (Fig. 2.4c) was coated with the silver ink. When compared to the hydrophobic silver ink inkjet printed by the Dimatix, the electrodes sprayed by the Linomat coated more of the surface of the nitrocellulose. This affected the surface hydrophobicity of the electrode, thus making the hydrophobic electrode sprayed by the Linomat more surface hydrophobic. This phenomenon was observed by noting how the valve opened when actuated. Not only did the fluid front penetrated through the inkjet-printed valve, but also flowed over the surface of the electrode. Conversely, the fluid front of the Linomat-sprayed valve penetrated through the valve only. When observing the underside of the membranes, the Linomat sprayed electrode appeared to be thicker and darker than the Dimatix printed electrode. Therefore, due to the difference in the two types of valves, the flow rate after passing the inkjet-printed electrode was faster than the Linomat-sprayed electrode. Depending on the type of assay the valves would be applied to, the selection of the printing type is important.

The Linomat-sprayed hydrophilic electrode was similar to the inkjet-printed electrode in terms of its surface characteristics and fluid flow.

2.3.5 Application of silver valves in nucleic acid detection with gold nanoparticles in lateral flow assays

The silver valves printed on nitrocellulose could be applied to lateral flow assays in the detection of nucleic acids with gold nanoparticles. In previous studies done in our laboratory, we developed lateral flow assays (LFA) to model the detection of microorganisms[46], such as *Saccharomyces cerevisiae*. *Saccharomyces cerevisiae* rRNA, a

spoilage organism in food, was used as the target. Commercially manufactured gold nanoparticle reporters (Bioassay Works, Ijamsville, MD) were then conjugated with a sequence complementary to one end of the target and were immobilized in a conjugate pad, where target and gold reporter hybridization takes place. The conjugate complex would then bind to the test line and control line, yielding a positive result, which was shown as two red lines. If there were no presence of target in the sample, the gold nanoparticles would only bind to the control line, yielding a negative result, which was shown as one red line. To ensure that the majority of conjugate reporter has been effectively washed up the test strip, PBS was dispensed after a period of incubation. In this project, we incorporated our valves into the lateral flow assay system (Fig 2.5). Instead of dispensing a secondary buffer solution after incubation, we were able to dispense both the sample and buffer solution at subsequent times. The valve was then actuated at the appropriate time to allow the secondary buffer solution to wash the sample up the test strip towards the test and control lines. A stronger fluid flow was desired in this assay because we needed to wash the sample and excess gold nanoparticles up towards the test and control lines from the extended part of the test strip where the valves were located. There seems to be no observed effect with the downstream chemistry of the electrodes such as electrolysis of the PBS or release of silver or other chemicals in this assay. It would be beneficial for future work to further investigate the downstream chemistry of the electrodes. With this simple application, it shows that we can develop more complex assays. With the incorporation of a relay attached to a power source, we can actively control the rate of the fluid flow in a LFA, which could be valuable when designing a paper fluidic device to be used in a low resource setting.

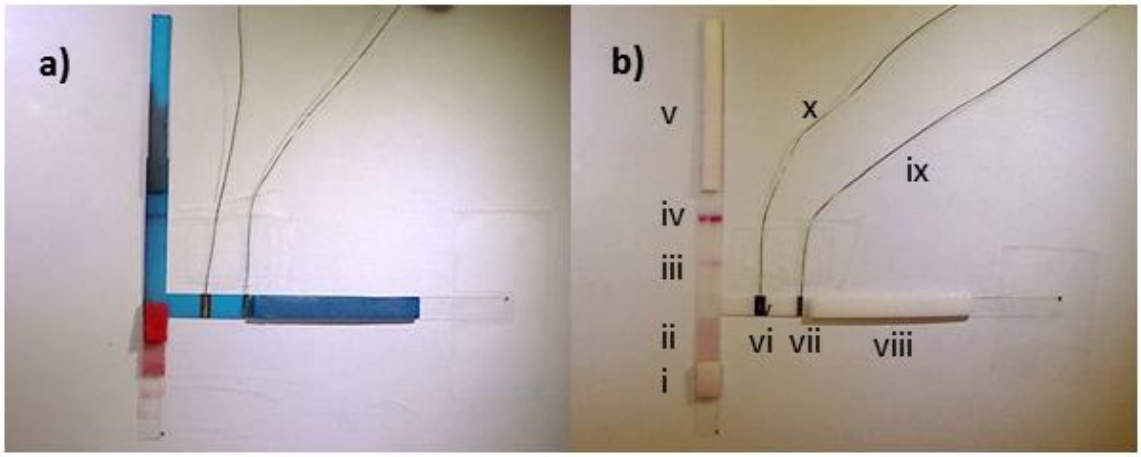

Fig. 2.5. Application of valves in the detection of *S. cerevisiae* rRNA in lateral flow assays. a) Visualization of the flow of the "sample" (red dye) and "buffer" (blue dye) b) Valves incorporated in the lateral flow assay. A positive result is shown. (i. Sample pad ii. Conjugate pad iii. Positive test line iv. Positive control line v. Absorbent pad vi. Hydrophobic electrode/valve vii. Hydrophilic electrode viii. Buffer pad ix. Wire/Negative terminal x. Wire/Positive terminal.

2.4 Conclusion

Paper-fluidics provide an inexpensive, portable, sensitive and specific method of analysis, which could be used in low resource settings. With the application of our novel valves we were able to actively control the fluid flow, which allows us to run more complex assays in the future. The valves were actuated by the application of potential from an external power source, which controlled the fluid flow of the buffers. Furthermore, we were able to apply our valves to a lateral flow assay for the detection of nucleic acids, which could be used for the detection of microorganisms. In our case we detected *Saccharomyces cerevisiae* rRNA sequences. This application can be further applied to assays that detect foodborne pathogens and for disease causing bacteria prevalent in low resource settings. Future studies will be developed to further characterize the valves, such

as applying different voltage cycles and investigating the downstream chemistry of the electrodes.

CHAPTER 3

INKJET-PRINTED PEDOT:PSS ELECTROWETTING VALVES FOR MULTIPLEXED PAPER-FLUIDIC DEVICES

3.1 Introduction

In recent years, paper-based devices have become a focus for the development for rapid and low-cost diagnostics in medical, environmental and food production settings [12, 14-15]. Using porous paper-based materials allows for lower production costs and more portability as they are thin, lightweight, and do not require external pumps for transport of fluids due to wicking through capillary action[3]. Paper-fluidic devices can also be modified to chemically incorporate functional groups for binding analytes, thus maintaining the rapid, sensitive and specific attributes of polymeric microfluidic devices[3, 15]. With new technological advancements, numerous approaches have been used to fabricate paper-fluidic devices, such as photolithography and wax printing[3], with inkjet printing being a popular method of low cost and effective patterning in recent years[3, 12, 73].

Due to the versatility and the ease of patterning using inkjet printing, metal-based nanoparticle inks have been developed to deposit conductive structures[79, 83]. Silver nanoparticle-based inks have been patterned via inkjet-printing for use in transistors, solar cells and most recently, on paper to be functionalized into electrowetting valves[33]. Despite the relatively high conductivity of silver, it may not be suitable in some applications due to oxidation in many aqueous environments. Gold nanoparticle-based inks have also been used and are chemically inert to oxidation and acids[83]. However, similar to silver-based inks, they require high sintering and annealing temperatures, which adds complexity to the

manufacturing process and is not compatible with some substrates, such as nitrocellulose. This common paper-fluidic substrate has a combustion temperature of 160°C. Furthermore, the deposition of silver and gold nanoparticle inks is difficult to control, as they tend to clog the printing nozzles due to fast evaporation of the solvent. Metal-based inks also block the pores of paper, which hinders the fluid flow in a paper-fluidic device[33]. This can be undesirable in certain applications, such as electrowetting on dielectrics (EWOD). Finally, gold and silver nanoparticle derived inks may be cost prohibitive to roll to roll manufacturing of low cost devices.

Alternative conductive inks that are non-metal-based have potential use in inkjet printing on porous materials. Poly(3,4-ethylenedioxythiophene):poly(styrenesulfonate), also known as PEDOT:PSS, is a conductive polymer and is used in light emitting diodes and solar cells due to its optical transmittance, tunable conductivity and ease of application[84-87]. Both screen and inkjet-printed PEDOT:PSS have been used to fabricate organic transistors[88-89] and pattern highly conductive electrodes[90] on flat polymeric surfaces, such as polyethylene terephthalate and polyethylene naphthalate. Recently, the interest in patterning conductive polymers on paper-based materials have grown due to its low process cost and recyclability[91]. Nitrocellulose membranes are now widely used as a platform for paper-fluidic devices due to their tunable pore size, ability to bind to biomolecules and ability for dry reagent storage for analyte detection[15]. The utilization of inkjet printing of conductive polymers and the use of paper-based materials as a platform, can enable roll-to-roll manufacturing to produce low cost, portable, rapid and sensitive paper-fluidic devices.

One of the challenges with paper-fluidics is the ability to control fluid flow and delivery within the device. In this study, we have developed three-dimensional flow through valves/electrodes on paper that could actuate on demand using electrowetting on dielectrics. The electrodes were first established by inkjet printing PEDOT:PSS onto nitrocellulose and optimizing the print parameters that would enable successful functionalization of the valves. The electrodes were further characterized by ensuring a continuous conductive layer was formed throughout the membrane, which was confirmed by measuring sheet resistance and optical microscopy. The effect of wicking of nitrocellulose after printing was also studied to ensure fluid flow rate was not hindered. After characterization, the electrodes were functionalized with 3,3,4,4,5,5,6,6,7,7,8,8,9,9,10,10,10-heptadecafluoro-1-decanethiol (R_f-thiol), where the thiol forms a covalent bond with the carbon backbone of the PEDOT:PSS. By functionalizing the PEDOT:PSS with a self-assembled thiol layer, we were able to create a hydrophobic electrowetting valve that would actuate with an applied potential. The relationship between the amount of applied potential and time to actuate the valves was characterized. Surface chemistry of the electrodes was quantified by X-ray photoelectron spectroscopy (XPS). Furthermore, a multi-valved paper-fluidic device was also fabricated to demonstrate its efficacy for multiplexed assays or monitoring over time. The successful fabrication of inkjet-printed polymer electrodes will enable high throughput production of low cost point of care diagnostics that are capable of timed fluid delivery for multiplexed analysis.

3.2 Materials and Methods

3.2.1 Materials

All chemicals and reagents were of analytical-reagent grade. Poly(3,4-ethylenedioxythiophene)-poly(styrenesulfonate) (0.8% in H2O, conductive inkjet ink) and 3,3,4,4,5,5,6,6,7,7,8,8,9,9,10,10,10-heptadecafluoro-1-decanethiol (R_f-thiol) (≥96.0%) were obtained from Sigma Aldrich (St. Louis, MO, USA). Poly(methyl methacrylate) (PMMA) in anisole (50PMMA) was obtained from MicroChem (Newton, MA, USA). Ethyl alcohol (absolute, 200 proof, 99.5+%, ACS reagent) was obtained from Arcos Organics (New Jersey, NJ, USA). Phosphate buffered saline (PBS) solution (40 mM sodium chloride, 50 mM sodium phosphate dibasic, pH 6.8) was prepared.

Nitrocellulose membranes (245 x 25 mm, AE 98, Whatman®, Pittsburg, PA, USA) with 120 µm thickness were used. Double sided medical tape (3M, St. Paul, MN) with dimensions of 38 x 279 mm and plastic backing (Highland Transparency Film, 901) was used.

3.2.2 Inkjet printing of PEDOT:PSS

An inkjet-printable PEDOT:PSS ink was patterned onto nitrocellulose membrane as electrodes using a Dimatix Materials Printer (Fujifilm DMP-2800). The conductive ink (4 mL) was degassed in a sonicating bath and filtered (0.45µm syringe filter) into a 10 pL inkjet cartridge (Fujifilm Dimatix, Santa Clara, CA). The electrodes were printed using a drop spacing of 15 µm and a line width of 0.3 to 1.0 mm. The cartridge temperature was set at 25±3°C and a plate temperature of 38°C was used for drying of the ink. The firing voltage was set at 20 V for all sixteen nozzles and all working nozzles were used to print

the electrodes. Tickle frequency of 5.0 Hz was enabled to prevent clogging of the nozzles when the printer is idle. Multiple layers were printed to determine the effects of conductivity, surface morphology and chemistry of the electrodes. The number of layers printed ranged from one to fifteen layers on the front of the nitrocellulose along with one to ten layers on the back side of the nitrocellulose, depending on the application of the electrode.

3.2.3 Characterization of PEDOT:PSS electrodes

3.2.3.1 Sheet resistance measurements

Sheet resistance measurements were conducted with a Signatone probe station (H150-W) (Fig. A.3). A two point probe test was performed to ensure ohmic contact with all four probes by conducting a voltage sweep of -1V to 1 V. The linear portion of the IV curve was determined which was used as the guideline for the current sweep of the four point probe measurements. The voltage difference was measured and the sheet resistance (R_s) was calculated using the following formula: $R_s = 4.53(V_{diff}/I)$, where V_{diff} is the voltage difference measured and I is the current used.

3.2.3.2 Electrode thickness measurements and conductivity measurements

The thickness of the inkjet-printed PEDOT:PSS electrodes were measured using an optical profilometer (Zeta Instruments, San Jose, CA) with the use of an image capturing software to measure the penetration depth of the PEDOT:PSS. The membranes were first freeze fractured with liquid nitrogen and the samples were mounted onto glass slides using double sided tape with the cross sections facing up. The edges and the center of the electrodes were measured and averaged (n=3) to calculate the electrode thickness.

Conductivity (σ) of the electrodes was estimated with the following formula: $\sigma = 1/R_s h$, where R_s is the sheet resistance and h is the thickness. For homogeneous materials, σ is a fundamental property. But because the PEDOT:PSS ink penetrated into the nitrocellulose membrane, conductivity was an apparent property which depended on the variations in the structure of the conductive layer[92].

3.2.3.3 Contact angle measurements

Contact angle measurements were measured on a Krüss DSA100 (Hamburg, Germany) goniometer equipped with a direct dosing system (DO3210, Krüss, Hamburg, Germany) at room temperature under atmospheric conditions to determine the wettability of PEDOT:PSS functionalized with a thin film of fluorinated thiol. The Tangent Method 2 from the Drop Shape Analysis software (Version 1.91.0.2) was used to calculate advancing contact angle with a single drop volume of 2 µL HPLC water and a droplet rate of 25 µL/min. For each drop, an image was recorded every 0.10 s and an average of the recorded images was calculated to obtain a mean contact angle (n=4).

3.2.3.4 X-ray photoelectron spectroscopy

X-ray photoelectron spectroscopy (XPS) was carried out on a Physical Electronics Quantum 2000 spectrometer (Physical Electronics Inc., Eden Prairie, MN) using Al Kα monochromatic X-ray source at spot size of 200 µm at 37.5 W. All data were collected at a 45° takeoff angle relative to the plane of the sample surface. Survey scans of every sample were recorded at pass energies of 187.85 eV with a step size of 1.6 eV. High resolution spectra were obtained at 46.95 eV with a step size of 0.2 eV. The determination of elemental compositions and deconvolution of the high resolution spectra were

performed using Multipak V9.3 software (Physical Electronics Inc., Eden Prairie, MN). The high resolution spectra were fitted with the Gaussian-Lorentzian model (90% Gaussian).

3.2.3.5 Optical microscopy

Optical micrographs (Zeta Instruments, San Jose, CA) were captured at 20x magnification.

3.2.4 Application of inkjet-printed PEDOT:PSS

3.2.4.1 Fabrication of test strips

The electrodes were designed using AutoCAD (Autodesk Inc., San Rafael, CA) and were converted (ACE 3000, Version 6, Numerical Innovations) into a pattern file for compatibility with the Dimatix Materials Printer (Fig. A.1). Fifteen layers of PEDOT:PSS were printed on the front side of the nitrocellulose and ten layers were printed on the back side of the nitrocellulose, using the fiducial camera to ensure the electrodes were superimposed on each other. The pre-printed nitrocellulose was then backed onto a plastic sheet using double sided tape and a PMMA barrier was printed on the membrane to form a channel for fluid transport. The PMMA ink was jetted with the following settings: drop spacing of 15 µm, cartridge temperature of 25±3°C, plate temperature of 38°C, a firing voltage at 36 V and 6 layers of ink was deposited onto the membrane. The test strips were then heated at 95°C for 2 minutes to evaporate any excess solvents and were placed in a desiccator at 20°C until further use.

3.2.4.2 Functionalization of PEDOT:PSS with a fluorinated thiol layer

Inkjet-printed PEDOT:PSS electrodes were treated with R_f-thiol by carefully depositing with a micro tipped glass pipette on PEDOT:PSS patterned areas. This resulted in the formation of a fluorinated thiol layer depicted in Figure 3.1. The functionalized electrodes were then stored in a desiccated container.

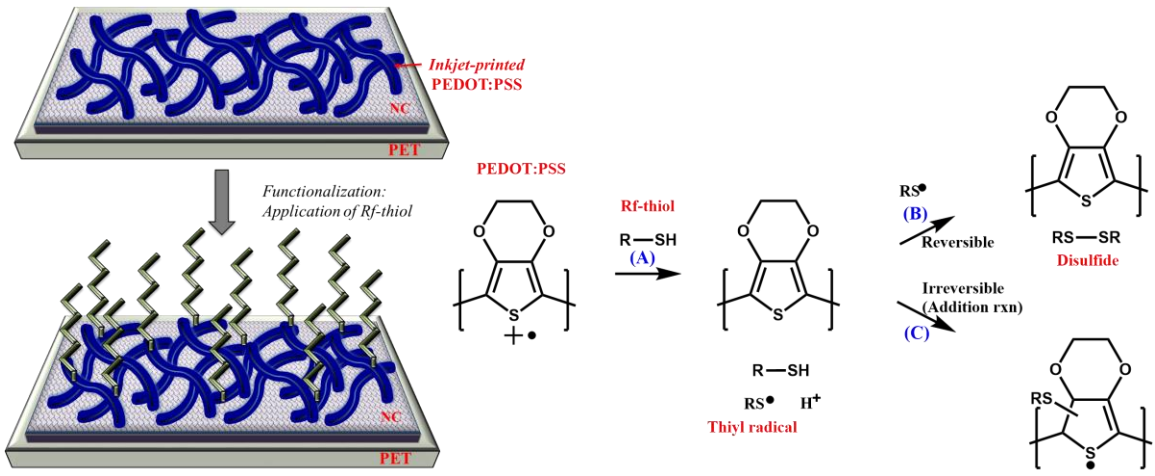

Fig. 3.1. Schematic diagram of functionalization of PEDOT:PSS with R_f-thiol and their reaction mechanisms. In step (A), PEDOT is reduced, forming a thiyl radical. This partitions into pathway (B) forming a disulfide, which is reversible by reoxidation and/or pathway (C), an addition process that is irreversible.

3.2.4.3 Actuation of electrodes using electrowetting on dielectrics

PEDOT:PSS electrodes were functionalized with a fluorinated thiol layer by depositing 0.5 µL of 75% R_f-thiol in absolute ethanol. The functionalized electrodes were then applied in a paperfluidic device as a hydrophobic valve. A device holder fabricated from 2 pieces of PMMA with spring loaded pogo pins as electrode contacts were connected to the paperfluidic device via the PEDOT:PSS electrodes. 200 µL of PBS was deposited

on a sample pad and allowed to flow up the paper-fluidic device. A power supply (Extech DC power supply 382260, Nashua, NH) was used to actuate the valves with an applied potential, which disrupts the thin film of fluorinated thiol.

3.2.4.4 Fabrication of paper-fluidic device

The paper-fluidic devices were fabricated and assembled using the same method as the test strips. Figure A.2.a in Appendix A shows the patterns of the printed PEDOT:PSS electrodes on the front side and the back side of the nitrocellulose. The device layout of the electrodes and PMMA barriers are shown in Figure A.2.b.

3.3 Results and Discussion

3.3.1 Inkjet printing and electrical characterization of PEDOT:PSS

Conductive electrodes were fabricated by inkjet printing PEDOT:PSS onto nitrocellulose. Due to the porous structure of nitrocellulose, PEDOT:PSS was printed on the front and back sides of the membrane with varying electrode layers and widths. It is important that a continuous coating of ink is formed through the thickness of the membrane (Fig. A.4) in order to achieve ohmic contact (conductivity) and yet not affecting the wicking ability of the nitrocellulose.

3.3.2 Front printing

Multilayers of PEDOT:PSS were initially printed on the front side of the nitrocellulose membrane and then characterized their electrical properties as a function of the number of layers. The degree of sheet resistance and conductivity measured using a four-point probe system is shown in Table 3.1. Increasing the number of printed layers

resulted in decreased sheet resistance. This results in the increase in concentration of the conductive polymer in the patterned area, which allows for more connectivity of the PEDOT:PSS interlayer. The sheet resistance was significantly different ($p<0.05$) when compared to all printed layers (Table 3.1). Printing more than 15 layers resulted in sheet resistances that were not significantly different (data not shown). This suggests that the intrinsic conductivity of the printed material was achieved. Sheet resistance assumes that the material measured is a thin film, thus it does not account for the thickness in the calculation. Because the PEDOT:PSS ink penetrated into the nitrocellulose membrane, it was important to study how thickness affects bulk resistivity/conductivity of the electrodes. Resistivity is defined as follows: $\rho = R_s h$, where ρ is the bulk resistivity, R_s is the sheet resistance and h is the thickness of the electrode[92]. Conductivity, the inverse of resistivity, was calculated with the following equation: $\sigma = 1/\rho = 1/R_s h$, where σ is the conductivity of the electrodes, R_s is the sheet resistance and h is the thickness of the electrode[92]. Table 3.1 shows that as multiple layers are printed, the conductivity of the electrodes increased. It is observed that the thickness of the electrodes from multilayered printing did not affect the conductivity in this scenario, as the sheet resistances were significantly different. Figure 3.2 depicts the inverse relationship between calculated bulk resistivity from sheet resistance and conductivity.

Table 3.1. The effect between the number of PEDOT:PSS layers printed on the front of nitrocellulose and the sheet resistance, thickness and conductivity of the ink.

Number of Layers	Sheet Resistance (Ω/□)	Thickness (μm)	Conductivity (S/m)
1	481,000 ± 48,300	50.14 ± 14.92^{x}	0.04 ± 0.00^{m}
3	24,600 ± 2,250	50.50 ± 7.48^{x}	$0.81 \pm 0.08^{m,n}$
5	3,360 ± 160	$53.03 \pm 6.71^{x,y}$	5.62 ± 0.26^{n}
7	1,490 ± 271	$54.49 \pm 7.18^{x,y}$	12.59 ± 2.08
9	647 ± 40	$62.31 \pm 7.19^{y,z}$	24.86 ± 1.49
11	425 ± 38	$63.31 \pm 3.49^{y,z}$	37.37 ± 3.29
13	305 ± 19	65.07 ± 4.86^{z}	50.52 ± 3.35
15	238 ± 10	65.81 ± 5.39^{z}	63.86 ± 2.91

Data within column sharing the same alphabetical superscript (x-z) and (m-n) are not statistically different (p>0.05). Data with no alphabetical superscript are statistically different (p<0.05).

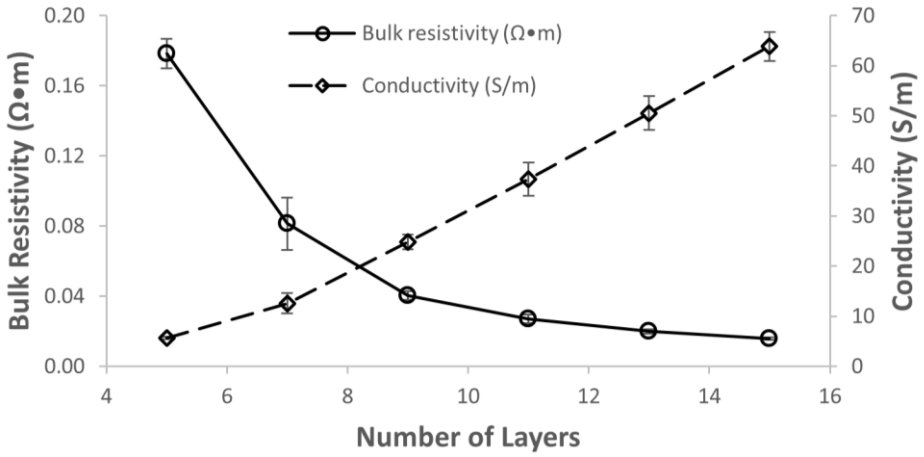

Fig. 3.2. Bulk resistivity (Ω•m) and conductivity (S/m) versus number of printed layers on the front side of nitrocellulose.

3.3.3 Back printing

Multilayered printing (> 15 layers) on the front resulted in the accumulation and drying of the PEDOT:PSS with 65.81 ± 5.39 µm in the membrane, which had a thickness of 120 µm (Fig. A.4). With each drop of jetted ink being 10 picoliters in volume, there was not sufficient for penetration through the 120 µm thick membrane. Printing more than 15 layers on one side not only did not increase penetration, but it also resulted in decreased wicking ability of the membrane. Thus, PEDOT:PSS was printed on the back side of the nitrocellulose, superimposing on the electrodes on the front. Printing the first four layers on the back did not significantly affect the overall sheet resistance and conductivity of the membrane (Table 3.2), as the printed ink layers on the front and back were still not in contact (Fig. A.4). Printing from six layers onwards reduces the sheet resistance as the gap between the front and back electrodes decreases (Fig. A.4), resulting in increased ohmic contact. The sheet resistance was reduced due to more ink penetration through the paper, increasing the thickness of the electrodes. However, the conductivity was decreased, due to the increased thickness of the electrodes. As discussed above, conductivity is a property that has an inverse relationship with thickness. When printing the 10^{th} layer, it was observed that the ink was able to penetrate through and form contact with the front layers (Fig. A.4), increasing the conductivity. However, slight compression of the membrane (decrease in thickness) was observed, due to a compromise of the nitrocellulose structure after multilayered printing. Overall, printing 10 layers on the back allowed for more connectivity and at the same time not hindering the wicking ability of on the membrane. Printing more than 12 layers resulted in obstructed fluid flow (data not shown).

Table 3.2. The effect between the number of PEDOT:PSS layers printed on the back (and 15 layers printed on the front) of nitrocellulose and the sheet resistance, thickness and conductivity of the ink.

Number of Layers	Sheet Resistance (Ω/□)	Thickness (µm)	Conductivity (S/m)
0	238.34 ± 10.40^{a}	65.81 ± 5.39^{x}	63.86 ± 2.91^{m}
2	247.61 ± 10.76^{a}	65.81 ± 5.39^{x}	61.46 ± 2.67^{m}
4	234.90 ± 4.66^{a}	65.81 ± 5.39^{x}	64.71 ± 1.28^{m}
6	199.14 ± 13.49^{b}	113.13 ± 1.96^{y}	44.54 ± 3.11^{n}
8	195.50 ± 11.87^{b}	108.99 ± 2.77^{y}	47.06 ± 2.86^{n}
10	158.46 ± 3.67^{c}	102.85 ± 7.05^{z}	61.39 ± 1.43^{m}

Data within column sharing the same alphabetical superscript (a-c), (x-z) and (m-n) are not statistically different ($p>0.05$). Data with no alphabetical superscript are statistically different ($p<0.05$).

3.3.4 Effect of multilayered printing on the wicking/fluid flow of nitrocellulose

The effect of electrode width size with multilayered printing on the connectivity (ohmic contact) and wicking ability of nitrocellulose was also determined. It is important that defined electrodes are printed, and at the same time not hindering fluid flow on the membrane. Table 3.3 shows that this was achieved with print settings of 0.30 mm electrode width, 15 layers on the front, and 10 layers on the back. The actual printed electrode width measured 0.43 ± 0.0034 mm, which was ~30% increase due to the wetting properties and lateral diffusion of the ink in the membrane. Printing electrode widths more than 0.30 mm (*i.e.*, 0.75 and 1.00 mm) on the membrane resulted in disrupting the pores of the substrate, which is observed by the degree of wrinkling (Fig. 3.3) and hindrance of fluid flow (Table 3.3) in the paper. The optimal print settings, bolded in Table 3.3, were used in the rest of the study.

Table 3.3. Effect of number of printed layers (back and front) and ohmic contact on nitrocellulose on the fluid flow.

Width (mm)	Number Of Layers (Front)	Number Of Layers (Back)	Ohmic Contact? (Y/N)	Flow of Nitrocellulose? (Y/N)
0.30	10	10	N	Y
0.30	**15**	**10**	**Y**	**Y**
0.30	15	15	Y	N
0.30	20	20	Y	N
0.60	15	10	Y	N
0.75	10	10	Y	N
0.75	15	15	Y	N
0.75	20	20	Y	N
1.00	15	3	N	Y
1.00	15	5	Y	N
1.00	15	8	Y	N
1.00	15	10	Y	N

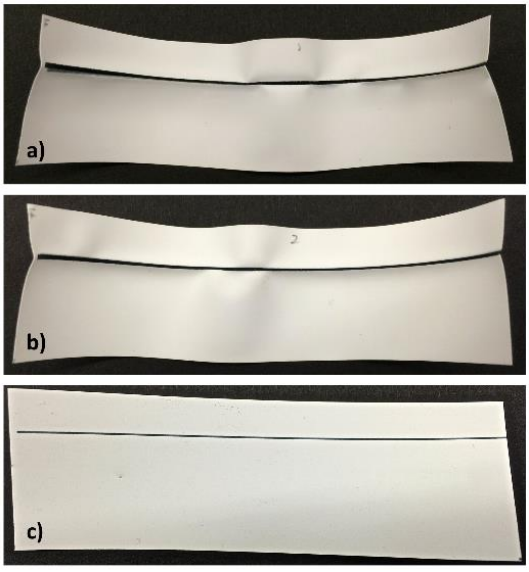

Fig. 3.3. Multilayered printing with varying PEDOT:PSS electrode widths on nitrocellulose. a) 1.00 mm; b) 0.75 mm; and c) 0.30 mm.

3.3.5 Functionalization of inkjet-printed PEDOT:PSS as a method of fluid control

3.3.5.1 Design of test strips

After optimizing the print setting of PEDOT:PSS electrodes, we fabricated 3D flow-through valves to control the fluid flow on a paper-fluidic device. With paper-fluidics becoming more sophisticated with multiplexed designs, there remains a need for fluid flow control. Our 3D flow-through valves/electrodes on paper is based on the phenomenon of electrowetting on dielectrics (EWOD), where there are four main components – an ionized solution that serves as a medium, a conductive material that act as electrodes, the dielectric which provides capacitance between the electrodes and the medium, and the hydrophobicity at the solid-liquid interface[80]. Two PEDOT:PSS electrodes were printed on nitrocellulose (hereafter termed as test strips), one as a counter/hydrophilic electrode and the other as the working/hydrophobic electrode to act as a valve for fluid control (Fig. 3.4). The counter electrode was printed preceding the hydrophobic electrode to act as a conductive substrate for the actuation of the valve. The working electrode was rendered hydrophobic by careful application of thiolated fluorocarbon along the printed area. Solubilized PMMA was printed as physical barriers to direct fluid flow towards the absorbent pad (Fig. 3.4).

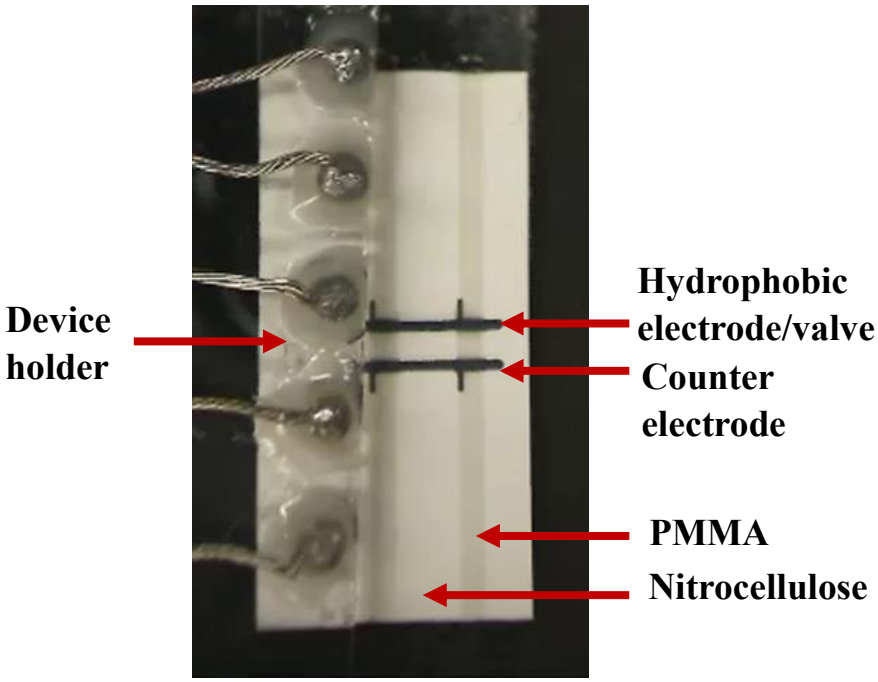

Fig. 3.4. Inkjet-printed PEDOT:PSS test strip with device holder attached.

The 3D flow-through valves were tested by dispensing the ionized solution PBS onto the buffer pad (Fig. 3.4). The ionized solution was wicked up by capillary action towards the electrodes and flowed past the counter/hydrophilic electrode (the conductive material). The fluid front then stopped at the hydrophobic valve (the dielectric) due to the fluorocarbon thin film. Potential was applied to the electrodes to actuate the valve and disrupt the fluorinated layer[78]. To actuate the valve, the positive terminal was connected to the hydrophobic electrode/valve and the negative terminal was connected to the counter electrode. For the valve to function, the negative terminal must be in contact with the liquid medium, where the applied potential (the threshold voltage) creates charges on the liquid and electrode interface and change the wettability of the hydrophobic electrode (dielectric)[81]. At this point, the wettability of the hydrophobic valve is still reversible and can be detected by a change in the contact angle. The applied potential was allowed to run

until the contact angle is irreversible, which enables a permanent change in the wettability of the hydrophobic valve (dielectric)[81] and opens the valve indefinitely. This type of applied potential is termed as the breakdown voltage[81] or the phenomenon is called the dielectric breakdown in dielectrics[80].

In the previous section, the optimal print setting was established to allow for high conductivity of the electrodes, as this is one of the limiting factors of electrowetting. Furthermore, the bare electrodes without the application of the thiolated fluorocarbon should not physically hinder the wicking of the membrane, so that once applied with a fluorocarbon layer, the electrode is truly rendered hydrophobic. Thus, the stop of fluid flow at the valve is solely due to the hydrophobic interactions between the substrate and the liquid interface.

3.3.5.2 Understanding the relationship between valve actuation and applied potential

One of the other limiting factors for the rate of valve actuation is the applied potential and the distance between the counter and hydrophobic electrode. To have a better understanding of how the 3D flow-through valves operate, they were actuated at different voltages to determine the effect on the valve actuation time (Fig. 3.5 and 3.6). The different voltages tested were 0, 4, 9, 12 and 16 V with an alternating current cycle. The distance between the hydrophobic electrode/valve and counter electrode was 3 mm. It was observed that as voltage increased, the actuation time of the valves decreased (Fig. 3.5). This is because as more potential was applied to the valve, the faster the fluorocarbon layer was disrupted, which decreased the time for the fluid front to flow past the valve. In our

previous study, we found that there was no significant difference in the time required to open the valves when compared to the distance between the counter and hydrophobic electrode/valve[33]. The electrodes were printed as close proximity to each other to minimize device size and yet still feasible to accurately double side print the electrodes and to apply the fluorocarbon layer. With the ability to actuate the valves on demand and at low voltages where a battery-sized powered source (e.g. commercially available 9V battery) could be used, it allows this technique for fluid flow control to be potentially used in low resource settings.

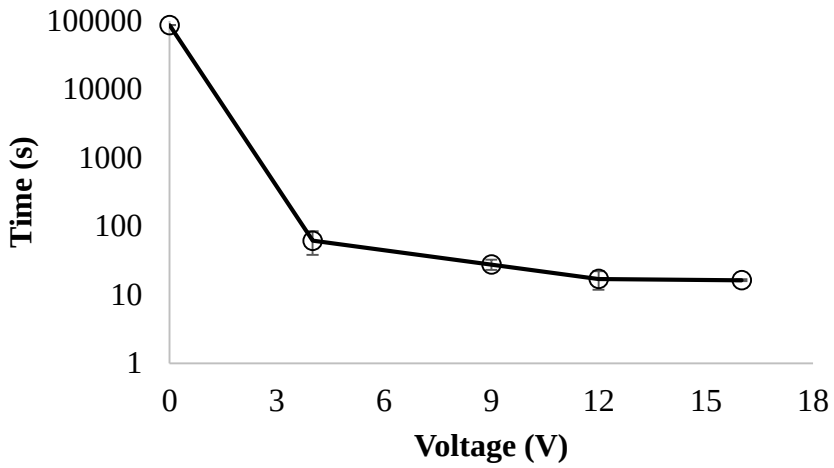

Fig. 3.5. Amount of actuation time (seconds) vs. amount of voltage applied to electrodes.

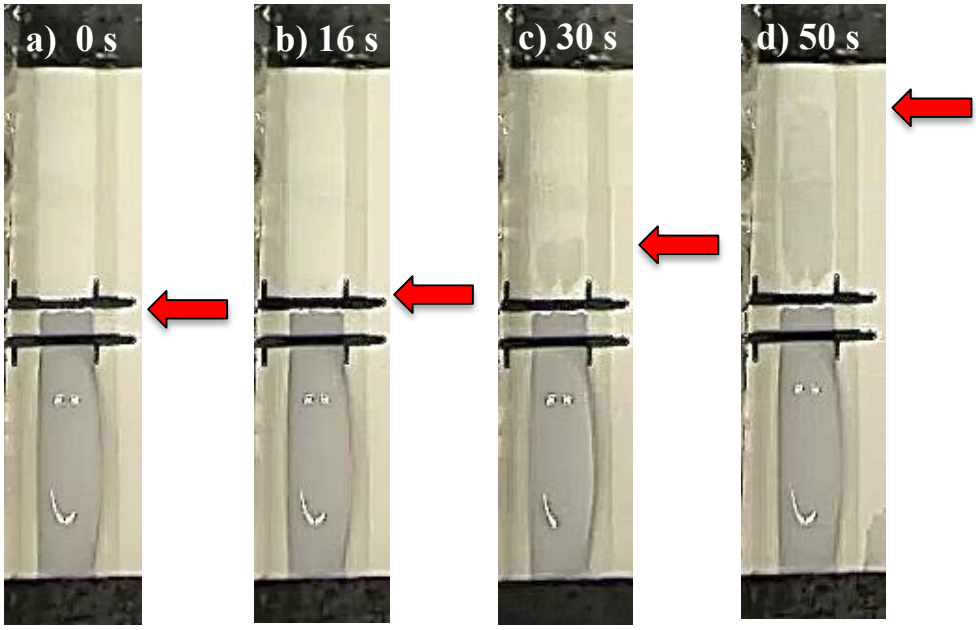

Fig. 3.6. Photographs of test strip valves. a) Fluid front flowed past the counter electrode and stopped at the hydrophobic valve. A potential of 16 V has been applied to the electrodes. b) Thiolated fluorocarbon layer disrupted by the applied potential, therefore fluid front flowed past the valve. c) Flow of fluid front after passing the valve for 30 seconds. d) Flow of fluid front after passing the valve for 50 seconds.

3.3.5.3 Characterization of the thiolated PEDOT:PSS electrodes/valves on nitrocellulose

The surface chemistry of the thiolated PEDOT:PSS electrodes on nitrocellulose was quantified by X-ray photoelectron spectroscopy (XPS) to ensure that covalent bonding of the thiol occurred. Both survey scans (Table 3.4, Fig. A.5) and high resolution scans (Fig. 3.7) for C 1s, N 1s, O 1s, F 1s and S 2p were performed to quantify the change in surface atomic composition and specific bond formation when R_f-thiol is applied. When compared to nitrocellulose, inkjet-printed PEDOT:PSS contains sulfur of 3.9%, which is part of the structure of the polymer (Fig. 3.1). Furthermore, when R_f-thiol was added to PEDOT:PSS, 11.4% of fluorine was detected, which coincides with the long chain fluorocarbons attached to the thiolated ends.

Table 3.4. Atomic concentrations (%) PEDOT:PSS electrodes with R_f-thiol obtained from XPS.

Treatment	C	O	N	S	F
Nitrocellulose	45.1	43.8	10.7	0.3	0.2
PEDOT:PSS	53.2	37.6	4.7	3.9	0.6
PEDOT:PSS/R_f-thiol	48.2	33.0	3.5	3.8	11.4

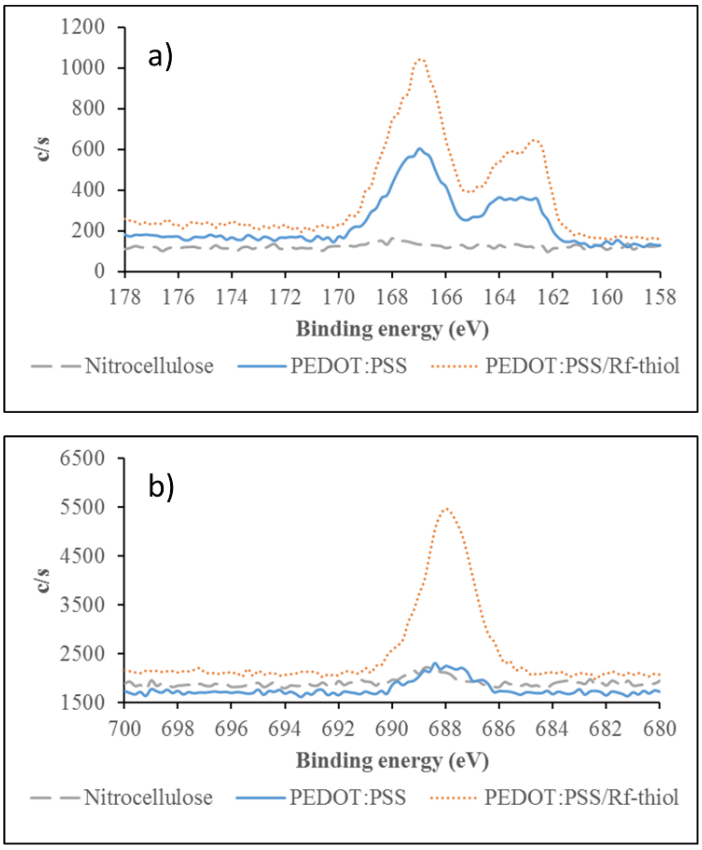

Fig. 3.7. High-resolution XPS data for nitrocellulose, PEDOT:PSS and PEDOT:PSS with R_f-thiol for a) sulfur (S2p) and b) fluorine (F1s).

To further confirm that R_f-thiol was covalently bound onto the inkjet-printed PEDOT:PSS, high resolution XPS scans for sulfur (S_{2p}) and fluorine (F_{1s}) were performed

(Fig. 3.7). The analysis of sulfur showed that the intensity of the peaks at binding energies were 162.6 eV and 163.6 eV (Fig. 3.7.a). This suggests that there was sulfide linkage with the carbon backbone of PEDOT:PSS as $S_{2p3/2}$ and $S_{2p1/2}$ peaks for bound thiols are known to be 162 eV and 163.2 eV respectively[93-94]. Conversely, the sulfur peak for unbound thiols appear at 164.4 eV (Fig. 3.7.a), where $S_{2p3/2}$ and $S_{2p1/2}$ are known to be around 164 eV and 165 eV, respectively[93]. Incomplete adsorbate binding of thiol to PEDOT:PSS can be seen at the peak (167.0 eV), which is greater than the binding energy of 166.0[93]. Furthermore, the analysis showed that there were distinct intensity changes in the electrodes for fluorine after the deposition of R_f-thiol, as there is an increase in fluorinated carbons, with a peak observed at 688.0 eV (Fig. 3.7.b). With both high resolution scans of fluorine and sulfur, the data suggests that R_f-thiol has covalently bound to PEDOT:PSS.

The covalent bonding of R_f-thiol onto PEDOT:PSS can be indirectly observed by measuring the electroactivity of the polymer over time. According to a study by Molino et al.[95], a solution of fluoroalkanethiols can react with the thin films of PEDOT to alter their surface energies. Thiols are known to reduce conducting polymers, like PEDOT, into their neutral non-conducting forms and produce disulfides. The reaction mechanism, as shown in Figure 3.1, where PEDOT:PSS is reduced by thiol, resulted in the formation of a thiyl radical (Pathway A). The thiyl radical can form a disulfide (Pathway B), which is reversible, or follow through with an addition reaction (Pathway C), which is irreversible. The heterocyclic radical can react with additional thiols, forming more thiyl radicals. The addition reaction breaks down the backbone of the polymer, which decreases its electroactivity[96]. Pathway B and C are competitive in PEDOT:PSS, which means that the

addition of thiols will have less of an effect on electroactivity of the polymer. This can be seen in Table 3.5, where an increase in sheet resistance is observed over time, which also suggests that the thiols are covalently bonded to the carbon backbone of the polymer. The problem of losing electroactivity could be overcome if the reaction was only at the surface of the films, by printing multiple layers and using a substrate with high surface area like paper or membrane[95]. The sheet resistance of the thiolated electrodes on nitrocellulose was measured to monitor the electroactivity (Table 3.5). Even though there was increase in sheet resistance after 180 min, the electroactivity is still sufficient for its performance as a valve.

Table 3.5. Sheet resistance of inkjet-printed PEDOT:PSS with fluorocarbon thiol layer.

R_f-thiol (µL)	**Incubation time (min)**	**Sheet Resistance (Ω/□)**
0	0	158.5 ± 3.666
0.5	30	194.5 ± 2.774
0.5	180	513.9 ± 34.39

3.3.5.4 Application of EWOD in a multiplexed paper-fluidic device

For the application of paper-fluidic devices in low resource settings, it is ideal that the device be low-cost, portable, easy to dispose of, easy to use and capable of performing multiplexed assays. In this part of the study, we fabricated a paper-fluidic device that had valves/electrodes functionalized with thiolated fluorocarbons printed in front of lateral channels leading to "detection zones" (Fig. 3.8 and A.2). To prove that the concept of multiplexing was possible, PBS solution was used as the sample liquid and were flowed toward the circular areas ("detection zones"). In a real sample situation, the circular areas

would have reagents deposited and dried, which would react with the sample, indicating either a signal that we could either measure quantitatively or determine qualitatively. The outline of the device was bordered by inkjet-printed PMMA and had a main channel where sample fluid is continuously wicked up towards the absorbent pad. The fluid flow in the channel is dependent on the porosity of the membrane and on the volume uptake of the absorbent pad. The main channel was connected with three side/lateral channels where the valve was placed at the inlet leading to the "detection zones". The electrodes were printed precisely at the opening of the lateral channels to ensure no residual fluid was caught in the area between the PMMA and the hydrophobic valve, which can affect the sampling of the fluid in a timed assay. The valves were able to effectively block the fluid flow into the lateral channels until the fluid needed to be sampled in the detection zone. This could be beneficial in a situation where an assay requires sequential sampling over time. Thus, valves that could actuate on demand is desired. Here, potential (16 V) was applied to actuate the valves until fluid flowed past and reached the detection zone. A timed relay was attached to the device, where a self-written program was used to control the timing of the applied potential. This allows users to automate and customize the timing of the actuation. With this multi-valve device, we were able to achieve sequential actuation of three valves, which could be useful in a multiplex assay designed to be performed in a low resource setting.

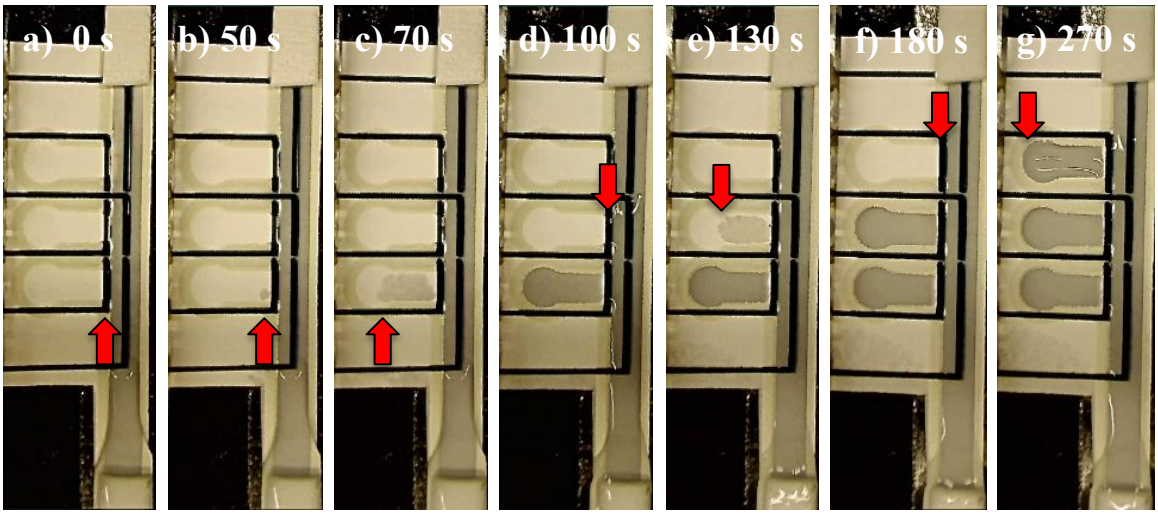

Fig. 3.8. Images of paper-fluidic multi-valve device. a) Fluid front flowed along the main channel towards the absorbent pad. Fluid flow has been effectively blocked from the three lateral channels. b) Hydrophobic layer of first valve disrupted by the applied potential (16V) and fluid front flowed past the first valve. c) Flow of fluid front after passing the valve for 20 seconds (70 seconds). d) After 50 seconds of actuation, the fluid has reached the detection zone in the first lateral channel. A potential of 16 V applied to the second valve which disrupted the fluorocarbon layer. e) Flow of fluid front after passing the second valve for 30 seconds (130 seconds). f) A potential of 16 V applied to the third valve which disrupted the fluorocarbon layer. g) After 90 seconds of actuation, the fluid has reached the detection zone in the third lateral channel.

3.4 Conclusion

The increasing need for more portable, inexpensive, easy to use and rapid diagnostics has led to fabrication of paper-fluidic devices using inkjet printing for low cost fabrication and effective patterning. This project involved optimizing inkjet printing of PEDOT:PSS on nitrocellulose for functionalization of thiolated electrodes and their application in controlling fluid flow for use as multiplexed device. Multilayered printing of PEDOT:PSS on the front and back of the membrane with a fine width created a high definition three-dimensional electrode. The printed PEDOT:PSS was rendered hydrophobic by a fluorinated thiol layer, which enabled control of fluid flow on

nitrocellulose by electrowetting on dielectrics and allowed timed fluid delivery to a specified area on demand. The hydrophobic 3D flow through valves/electrodes were actuated by an applied potential, with some voltages that were low enough to be sourced from a 9 volt battery. The overall study demonstrated the feasibility of inkjet printing PEDOT:PSS electrodes on paper, which was functionalized to control fluid flow. We have also fabricated a multi-valved device, where a working prototype was shown to effectively direct fluid into a specific area over time. Further studies are desirable to test the potential use of the device for a multiplexed assay with real world samples for rapid diagnostic purposes.

CHAPTER 4

DEVELOPMENT AND FABRICATION OF PAPER-BASED DEVICES WITH INKJET-PRINTED POLY(METHYL METHACRYLATE) PHYSICAL BARRIERS AND PASSIVE DELAY VALVES

4.1 Introduction

Paper-based devices have become the focus in recent years in the development for rapid and low-cost methods for diagnostics in medical, environmental and food production settings[12, 14-15]. These characteristics are essential in developing countries where the resources to perform complex analytical chemistry can be limited[3]. Paper-based devices were first introduced by Müller *et al*., but was later further innovated and developed by the Whiteside's group at Harvard University where they fabricated and applied new techniques in building a basic paper-fluidic device[73]. Paper-fluidic devices are able to retain the sensitivity and specificity of microfluidic devices but subsequently are easier to use and often do not require additional instrumentation. Lateral flow test strips, the predecessor of paper-fluidic devices, have been developed for many applications which range from nucleic acid and antibody detection for diseases in developing countries to commercially available home pregnancy tests[97]. With the growing interest in replacing microfluidic devices with paper-fluidic devices, multistep assays and tests are performed on these devices. These assays require more than one type of reagent being passed through, therefore, there is a need for physical barriers and channels for the development of more complex paper-based devices.

One of the earliest methods in developing two-dimensional paper networks is a method called fast lithographic activation of sheets (FLASH)[25]. Microchannels in the paper-based device were created by using a modified photolithographic method without the need of a cleanroom and with the use of an inkjet printer, UV lamp and hot plate. This results in hydrophobic photoresist barriers that can be as small as 200µm. However, this method can be inconvenient as they still require the use of a mask and UV curing, which complicates the fabrication process. Another method in creating channels in paper involves cutting the paper into strips with multiple inlets with different dimensions[28]. This method relies on the capillary flow and wet-out of the paper, which changes as the dimensions of the paper changes. The disadvantage with this method is the limited ability to create more complex designs without the use of a laser cutter. Another type of approach is the use of electrowetting valves to actively control the flow by actuating the valve with an applied potential[33]. However, this would require the use of an external power source for the actuation and a relay for the timing. A significant breakthrough in the fabrication of paper-fluidic devices was seen when wax printing was used to create hydrophobic barriers to make channels. This method involves using a relatively inexpensive and commercially available wax printer, to create barriers[23, 27, 31]. The method is simple, cost efficient and rapid, but the main disadvantage is the precision, feature size and temperature stability. Poly(dimethylsiloxane) (PDMS) dissolved in hexanes were patterned into channels onto filtered paper using a modified desktop plotter[26]. This method allows the ability to easily create channels that can be folded, without destroying the integrity of the barrier. However, the accuracy and precision of the modified plotter, which uses a series of eight altered felt

tip pens, is much lower than a materials inkjet printer, where it is designed to print different types of customizable inks in a precise and accurate manner.

Our method to create channels and barriers in paper-based devices takes advantage of using polymer based inks and inkjet printing[98]. The polymer in our ink, poly(methyl methacrylate) (PMMA), which is commonly used as conventional photoresists[26], is dissolved in anisole, a relatively non-toxic organic solvent that is a precursor to perfumes and pharmaceuticals[99]. PMMA is also commonly used to fabricate intraocular lenses due its biocompatibility[100].The PMMA ink was inkjet-printed onto plastic backed nitrocellulose using a Dimatix Materials Printer with our desired pattern to create our paper-based microfluidic device. To create channels in our device, PMMA was printed until it penetrated through the nitrocellulose membrane and physical barriers were formed. Furthermore, passive delay valves were also inkjet-printed using the PMMA ink to create barriers within the channels. The valves were fabricated by altering the drop spacing of the ink, creating effective delay barriers, which decreases the rate of capillary action of the throughput solution. A study was done to determine the timing of the valves and how it affects the capillary flow rate. The PMMA patterned channels and valves were later used to create a paper-based device where an amplified nucleic acid assay was applied for the detection of nucleic acid targets. By inkjet printing PMMA in anisole, we were able to achieve a rapid, cost efficient and precise method to create channels and valves on paper that would be compatible with many solutions and were fabricated without the need of heavy instrumentation. This concept would bring us closer to reaching our goal in the

fabrication of rapid and low cost devices for the use in developing countries, where cost and portability are important issues.

4.2 Materials and Methods

4.2.1 Optimizing properties of PMMA ink

The polymer ink, PMMA dissolved in anisole, was obtained from MicroChem (Newton, MA) with a concentration of 11% in anisole. The properties of the ink are as follows: solids content was 11.03%, a viscosity of 6.29 cst at 25°C, 0.4% solvent impurities by GC and a filtration level of 0.2µm. The polymer ink was further characterized by measuring apparent shear viscosity in different concentrations at 35°C using a dynamic shear rheometer (Kinexus Rheometer, Malvern Instruments Ltd., MA, USA), so that it was optimized for inkjet printing (Fig. 4.1). A cone and plate measurement cell measured the apparent shear viscosity with the instrument software (Kinexus rSapce, version 1.30, Malvern Instruments Ltd., MA) using 10 s^{-1} as the shear rate, which mimics the jetting of the ink from the cartridges during printing.

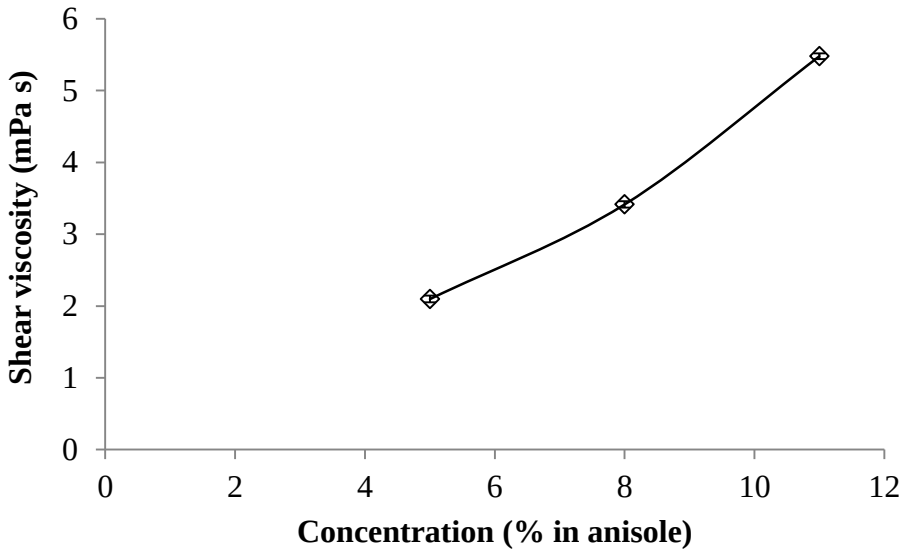

Fig. 4.1. The apparent shear viscosity (mPa s) of PMMA ink was measured at 5%, 8% and 11% in anisole at 35°C with a shear rate of 10 s^{-1}. Values shown represent the average of n=4 with the error bars representing the standard deviation.

PMMA ink was dispensed and dried onto pre-cleaned polyethylene terephthalate (PET) film and the contact angle was measured by using a Krüss DSA100 (Hamburg, Germany) goniometer equipped with a direct dosing system (DO3210, Krüss, Hamburg, Germany) at room temperature under atmospheric conditions. PET was first cleaned with sonication in a 15% isopropanol bath and was then rinsed in deionised water. The PMMA ink (50 µL) was then spincoated onto the PET film with a spin setting of 500 rpm for 10 seconds, followed by 2500 rpm for 30 seconds. The advancing contact angle was measured with the Drop Shape Analysis software (version 1.92.0.2) using the circle fitting method. A water droplet with a volume of 5 µL (HPLC Grade, Fisher Scientific, Fair Lawn, NJ) was dispensed onto the PET film at a rate of 25 µL/min. The advancing contact angle was measured every 0.10 s and recorded with the mean contact angle as a single measurement.

4.2.2 Inkjet printing of the polymer ink

To inkjet print our polymer ink, we used a Dimatix Materials Printer (Fujifilm DMP-2800) and a 10 pL cartridge. The ink was jetted with 16 nozzles at 36V using a customized waveform for the ink at 35°C. The increased temperature of the cartridge allowed the ink to jet accurately out of the nozzles with minimal tailing and satellites. The printing surface was also raised to 35°C to aid in the drying of the solvent. The ink was printed on backed nitrocellulose membrane (FF120HP, Whatman International Ltd., Piscataway, NJ, USA), which was used throughout the entire project. The width of the lines that were inkjet-printed were based on the spreading of the solvent on the nitrocellulose, which depended on the amount of ink printed, the number of layers applied, and the application of the ink and whether it was to create channels or delay valves. All of the patterns inkjet-printed were constructed using computer aided design software (AutoCAD, Autodesk, Inc.).

4.2.3 Fabricating physical barriers with PMMA ink

Precut nitrocellulose membrane measuring 15 x 15 mm was placed on the printing surface and was held down using non-permanent double sided tape (3M, St. Paul, MN). On each piece of nitrocellulose membrane, a 7.5 x 7.5 mm square with a line width of 0.5 mm or 1 mm was printed using PMMA ink with a drop spacing of 10 µm or 15 µm. For each drop spacing setting, different number of layers with the same square pattern were printed, ranging from 10 down to 3 layers. After printing, the nitrocellulose squares were carefully removed and dried on a hotplate (Thermo Scientific, Waltham, MA) set at 130°C for 5 minutes to evaporate any excess solvents. To test the holding time of the barriers, 10

µL of diluted blue food color dye (McCormick & Co., Inc., Hunt Valley, MD) was pipetted into the middle of the squares and was timed for its holding ability (Fig. 4.2).

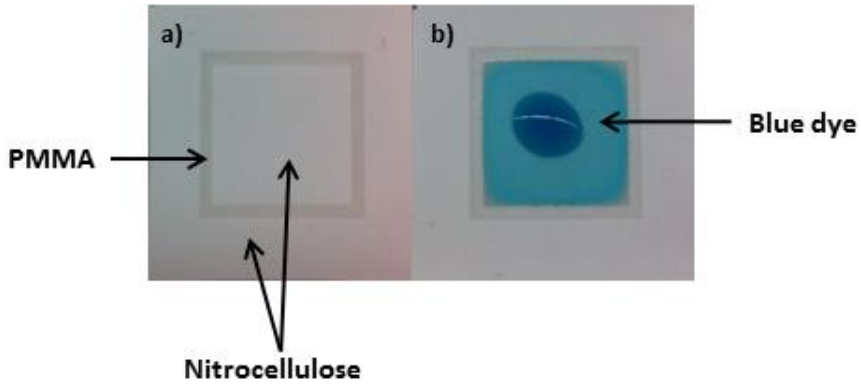

Fig. 4.2. An inkjet-printed 7.5 x 7.5 mm PMMA square with a line width of 1 mm with 5 layers at 15 µm drop spacing. A) Square after heating. B) Square after pipetting 10 µL of blue dye. The blue dye dried before it could pass through the PMMA.

4.2.4 SEM imaging

The nitrocellulose membrane was sputter-coated with a thin layer of gold (Cressington 108, Cressington Scientific, Watford, UK) for 60 seconds. The surfaces of the PMMA barriers were captured by the FEI Magellan 400 field emission scanning electron microscope (FEI, Hillsboro, OR). All of the images were captured at 2.0 kV.

4.2.5 Fabricating passive delay valves with PMMA ink

To construct the passive delay valves, a rectangle pattern measuring 16 x 0.5 mm was printed in the middle of a PMMA patterned square (16 x 16mm) with drop spacing ranging from 15 µm to 30 µm. Alongside, different number of layers, ranging from 1 to 6 layers, of the valves was also printed. The nitrocellulose was then removed and dried on a hotplate (Thermo Scientific, Waltham, MA) set at 130°C for 5 minutes. To test the valves,

the nitrocellulose was cut vertically into three pieces, each 4 x 15 mm in dimension and 7.5 µL of blue dye was pipetted onto the nitrocellulose. The valves were timed individually to determine how long it delayed the capillary flow.

4.2.6 Characterizing and testing delay valves with PMMA patterned channels

After optimizing the delay valves in the previous step, they were incorporated into PMMA patterned channels where they were further characterized. A nitrocellulose test strip was fabricated by patterning a rectangle measuring 23 x 25 mm with 5 mm channels (Fig. 4.3). All lines were printed in 1 mm widths. A series of delay valves were printed ranging from 0.5 mm to 3.0 mm in width across the first three channels, leaving the last channel empty for the control. 7.5 µL of blue dye were pipetted simultaneously into each channel with a multichannel pipette and the timing of the different delay valves was recorded.

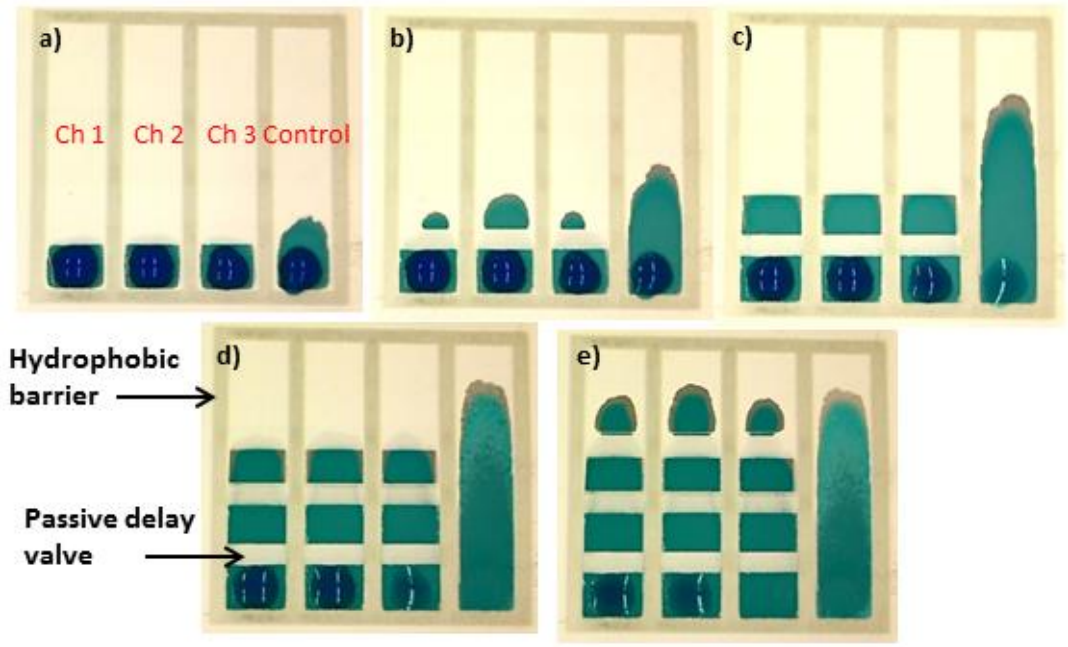

Fig. 4.3. Characterizing and testing delay valves with PMMA patterned channels printed on a nitrocellulose test strip. A volume of 7.5 µL of blue dye was pipetted into each channel. a) Time at 0 seconds; b) Time at 18 seconds; c) Time at 66 seconds; d) Time at 125 seconds; and e) Time at 154 seconds.

4.2.7 Application of the paper-based device with PMMA channels and valves

- **Design and fabrication of the paper-based device with PMMA channels and valves**

Nitrocellulose membrane was patterned with PMMA ink in a 26 x 27.75 mm design with three channels (Fig. 4.4). Channel 1 and 2 contained no valves, while Channel 3 had six 1.5 mm valves. The openings in Channel 1 and 3 were each blocked off with one 1.5 mm valve. At the top of the device, a piece of 30 x 8 mm absorbent pad was taped to the nitrocellulose to allow for wicking of the fluids. To test the flow of the channels, 15 µL of red dye and 100 µL of green and blue dye was pipetted into a 96- well microtiter plate into

three subsequent wells. The device was placed into the wells and video recording software was used to capture the flow.

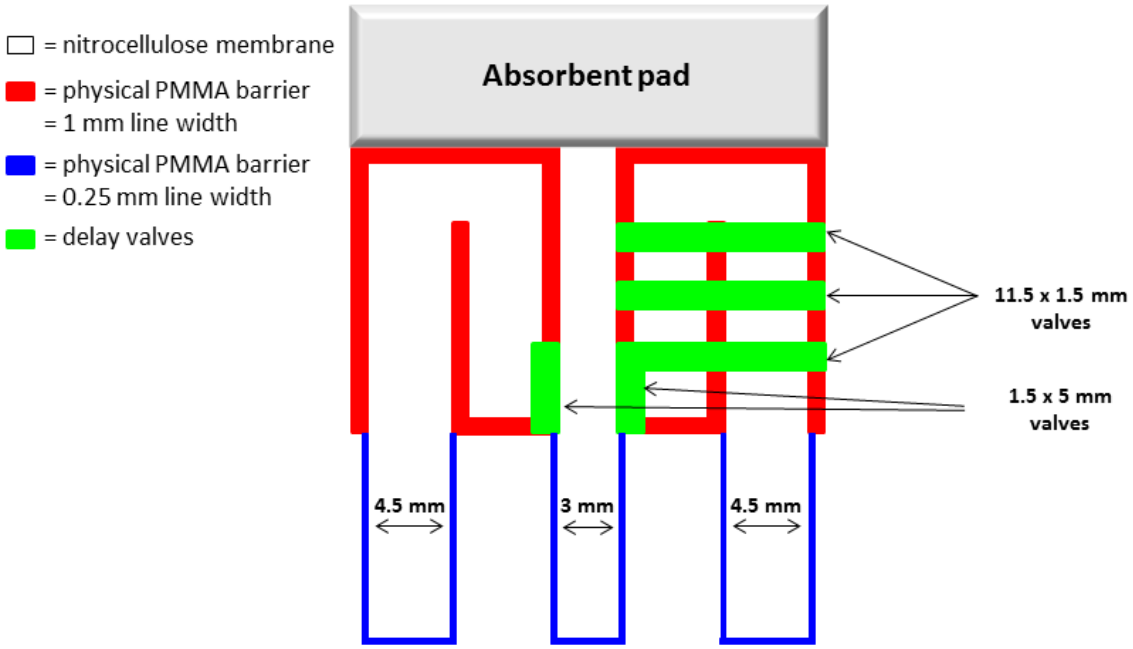

Fig. 4.4. Schematic diagram of the paper-based device.

- **Immobilization of oligonucleotides for test and control regions**

The test and control line solutions were prepared by mixing 2 µL of 300 µM biotin capped oligonucleotide (Table 4.1), 2 µL of streptavidin and 6 µL of 0.4 M $NaHCO_3/Na_2CO_3$, pH 9.0, containing 5% methanol and incubated for 20 minutes. The test and control regions were created by pipetting 0.5 µL of the corresponding oligonucleotide mixture in Channel 2, making sure both regions do not congregate (Fig 4.4 and 4.9). The device was then placed into a vacuum oven to dry at 40°C and -15 mmHg for 1.5 hours. The membrane was then blocked with 35 mL of blocking solution (0.015% sodium caseinate, 0.3% polyvinylpyrrolidone (MW 8000), 0.001% Tween 20 brought to volume

with 10 x TBS), agitating for one minute. The paper-based device was then dried in a vacuum oven at 25°C and -15 mmHg for 2 hours.

Table 4.1. Nucleic acid sequences used for the paper-based device.

NAME	**SEQUENCE**
Test line	[Biotin]GGGCATCACAGACCTG
Control line	GGAGGGCAAGTCTGGT[Biotin]
Reporter (gold nanoparticle)	ACCAGACTTGCCCTCC[Biotin]
Target	GGAGGGCAAGTCTGGTACCATCCGCTGGATTATGGCTGA ACGCCTCTAAGTCAGAATCCATGCTAGAACGCGGTGATTT CTTTGCAGGTCTGTGATGCCC

- **Testing of the paper-based device**

A 96-well microtiter plate was used as a holder for the device, where the washing buffer, the target solution and the silver enhancer (Catalog No. 50-22-02, KPL, Gaithersburg, MD) was pipetted into subsequent wells. Phosphate buffered saline (100µL), which was used as a rinse buffer was pipetted into the first well. The target solution was prepared by incubating 12.5 µL of *target* oligonucleotide (200 fmol μL^{-1}), 12.5µL of streptavidin linked gold nanoparticle conjugates and 50 µL of PBS, in the second well. Equal volumes of Solution A and B from the silver enhancer kit (KPL, Gaithersburg, MD) were mixed and 100µL of the mixed solution was pipetted into the third well. The prepared paper-based device was placed into the three wells and the flow and results were captured by video recording software.

4.3 Results and Discussion

4.3.1 Inkjet printing PMMA ink

The polymer ink was characterized and optimized prior to inkjet printing using the Dimatix Materials Printer. According to Fujifilm, ink with a viscosity of 2 to 30 mPa·s allows for optimal jetting of the ink from the nozzles. Anisole was used as the solvent because it had enough surface tension to hold the ink in the nozzle without any dripping. It also easily evaporated, which was beneficial for our purposes of creating physical barriers with PMMA on nitrocellulose due to shorter and less vigorous heating times. Thus, it was determined that 11% PMMA in anisole had the properties closest to an ideal ink for the Dimatix Materials Printer due to its viscosity of 5.480 ± 0.004 mPa S at 35°C.

After optimization, the polymer ink was then injected into a 10 pL cartridge, where the settings, such as jetting frequency, jetting voltage and waveforms were determined. The calibration settings of the nozzles were adjusted until ink drops jetting out were straight, had no tails and at the ideal speed. This resulted in a setting of 36V at 35°C.

The apparent advancing water contact angle of PMMA dried on pre-cleaned PET was 78.0 ± 2.33°, which suggests that the PMMA is hydrophilic, when an angle of greater than 90° is termed as hydrophobic. Because the PMMA ink only acts as a physical barrier in the nitrocellulose membrane, wettability of the ink is not an important factor. In fact, because the PMMA has a contact angle of less than 90°, it can be beneficial when using throughput solutions containing protein as we can minimize the loss of activity of the proteins. Hydrophobic interactions between proteins and a hydrophobic material can

decrease the activity, due to a loss of protein conformation, which can eventually lead to protein denaturation.

4.3.2 Fabricating and testing physical barriers and channels with PMMA ink

In order to create effective barriers in the nitrocellulose, the ink was needed to penetrate deep enough into the membrane so that the anisole could dissolve and collapse the cellulose fibers[22]. The anisole was able to disrupt the integrity of the nitrocellulose, resulting in the collapsing of the fibers. When the solvent evaporated, the PMMA was left behind with the disintegrated fibers, creating an effective barrier.

The nitrocellulose membrane (FF120HP), including the backing, only measured 200 µm in thickness. Theoretically, the use of a thinner piece of nitrocellulose to create physical barriers allowed us to use less ink to create the same wettability when compared to a thicker membrane. The plate where the nitrocellulose was placed was also heated to 35°C to speed up the evaporation of the solvent.

To create the PMMA barriers, a square measuring 7.5 x 7.5 mm with a line width of 0.5 mm was patterned onto the membrane (Table 4.2). 10 µL of blue dye was pipetted into each square box and was timed for its holding ability.

Table 4.2. Print settings and testing of the physical barriers measuring 0.5 mm in width.

Resolution/Drop spacing (µm)	**Layers**	**Line resolution**	**Hold time**
15	5	Defined	3 minutes
15	6	Defined	6 minutes

Even though the lines printed were defined, but the holding ability of the lines was insufficient. We require the barriers to have extended holding times so that we can run longer assays on the paper-based device. Therefore, we increased the line width to 1 mm, which was again patterned into a 7.5 x 7.5 mm square (Table 4.3). 10 µL of blue dye was pipetted into each square box and was timed for its holding ability.

Table 4.3. Print settings and testing of the physical barriers measuring 1.0 mm in width.

Resolution/ Drop spacing (µm)	**Layers**	**Line resolution**	**Ink penetration**	**Hold time**
15	3	Defined	Ink slightly penetrated through to plastic	0 seconds
15	5	Defined	Ink completely penetrated through Nitrocellulose (NC) became translucent	Indefinite
15	6	Defined	Ink completely penetrated through NC became translucent	Indefinite
15	10	Not defined	Ink completely penetrated through NC became translucent	Indefinite
10	5	Not defined	Ink completely penetrated through NC became translucent	18 minutes

It was found that that at drop spacing of 15 µm, squares with 5, 6 and 10 layers had a hold time longer than the time tested. In these samples, the dye solution dried before the solution could pass through the barrier. On the other hand, the squares with 3 layers were

unable to hold the dye solution for any appreciable time. Printing with a higher resolution at 10 µm resulted in the lines becoming undefined, which can affect patterning of more complex devices in the future. It is important for the lines to be defined because we need to create narrow channels, which will require precision and accuracy. Therefore, the setting where the line is printed in 5 layers with a drop spacing of 15 µm and with a line width of 1 mm was chosen. This setting allowed us to use as little ink as possible without affecting the hold time or line quality.

4.3.3 SEM imaging of PMMA physical barriers and channels

In the SEM images, the PMMA evenly coated the nitrocellulose membrane, forming an effective barrier for the solution (Fig. 4.5). This shows that the inkjet printer was able to uniformly deposit drops of the ink on the membrane with enough definition so that the dye solution could be held.

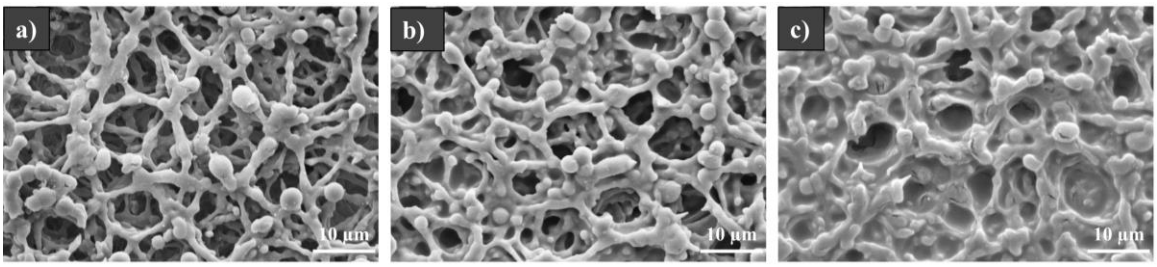

Fig. 4.5. SEM images of inkjet-printed PMMA on nitrocellulose. a) nitrocellulose (control); b) PMMA delay valve; and c) PMMA barrier.

4.3.4 Fabricating passive delay valves with PMMA ink

Following fabrication, the delay valves were tested for precision. Optimally, the valve would be able to delay the flow for an extended period of time and concurrently be

precise with respect to timing. Similar delay valves that decrease the flow rate of the solution have previously been developed, but most of them involve the introduction of a by-product from the valve itself, such as a surfactant[77] or sucrose[101]. Conversely, our PMMA delay valves should not be introducing any polymers into the running solution as we were able to reuse the valve with similar timings after drying. The other disadvantage is that they are single-use valves, whereas PMMA delay valves could be used multiple times. To study the relationship between drop spacing, the number of layers printed and the delay of the flow by the valves, nitrocellulose membranes were patterned with PMMA ink with different drop spacing layers to control the volume and resolution of ink deposited, which is similar to the fabrication of the physical barriers (Section 4.2.3). When printing at a drop spacing of 15 µm, only up to four layers were printed because of its physical blocking properties when five or more layers are printed. Using the Kruskal-Wallis ANOVA (OriginPro 9, Northampton, MA) for statistical analysis, we observe that there was no significant difference between printing different number of layers and the delay in flow, with a p-value of 0.195. When printing at a high resolution like 15 µm, relatively more anisole is deposited onto the nitrocellulose disrupting more of the membrane, but the amount of PMMA deposited is only enough to coat the surface of the substrate. The amount of PMMA deposited on the surface is not sufficient enough to physically block the disrupted membrane and thus delay the flow of the throughput solution. Thus, no significant difference is observed until a physical barrier is formed when five or more layers of the PMMA ink is printed at 15 µm.

At 25 µm drop spacing, a significant difference of 0.0103 was observed between printing different layers with six layers being the maximum number of layers printed. Because relatively less anisole was deposited on the membrane compared to 15 µm, less nitrocellulose was disrupted, allowing the PMMA to be collected on the surface, which effectively decreased the flow of the solution. However, at 30 µm drop spacing, no significant difference between layers was observed, with a p-value of 0.358. This is because not enough anisole is patterned onto the membrane, which affects the penetration of PMMA to effectively block the flow of the solution. This resulted in short delay times of the throughput solution. Due to the design of our paper-based device, 30 µm and one layer was chosen as the setting of our valves. The advantage with choosing this setting was that less PMMA ink would be used to fabricate our devices, which decreases the cost of production.

4.3.5 Characterizing and testing delay valves with PMMA patterned channels

Delay valves with different widths were printed with one layer at drop spacing of 30 µm and were tested by pipetting 7.5 µL of blue dye into each channel. Delay valves measuring 1.5 mm, 2 mm, 2.5 mm and 3 mm were tested (Fig. 4.6). Using the Kruskal-Wallis ANOVA, it is found that delay times are significantly different from each other with a p-value of 0.0151 as the width of the valve is increased. The data suggests that as the width of the valve is increased, a proportional delay time was added. This was because the blue dye required more time to travel through a larger area. To further test the valves for further applications, we also printed them in a series of 3, each measuring 0.5 mm, 1.5 mm, 2 mm and 2.5 mm (Fig. 4.6). Again, a Kruskal-Wallis ANOVA was performed and the

results show that the delay times were significantly different from each other with a p-value of 0.0156, as the width of the valve is increased. When comparing the timing between a single valve to a series of three valves, a one-sided Mann-Whitney test was performed for barrier widths of 1.5 mm, 2.0 mm and 2.5 mm. The p-values for the three widths were 0.05. An increase in time is observed because the blue dye needs to travel through more valves, which increase the resistance to the flow.

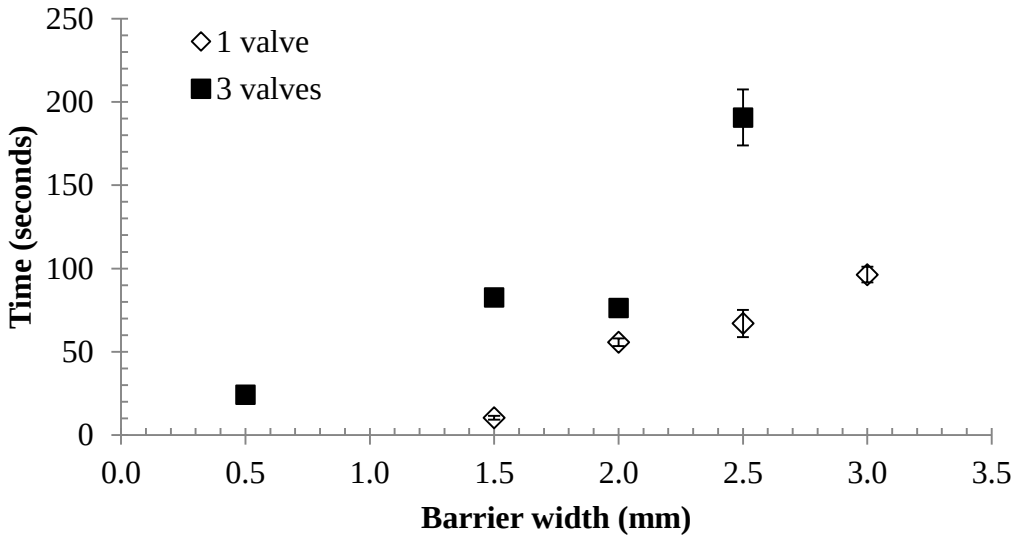

Fig. 4.6. A comparison between the relationship of the barrier width and the holding time for a single delay valve and a series of three valves with printer settings of 1 layer and a drop spacing of 30 µm. Values shown represent the average of n=3 with the error bars representing the standard deviation.

4.3.6 Application of the paper-based device with PMMA channels and valves

We developed and fabricated a paper-based device that would be able to perform a nucleic acid assay that was convenient, cost effective and user friendly. In a conventional nucleic acid lateral flow assay test, it requires the user to incubate the sample for a few minutes, followed by adding a washing buffer to wash the excess sample towards the

detection area and finally add a silver enhancer solution to increase the signal. However, this is laborious and time consuming. Thus, we developed a device that would include the sample incubation step, the washing step and the silver enhancing step into one[97, 102]. Furthermore, the sample preparation step was also designed to be easy, where the user would pipette the sample and solutions into corresponding wells and place the device into the wells to start the assay. The device was designed so that Channel 2 contained the sample and was wicked up towards the detection region (Fig. 4.7.). After a few minutes of incubation, the washing buffer, which was in Channel 1, would wash the rest of the sample towards the absorbent pad, ensuring that the largest signal would be achieved. Channel 1 did not contain any valves, but was longer in length, which also effectively delayed the flow of the buffer. After the wash, the silver enhancer, which was in Channel 3, would finally reach Channel 2 after being delayed by the valves. The enhancer would travel towards the detection region and enhance the signal. In Fig. 4.7, the flow of the washing buffer, sample and silver enhancer is depicted by the green, red and blue dye, respectively.

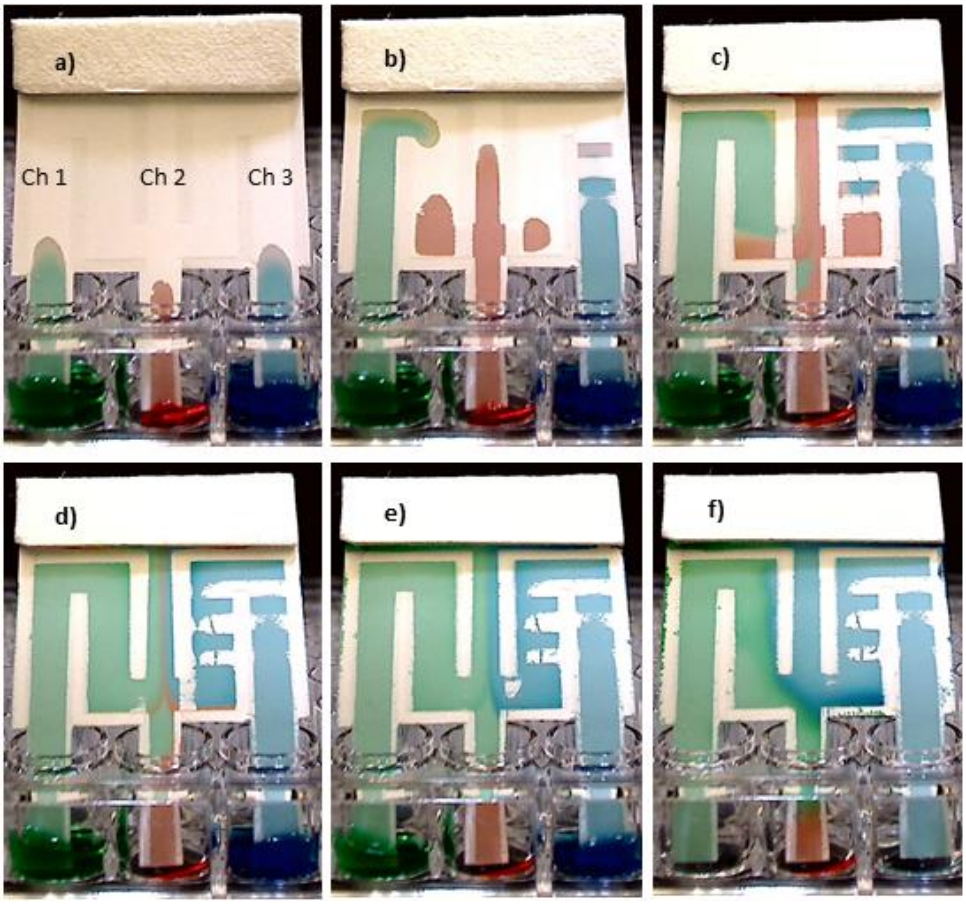

Fig. 4.7. Flow of dye on paper-based device. a) Time at 27 seconds; b) Time at 1 minute 46 seconds; c) Time at 4 minutes 54 seconds; d) Time at 9 minutes 31 seconds; e) Time at 24 minutes 20 seconds; and f) Time at 56 minutes 43 seconds.

In Fig. 4.8, we applied a nucleic acid assay on our paper-based device. Here, we demonstrate that the device is able to perform the detection, washing and signal amplification without the need to wait for subsequent additions of multiple solutions. With this device, users are able to perform multiple assays with ease and at a low, affordable price.

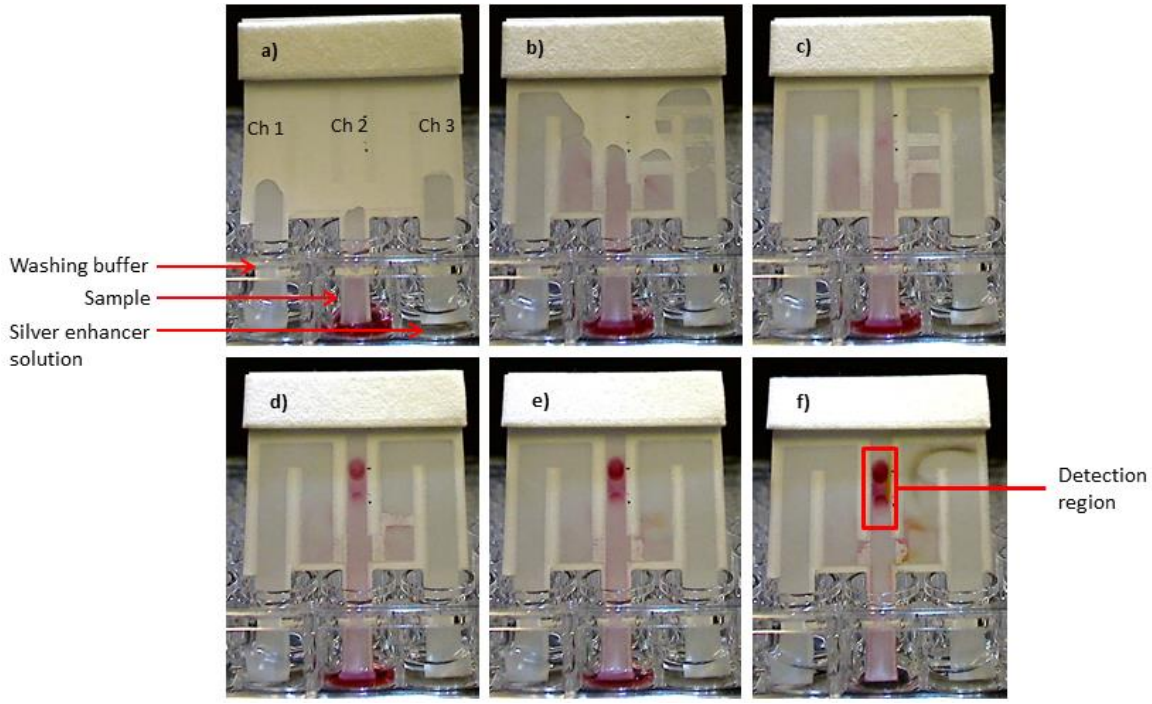

Fig. 4.8. Application of a nucleic acid assay on paper-based device. a) Time at 38 seconds; b) Time at 2 minute 30 seconds; C) Time at 4 minutes 1 second; d) Time at 7 minutes 51 seconds; e) Time at 11 minutes 43 seconds; and f) Time at 33 minutes 39 seconds.

4.4 Conclusion

With the development of paper-based devices, more portable, inexpensive, easy to use, sensitive and specific methods of analysis are produced. With the use of the PMMA ink, not only were we able to create physical barriers and pattern channels but we were also able to develop passive delay valves. The PMMA barriers were tested for their ability to hold solutions indefinitely while the delay valves were characterized by measuring the delay caused in capillary flow action. We further applied the channels and valves into a paper-based device where a silver enhanced nucleic acid assay was performed. This application showed that we are able to perform a multistep assay without the need for the user to wait for subsequent additions of solutions. This makes our paper-based device an

effective tool in low resource settings were equipment is limited and users may not be trained adequately. Future studies will be developed for the detection of diseases commonly found in low resource settings.

CHAPTER 5

DEVELOPMENT OF A VISUALLY QUANTITATIVE PHAGE AMPLIFIED LATERAL FLOW ASSAY FOR *E. COLI*

5.1 Introduction

Detection of pathogenic bacteria in food and healthcare sectors has become a focus in recent years[1-3]. With growing numbers of outbreaks, it is of public interest that rapid, accurate and sensitive detection methods be developed. According to the U.S. Centers of Disease Control and Prevention, between 2003 and 2012, there has been 4,930 confirmed cases of *E. coli* related illness with a total of 391 *E. coli* O157:H7 outbreaks (CDC, Atlanta, GA). Furthermore, in the recently published Food Safety Modernization Act, it requires the testing of agricultural water to have a detection limit of at least 10 CFU in 100 mL of sample (FDA, Silver Spring, MD).

Recently, there has been renewed interest in using lateral flow assays (LFAs) for rapid diagnostics due to its affordability and portability, yet still being sensitive enough for accurate detection[11-13]. The home pregnancy test kit is a product that exemplifies the benefits of using LFAs for detection. Currently, there are commercial LFA test kits available for detection of pathogenic strains of *Escherichia coli* (*E. coli)*, such as DuPont™ Lateral Flow System (DuPont, Wilmington, DE) and EMD Millipore's Singlepath® (EMD Millipore, Billerica, MA) for *E. coli* O157:H7. However, these tests rely on finding a mixture of antibodies to capture a broad range of strains of the bacteria, which can be expensive and laborious.

Bacteriophages, a type of virus that infect bacterial cells and hijack their metabolic mechanism through genetic transfer, have a range of specificity for hosts, and would be a great alternative to be used as a biosensing component in LFAs. There are many advantages in using phage as a detection probe, as they are relatively easy to culture, are host specific and have the ability to differentiate between viable and non-viable cells[50-51]. Most importantly, they are able to infect bacterial cells and release more phage after replication, which is termed as phage amplification or signal amplification. Microphage (Longmont, CO) developed a phage amplification-based LFA for clinical settings that detected for *Staphylococcus aureus* and antibiotic resistance determination on methicillin-resistant *S. aureus* (MRSA) in blood[52]. The total analysis time for the LFA, including amplification, was 5.5 hours compared to a conventional MRSA test of 48 hours. Phage amplification-based LFA is a promising technique for low bacterial count samples and can also be applied to detect for other pathogens, such as *E. coli*[51, 53].

A widely studied bacteriophage, T7, is able to infect a wide range of *E. coli* and has a replication cycle of 17 minutes at 37°C[103], in which at the end of its cycle, hundreds of phage progeny are produced. Therefore, with the amount of time it takes for *E. coli* to replicate, there would be a 100 fold increase in phage, thus making it ideal candidates for detection. This allows the phage to be used in signal amplification, which is especially desirable for samples with low levels of viable bacteria. Phage amplification can be further enhanced through kinetic studies to optimize the amount of phage and bacterial cells needed to produce detectable signals. Previously in our lab, we determined that when 10^3 CFU/mL of bacterial cells were incubated with 10^4 PFU/mL of T7 phage for 7 hours at 37°C, we were able to maximize the amplification of phage.

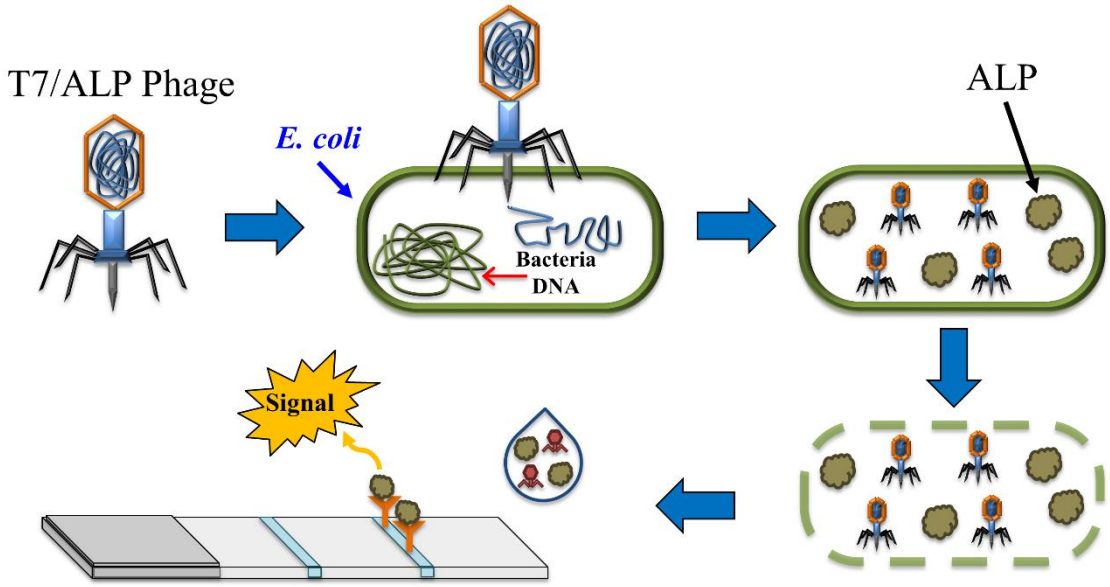

Fig. 5.1. Schematic diagram of phage amplification and ALP overexpression applied to a lateral flow assay.

With this knowledge, we decided to encode a gene into T7 phage to overexpress alkaline phosphatase (ALP) during replication, which would be used in a lateral flow assay with detectable colorimetric signals[104] (Fig. 5.1). Anti-ALP antibody was immobilized onto nitrocellulose membrane as a test line, which was used to capture ALP in the cell lysate sample. A colorimetric substrate, 5-bromo-4-chloro-3'-indolyphophate and nitro-blue tetrazolium (BCIP/NBT), was allowed to react with the captured ALP to produce a dark blue-purple precipitate (Fig. 5.2). With this method, we were able to obtain a limit of detection of $10^{6.8}$ PFU/mL for detectable colorimetric signals on the test strip. However, with this method, we were unable to differentiate the amount of phage from just visual observation and had to solely rely on image processing software to quantify the signal produced.

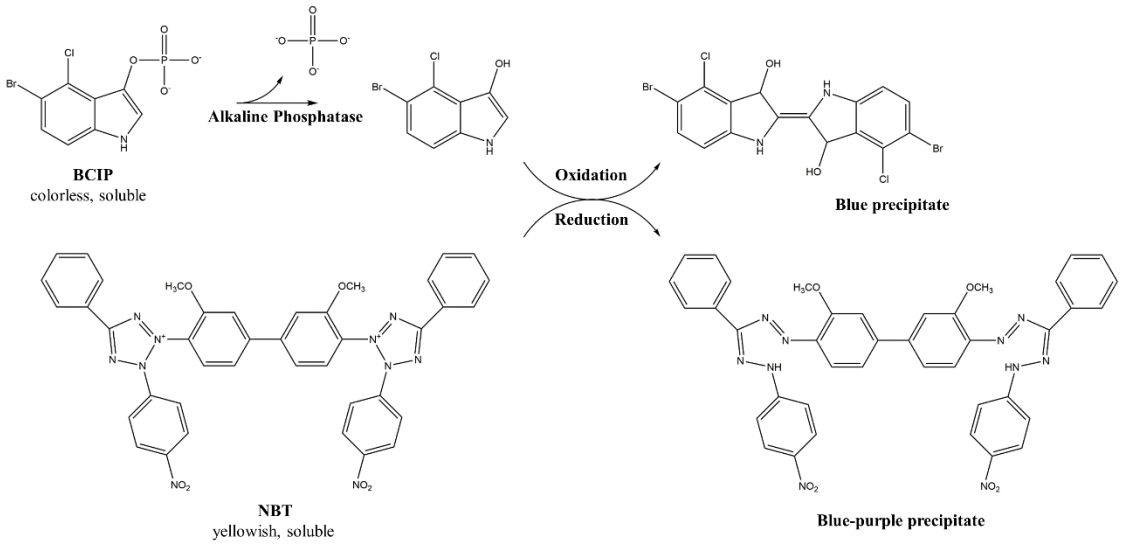

Fig. 5.2. Reaction scheme of NBT/BCIP colorimetric assay.

Therefore, in this study, we developed a visually quantitative lateral flow assay for phage-based detection. Our objective was to maintain the sensitivity and rapidness of the test, and be able to approximate the amount of phage in the sample using the naked eye. The end goal was to create a semi-quantitative assay that would be capable for both visual detection (for ease of use) and for colorimetric detection (for accurate quantitative results).

The objective was achieved by fabricating a barcode style (also known as ladder style) lateral flow assay, where multiple test lines were sprayed consecutively along the detection zone. Currently, there have been a few studies where a barcode style LFA was used for immunochromatographic[20, 105] and enzymatic detection[21]. Compared to a simple LFA, where there is only a single test line, a barcode LFA would have multiple lines immobilized, resulting in a band of lines when target is present. With the barcode design, the number of lines that light up are proportional to the concentration of analyte in the sample, which makes it visually quantitative. To obtain a quantitative readout of the

colorimetric reaction (NBT/BCIP), the signal of the lines were analyzed using image processing software.

5.2 Methods and Materials

5.2.1 Materials

Bacterial and Bacteriophage Strains

Anti-ALP antibodies were obtained from Abcam (ab7321, Cambridge, MA). Bacterial strain *E. coli* BL21 and bacteriophage T7 (T7Select® 415-1) were purchased from EMD Millipore (Billerica, MA). T7 bacteriophage were genetically modified to overexpress ALP using previously reported methods in our lab[104].

Solutions and Reagents

All chemicals and reagents were of analytical-reagent grade. 1 x PBS consisted of 10 mM Na_2HPO_4, 1.8 mM KH_2PO_4, 137 mM NaCl and 2.7 mM KCl, adjusted to pH 7.4. Luria Broth (LB) was prepared using 1% tryptone, 0.5% yeast extract and 1% NaCl, adjusted to pH 7.5. LB agar contained 1.5% agar in LB. One-step NBT/BCIP substrate solution (Cat No. 34042) was used directly in the assay. All of the above reagents were obtained from Fisher Scientific (Waltham, MA). Non-fat dried milk were purchased from (Omniblok™, American Bioanalytical, Inc., Natick, MA).

5.2.2 Assembly of the test sheets

Polyethylene terephthalate (Highland Transparency Film, 901) was cut into 40 x 100 mm rectangular sheets used for backing. Double sided tape (3M, St. Paul, MN) with

the dimensions of 38 x 215 mm was adhered along the bottom edge of the backing. A pre-cut 38 x 100 mm nitrocellulose membrane (AE 98 Fast, Whatman®) was gently pressed onto the double the sided tape.

5.2.3 Preparation of the test strips

The assembled test sheets were placed on the printing area of the Linomat IV (Linomat IV, CAMAG, Wilmington, NC, USA) and held down by magnets. Varying concentrations of anti-ALP antibody (0.01 to 0.5 mg/mL) were sprayed and immobilized as test lines for signal optimization studies. Test lines were sprayed 2 mm apart to achieve barcode style lateral flow test strips. The test sheets were allowed to dry in a vacuum oven at 20°C at -25 mmHg for 90 minutes.

The antibody containing membrane was blocked with 50 mL of blocking solution (1% non-fat dried milk in 1xPBS), shaking for 5 minutes. The test sheets were blotted dry and were agitated in 50 mL washing solution (1 x PBS) for 15 minutes. The blocked sheets were blotted dry and then dried in a vacuum oven at 20°C at -25mmHg for 2 hours.

Two 30 x 100 mm absorbent pad (CF5, Whatman International Ltd., Piscataway, NJ, USA) stacked together, were adhered onto the PET end of the test sheet with double sided tape. The assembled test sheet was then cut into 4 x 40 mm strips and stored in a desiccator at 20°C until further use.

5.2.4 Bacterial enumeration

An overnight culture of *E. coli* BL21 was grown in 35 mL LB at 37°C shaking at 200 rpm. The overnight culture was serial diluted and spread plated on LB agar to determine bacterial concentration.

5.2.5 T7/ALP bacteriophage stock solution

A subculture of 150 µL overnight culture was re-propagated into 35 mL of fresh LB at 37°C shaking at 200 rpm for 3 hours until $OD_{600} > 0.6$. An aliquot of 10 µL of T7/ALP stock was added into the subculture, shaking at 200 rpm at 37°C for 2 hours. The lysate was then centrifuged at 8000 rpm for 10 minutes at 20°C and the supernatant was passed through a 0.22µm sterile syringe filter. A double agar overlay plaque assay on LB agar was performed to determine phage concentration of the resulting stock solution. T7/ALP stock solution was diluted to construct a standard curve for ALP of the test strips.

5.2.6 Preparation of sample with cell lysate

An aliquot of 0.1 mL of phage stock serially diluted to 10^4 PFU/mL was added to 0.9mL of a known concentration of overnight bacterial culture. For the preliminary studies, 10^2 CFU/mL of bacterial culture was used. A negative control was prepared by mixing 0.1 mL of diluted phage stock and 0.9 mL of LB. The samples were incubated at 37°C for 7 hours, shaking at 200 rpm. After incubation, the cell lysate was passed through a 0.45µm syringe filter and stored at 4°C until further use.

5.2.7 T7/ALP phage-based barcode lateral flow assay

An aliquot of 100 µL of cell lysate was pipetted into a 10 x 75 mm glass test tube (Fisher Scientific, Waltham, MA) and a barcode test strip was dipped into the solution. The strip was allowed to incubate at 20°C until all of the cell lysate was wicked up. The test strip was then transferred into a tube where 30 µL of 1 x PBS was used as washing solution. After washing, the test strip was transferred into 1 mL of preheated NBT/BCIP solution at 37°C. After incubation for 2 hours, the test strips were blotted dry and an image of the test lines were captured using a mobile camera. The signal from the test line were quantified using an image processing software (Image J, NIH, Bethesda, MD) (Fig. 5.3).

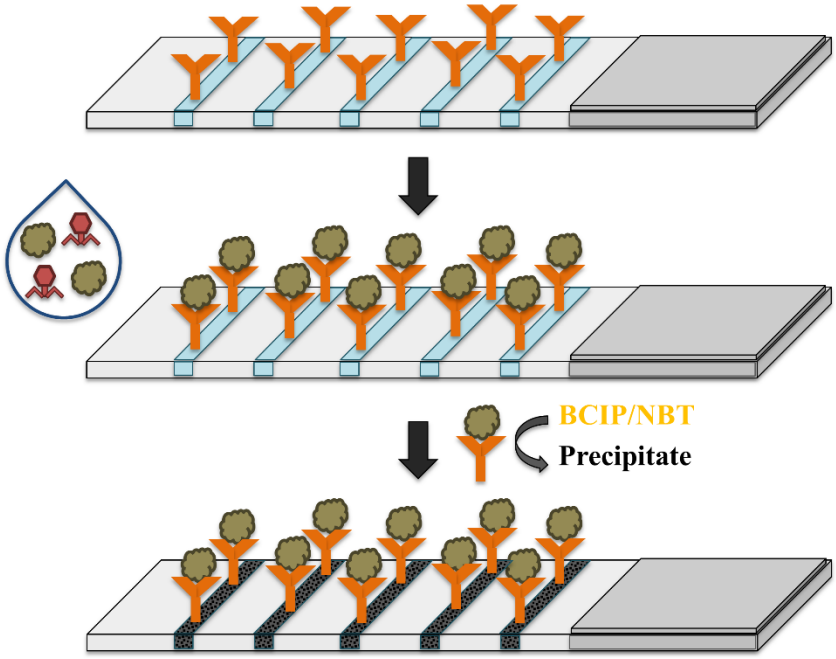

Fig. 5.3. Schematic diagram of T7/ALP phage-based barcode lateral flow assay.

5.3 Results and Discussion

5.3.1 Design of the test strip

A barcode-style phage-based lateral flow assay was used to visually quantify the colorimetric signal produced by ALP from T7/ALP cell lysate. In this study, T7 bacteriophage was genetically modified to overexpress ALP. Once T7/ALP phage infects and hijacks the metabolic activity of *E. coli*, ALP will be overexpressed and be released when the cell is lysed. With the overexpression of ALP, it was possible to obtain a detectable signal by immobilizing anti-ALP antibody on the test line and capturing the overexpressed ALP. The signal produced by the captured ALP is proportional to the phage titer of the cell lysate and the number and intensity of the lines that appear after adding the colorimetric substrate.

5.3.2 Optimizing the test line

Anti-ALP antibody was deposited onto nitrocellulose as test lines to capture overexpressed ALP in cell lysate. In this study, our goal was to determine the minimum amount of antibody that was needed to capture ALP and produce a visible colorimetric signal. Anti-ALP antibody solutions ranging from 0.01 to 0.5 mg/mL were sprayed onto nitrocellulose with a test line concentration of 0.02 to 1.0 μg/cm. Results show that 0.05 mg/mL was the minimum concentration needed to visually identify the test line (Fig. 5.4). Therefore, 0.05 mg/mL was chosen as the test line concentration in the barcode style assay. A total of 5 lines were sprayed on each test strip due to the length of the nitrocellulose and the practicality of fabricating the test strips.

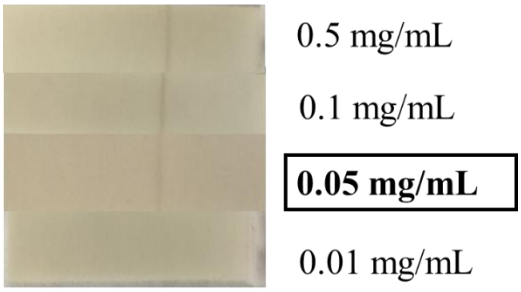

Fig. 5.4. Different anti-ALP antibody concentration for test lines (only a single line was sprayed for optimizing test line concentration).

5.3.3 Optimizing the blocking of nitrocellulose

Blocking of nitrocellulose is performed to reduce the amount of non-specific adsorption of the analyte to the membrane. Over-blocking of the membrane can result in the unsuccessful capture of analyte at the test line due to blocked reaction sites[14]. Under-blocking can result in non-specific binding of the analyte in other regions of the membrane, resulting in smeared lines. It was conclusive that 5 minutes of blocking in 1% non-fat dried milk, followed by 15 minutes of washing in 1 x PBS was adequate (Fig. 5.5).

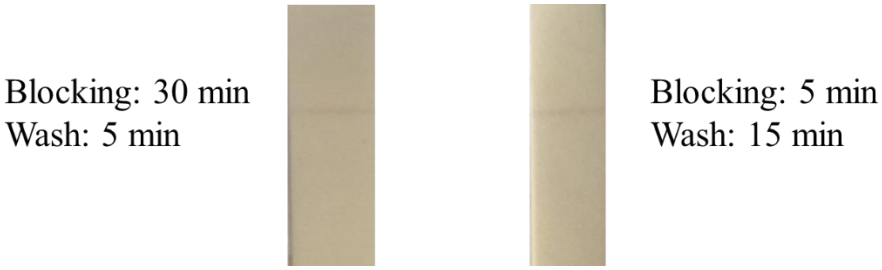

Fig. 5.5. Effect of blocking time of nitrocellulose with 1% non-fat dried milk and washing time with 1 x PBS.

5.3.4 Constructing the standard curve

A standard curve for phage amplification of the test strips was constructed by running dilutions of T7/ALP phage stock solution from 10^7 to 10^9 PFU/mL (Fig. 5.6). We

were able to distinguish the colorimetric signal up to a half log difference by visual inspection. Furthermore, each set of test lines were quantified and signal to noise ratio was determined and were standardized against a negative control test strip. The signal to noise ratio between dilutions were significantly different, which corresponds to the visual indication. This also suggests that the barcode style test strips were sensitive to the analyte concentration. Through this study, we were also able to determine the limit of detection of the test strips, which was 10^7 PFU/mL or in other words, 10^6 PFU.

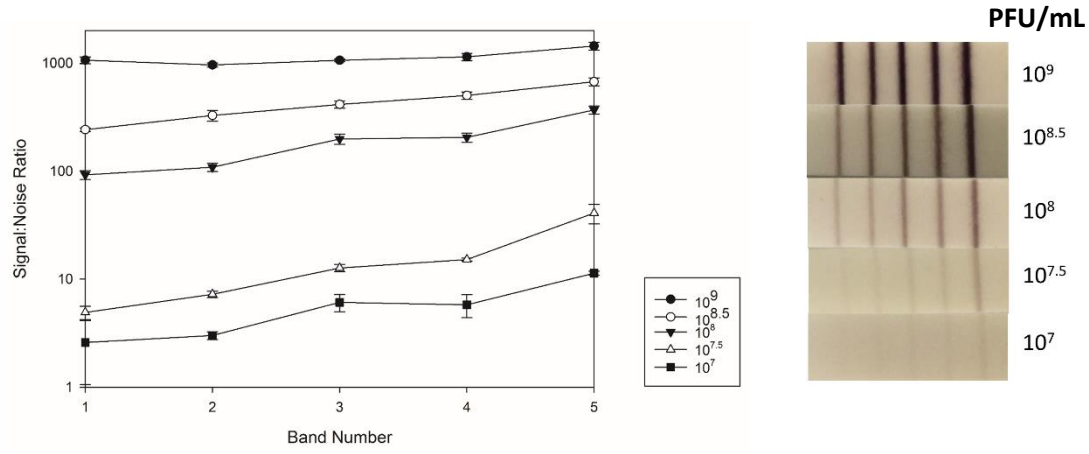

Fig. 5.6. Standard curve for barcode style phage amplification LFA. The phage were serially diluted from T7/ALP phage stock solution.

5.3.5 Testing with cell lysate

The purpose of the barcode style phage amplification LFA was to determine the bacterial concentration in a low count sample and at the same time be able to visually quantify the signal. According to the Food Safety Modernization Act, the detectable limit of *E. coli* must be less than 100 CFU per 100 mL (or 1 CFU/mL). With a concentration step, we can in theory detect 10^2 CFU/mL in a 1 mL sample by filtering a 100 mL sample with an initial concentration of 1 CFU/mL. Therefore, in our case, a spiked sample containing 10^2 CFU/mL of *E. coli* was tested. To amplify the signal, 10^4 PFU/mL of

T7/ALP phage was added to the sample for 7 hours at 37°C. The resulting lysate was filtered and a 100 µL aliquot was run up the test strip. The standard curve was used to determine the degree of phage amplification. This resulted in a signal:noise ratio that corresponded to $10^{7.5}$ PFU/mL, which not only showed there was successful signal amplification, but it also provided indication of the initial bacterial concentration in the sample (Fig. 5.7). More importantly, the barcode assay provided visual quantification of the amount of analyte captured, in this case, 10^2 CFU/mL of *E. coli* after amplification produced 3 lines.

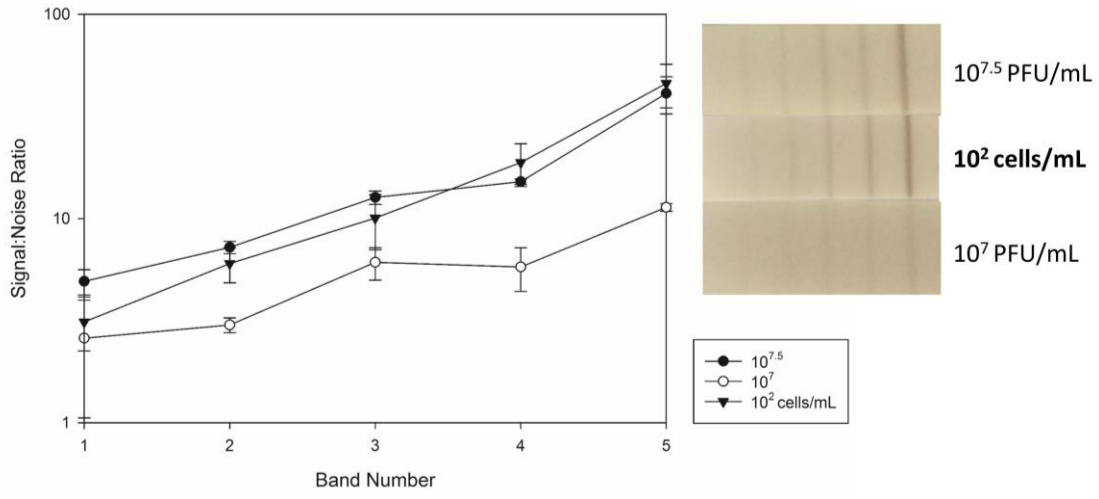

Fig. 5.7. Bacterial detection using barcode style phage amplification LFA. 10^2 CFU/mL of *E. coli* was incubated with 10^4 PFU/mL of T7/ALP phage for 7 hours at 37°C. This resulted in phage amplification signal of $10^{7.5}$ PFU/mL and a visual detection of 3 lines.

5.4 Conclusion

In this study, we developed a visually quantitative lateral flow assay for phage-based detection. Not only were able to achieve a relatively rapid and sensitive detection, but we were also able to approximate the amount of phage in the sample using the naked eye. The objective was achieved by fabricating a barcode style (also known as ladder style)

lateral flow assay, where multiple test lines were sprayed consecutively along the detection zone. Even though the barcode LFA had a detection limit of 10^6 PFU of T7/ALP phage, but we were able to detect an equivalent of 10^2 CFU/mL of *E. coli* cells with a seven hour amplification step. This showed the potential of meeting the requirements of FSMA, where the detection limit of an agricultural water test should be less than 100 CFU per 100 mL. Ultimately, we were able to create a sensitive and relatively rapid semi-quantitative assay that would be capable for both visual detection (for ease of use) and for colorimetric detection (for accurate quantitative results).

CHAPTER 6

DEHYDRATION OF BACTERIOPHAGE IN ELECTROSPUN NANOFIBERS: EFFECT OF EXCIPIENTS IN POLYMERIC SOLUTIONS

6.1 Introduction

In the recent years, bacteriophages have been actively studied to rediscover their potential use and application in the health and food sector as an alternative therapy to antibiotic treatment[106-107]. This is because extensive use of antibiotics has unfortunately led to the birth of new strains of drug resistant bacteria[108-109]. This dire situation is becoming a serious threat to public health, such that fresh produce and livestock can act as a reservoir[110-112] for the resistant bacteria and be transmitted to the human population[113-114].

Bacteriophages are viruses that are ubiquitous in nature and have no metabolic activity of their own but infect and replicate within a bacteria host that result in the lysis of the host[115]. In theory, bacteriophage will infect the targeted bacteria by injecting its viral DNA into the host and successfully hijacking the metabolic machinery of the cell (Fig. 6.1). When the bacteria replicates, the phage will replicate and lysozyme is subsequently produced, lysing the bacteria, and effectively killing it[115]. As bacteriophages can eliminate specific pathogenic bacteria by infecting and lysing its targeted host during the infection cycle, this specific destructive mechanism has potential application in the agriculture sector for decontamination of rinse water for post-harvest produce[116]. It was demonstrated that phage is effective against a broad range of foodborne pathogens, such as *Campylobactor*, *Listeria*, *Salmonella* and *Escherichia*[117-121]. Moreover, U.S. Food and Drug Administration (FDA) has now given much attention on decontamination of sanitary agricultural water

e.g., rinse water and irrigation water, as these water sources play a critical role in the initial contamination of fresh produce[122]. The recent foodborne illness outbreaks in the US linked to fresh produce, e.g., *Salmonella Poona* in cucumbers and Shiga toxin-producing *E. coli* O157:H7 in chicken salad containing contaminated celery[123], further stresses the need for decontamination of rinse water by using bacteriophages.

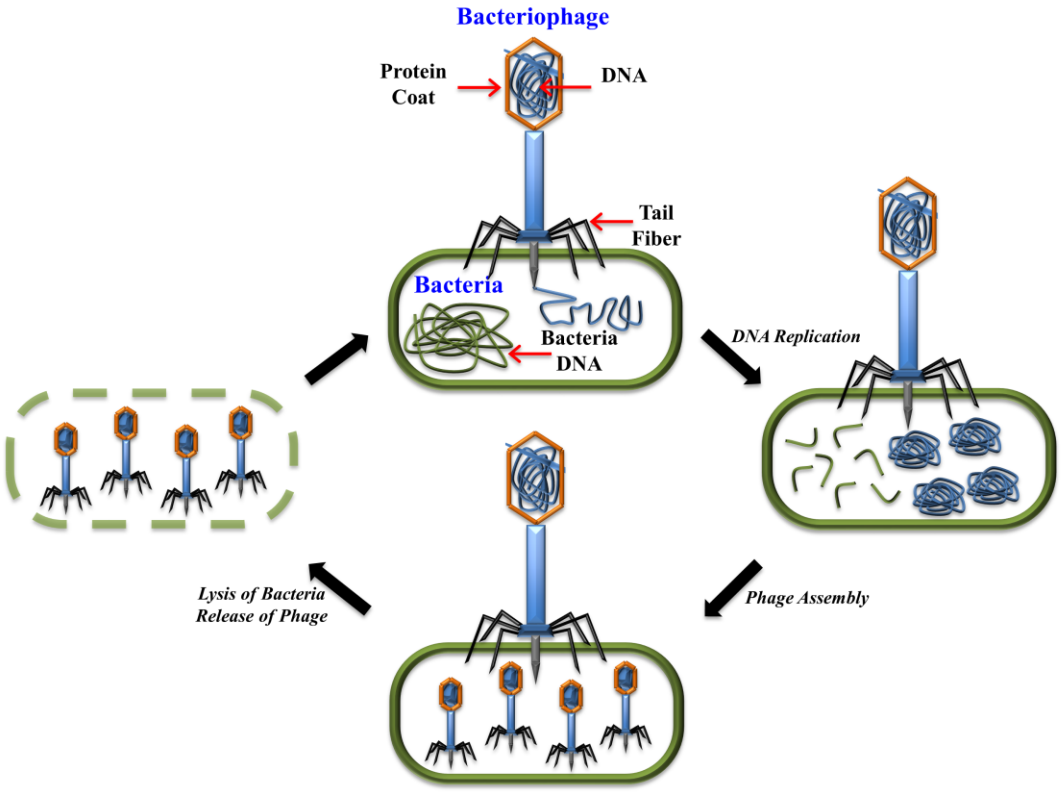

Fig. 6.1. Simplified sequence of bacteriophage infecting and lysing target bacteria.

Commercially available bacteriophages (*e.g.,* EcoShield™ and SalmoFresh™) are often stored in buffers and liquid solutions. This may be inconvenient and expensive to transport, store and maintain their viability. Therefore, there is a need to reduce the inconvenience and cost of operation and most importantly, to preserve the viability of the

phages for their intended use. Drying the bacteriophages may be the most feasible method to reduce the bulk volume and to preserve the bacteriophages[124-125]. One of the more commonly used methods for preservation and drying is by lyophilization, also known as freeze drying. A study demonstrated that freeze dried *S. aureus* bacteriophages (of 25 different species) could be stored for 12 to 18 years at -20°C under vacuum[126]. Although freeze drying is a commonly used method, it can be time-consuming and requires large machinery. An alternative potential method to dry and protect bacteriophage is by *electrospinning*. This is a simple, rapid and inexpensive drying method that produces nano- to sub-micron-scale fibers from a wide range of materials including polymer solutions or melts by application of high electric field to form a liquid jet [127-129]. A typical electrospinning setup involves three main components, 1) a high voltage power source, 2) a needle with syringe pump setup or capillary tube with pipette, and 3) a grounded flat metal sheet as a collector[127-129]. A high voltage is applied to create a fine stream of charged liquid jet that pulled out from the tip of the needle. The charged liquid jet is dried rapidly and produces nanofibers that are collected on a metal screen. An electrode is attached to the needle or pipette to induce charge on the liquid while another electrode is attached to the metal collector. Electrospun nanofibers have high surface area to volume ratio. The physical properties of the nanofibers can be influenced by the polymer solutions (*e.g.*, viscosity, conductivity), electrical potential, distance between the needle and metal collector screen, and conditions of the electrospinning chamber (*e.g.*, humidity)[127-129].

A few studies have used electrospinning to produce nanofibers of bacteriophage[130-135]. However, these studies demonstrated that the electrospun bacteriophages had low viability after electrospinning as a result of rapid dehydration of the polymer solutions that

caused drastic change to the osmotic environment surrounding the phage[136]. Nevertheless, a study done in our laboratory found that addition of trehalose in polyvinylpyrrolidone (PVP) polymer dispersed in storage media (SM) buffer had a protective effect on the bacteriophage during storage after the high voltage electrospinning drying process[133]. Thus, in the present study we further investigate the effect of salts (sodium chloride, magnesium sulfate) and organic component (Tris-HCl) found in SM buffer as well as sugar (sucrose) addition in PVP polymer solutions on the viability and infectivity of the bacteriophage after electrospinning and freeze drying. We also examined the effect of storage conditions, namely temperature and humidity. In the last part of the study, the overall effects of ambient storage on bacteriophage viability of electrospun nanofiber mats and freeze dried powders were compared to phage stored in polymeric solutions. The information obtained in this study may provide valuable insights on the shelf life of dehydrated bacteriophage by electrospinning.

6.2 Materials and Methods

6.2.1 Materials

Polyvinylpyrrolidone (PVP) with an average molecular weight of 1,300,000 was purchased from Sigma-Aldrich (St. Louis, MO, USA). Sodium chloride, magnesium sulfate heptahydrate, agar, yeast extract and tryptone were purchased from Thermo Fisher Scientific (Waltham, MA, USA). *E. coli* BL21 was purchased from EMD Millipore (Billerica, MA). Wild-type bacteriophage T7 stock was purchased from ATCC (BAA-1025-B2, Manassas, VA). Deionised (DI) water was obtained from a Barnstead™ Nanopure™ water filtration system at a resistivity of 18.2 MΩ/cm.

6.2.2 Bacteriophage harvesting

E. coli BL21 was cultured in Luria broth (LB, 1% tryptone, 0.5% yeast extract, 1% NaCl, pH 7.5) at 37 °C, shaking for 16 h, with a final concentration of 10^9 CFU/mL. An aliquot (0.3 mL) of the bacterial culture was mixed with 3.0 mL of warm top agar (LB with 0.75% agar) and subsequently spread onto a Luria agar (LA) plate (LB with 1.5% agar) for incubation at 37 °C. After 4 h incubation, 0.5 mL of bacteriophage T7 stock solution (10^6 PFU/mL) was added on the surface of LA plate and incubated for 4 hours. During this incubation step, the plaques were grown until the plate became cleared. To harvest the bacteriophage, 5 mL of a storage medium buffer (SM buffer, 1 M Tris-HCl, 0.1 M NaCl, 8 mM $MgSO_4$, pH 7.5) was added to the plate and was gently swirled every 30 min for 2 hours at 4 °C. The suspension stock was then collected and passed through a 0.22 μm sterile syringe filter, resulting in a highly concentrated bacteriophage stock solution (10^{10}-10^{11} PFU/mL). The lysate activity of the suspension was determined by a double agar overlay plaque assay.

6.2.3 Bacteriophage polymeric solutions

PVP polymer solutions were prepared by dissolving 1.5 g PVP polymer in a combination of different solutions (8.9 mL) adjusted to a final pH of 7.5 (see Table 6.1. for all PVP polymers solution formulations). Bacteriophage stock solution (1.0 mL) and red food dye (0.1 mL; McCormick, Hunt Valley, MD), for quantification of the fiber mats[137], were added into the PVP solution and gently mixed for 30 min.

Table 6.1. Formulations of PVP polymer solutions for electrospinning and freeze drying.

Formulation	Polymer	Solution	Bacteriophage Stock Solution	Red Food Dye
DI Water	15% PVP	18.2 MΩ of DI water	1.0 mL	0.1 mL
NaCl	15% PVP	0.1 M NaCl	1.0 mL	0.1 mL
$MgSO_4$	15% PVP	8.0 mM $MgSO_4$	1.0 mL	0.1 mL
Tris-HCl	15% PVP	1.0 M Tris-HCl	1.0 mL	0.1 mL
SM Buffer	15% PVP	0.1 M NaCl, 8 mM $MgSO_4$, 1 M Tris-HCl	1.0 mL	0.1 mL
SM Buffer and Sucrose	15% PVP 5% sucrose	0.1 M NaCl, 8 mM $MgSO_4$, 1 M Tris-HCl,	1.0 mL	0.1 mL
Sucrose	5% sucrose	18.2 MΩ of DI water	1.0 mL	0.1 mL

6.2.4 Electrospinning

The prepared polymer solution was drawn into a 5 mL sterile plastic syringe with a blunt 25 gauge stainless steel needle. The syringe-needle setup was placed on a syringe pump (Fisher Model 78- 01001, Holliston, MA). The positive terminal of the high voltage source (ES30P-5 W, Gamma High Voltage Research, Ormond Beach, FL) was then attached to the needle portion (Fig. 6.2). The syringe pump was set at flow rate of 0.5 mL/h for 20 min with a spinning voltage of 25 kV. The distance between the needle tip and the grounded aluminum foil sheet (collector) ranged from 10 to 12 cm. The humidity in the electrospinning chamber was kept below 10% RH, as the partial vapor pressure of water

(water activity, a_w) of the nanofibers will rapidly equilibrate to the ambient humidity. Therefore, the drying process of the nanofibers is limited to the relative humidity of the surrounding environment. After 20 min of electrospinning, the fibers collected on the aluminum foil, here after known as fiber mats, were cut out evenly and stored in centrifuge tubes. The tubes were then vacuum packed (25 inHg) and sealed in bags containing desiccant. An eight week storage study of the fiber mats was conducted under different storage conditions at 20°C, 4°C, and -20°C with relative humidity of 1%, 33% and 75%.

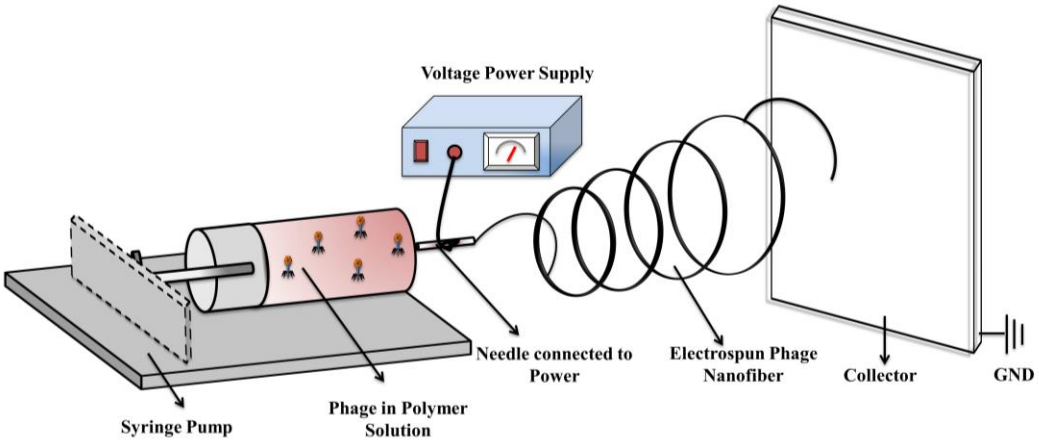

Fig. 6.2. Schematic diagram of electrospinning setup.

6.2.5 Freeze drying

The prepared polymer solutions were ten times diluted and pipetted into centrifuge tubes and were flash frozen with liquid nitrogen. The tubes were then dehydrated in a freeze dryer (Genesis Pilot Lyophilizer, SP Scientific, Warminster, PA) for 24 hours. Freeze dried powder tubes were vacuum packed (25 inHg) and sealed in bags containing desiccant. An eight week storage study of the freeze dried powder was conducted at 20°C at 1% RH.

6.2.6 Quantification of fiber mats and freeze dried powder[137]

Due to the difficulty of determining the mass of nanofiber mats and freeze dried powders, a red food dye was incorporated into the solution, in which absorbance was used as a measurement for the rehydrated solutions. A standard curve of the red food dye was constructed by plotting the absorbance at 523 nm at 100, 50 and 20 times diluted polymer solutions. Each of the dried samples (nanofiber mats and freeze-dried samples) was rehydrated in 0.5 mL SM buffer prior to absorbance measurements. The initial amount of bacteriophage in the samples were calculated according to the standard curve while the current viable bacteriophage counts were determined using a plaque assay test.

6.2.7 Quantification of bacteriophage viability

The plaque assay was used to quantify the amount of viable (active) phage after electrospinning and dehydration. A double agar overlay method was performed, where serial dilutions of the bacteriophage sample were prepared. An aliquot (100 μL) of each dilution was added to 300 μL *E. coli* BL21 overnight culture. Warm Luria top agar (3 mL) was added to the mixture and then poured onto an LA plate. After 3 h incubation at 37 °C, the number of plaques was counted for each dilution and reported as plaque forming units per mL (PFU/mL). Only dilutions that contained 25-250 plaques were counted.

6.2.8 Scanning electron microscopy

The morphology of the electrospun fibers was examined using scanning electron microscope (Magellan 400, FEI, Hillsboro, OR). The fibers were gold sputter coated for 35 s and imaged with an accelerating voltage of 5 kV. Diameters of the fibers were

analyzed using ImageJ software (n=12).

6.2.9 Statistical analysis

One-way analysis of variance (ANOVA) followed by Tukey's pairwise comparison (95% confidence interval, GraphPad Prism 6, La Jolla, CA) was used to determine statistical difference of fiber diameters between formulations after spinning and storage. All data points are calculated mean values (n=6) with error bars representing the standard deviations (SigmaPlot 12, San Jose, CA).

6.3 Results and Discussion

6.3.1 Bacteriophage nanofiber morphology

Electrospinning of bacteriophages dispersed in PVP polymer solutions containing different protectants produced nanofibers mats with fibers ranging from 100 to 200 nm in diameter (Table 6.2). In systems containing PVP (DI water) only or PVP with single salts (NaCl, $MgSO_4$, Tris-HCl), significantly thinner fibers (~100 nm) were produced when compared to systems with SM buffer and/or sucrose (~150 nm). In electrospinning, four key properties of the solution – i) conductivity, ii) surface tension, iii) dielectric properties, and iv) volatility, can affect the size and shape of the fibers[138]. In the presence of salts in buffer, such as NaCl, the solvent conductivity and charge density increases, which will increase the electrical distortion of the droplet shape and resulting in a thinner jet. With certain feeding rates of the solution, thinner jets can restrict the flow, which can lead to the formation of smaller fibers due to less solids reaching the collector[139]. In the presence of multiple salts, the surface tension of the solution increases and requiring a higher potential

to produce fibers[140-141]. This may explain the thicker fibers (150 to 200 nm) produced in systems containing SM buffer (Table 6.2).

Solid crystals were also observed on the surface of the nanofibers, with SM buffer system having the most salt crystals, as it contained all the individual salt components (Fig. 6.3). Similar salt crystal-forming phenomenon was also observed in a previous study[133] that used SM buffer in electrospinning bacteriophages. In the SM buffer and sucrose system, no apparent salt crystal was observed despite the presence of salts. This may be because the sucrose components formed a glassy outer layer on the nanofibers. Studies on spray dried and freeze dried microcapsules containing sugars have found that low molecular weight sugars form a glassy coating around the microcapsules upon rapid drying[142-145]. Moreover, the sucrose-containing systems produced significantly thicker fibers, which could be attributed to the glassy coating of sugar formed (Fig. 6.3, Table 6.2).

After 8 weeks storage at different temperatures, the diameters of all nanofibers were not significantly different (see Table 6.2 for diameters stored at 20°C, diameters stored at 4°C and -20°C are not shown). It was also observed that there were no signs of swelling or distortion of morphology in nanofiber mats (fiber mats spun with SM buffer or SM buffer/sucrose were chosen as representative formulations) (Fig. 6.4). However, at increased humidity of 33% RH, a significant average diameter increase was observed with SM buffer nanofiber mats (242 ± 32 nm) and a slight increase was observed for SM buffer/sucrose (206 ± 26 nm). Swelling, distortion and fusing at junctions were also evident in nanofibers spun with SM buffer stored at 33% RH (Fig. 6.5). At 75% RH, the morphology of the nanofibers for both formulations were distorted beyond recognition and

large fragments were formed (Fig. 6.5). The swelling and distortion of the fibers at elevated humidity were mainly due to water absorption of the nanofibers.

Table 6.2. Average nanofiber diameters of different formulations. Fibers were measured after electrospinning and after storage for eight weeks at 20°C and 1% RH.

Formulation	Fiber Diameter (nm)	Fiber Diameter after Storage (nm)
DI Water	105 ± 20^{a}	101 ± 17^{a}
NaCl	104 ± 15^{a}	101 ± 23^{a}
$MgSO_4$	107 ± 20^{a}	108 ± 28^{a}
Tris-HCl	114 ± 25^{a}	112 ± 22^{a}
SM Buffer	153 ± 41^{b}	151 ± 35^{b}
SM Buffer and Sucrose	175 ± 37^{b}	176 ± 25^{b}
Sucrose	161 ± 24^{b}	173 ± 39^{b}

Data within column sharing the same alphabetical superscript (a-b) are not statistically different ($p > 0.05$).

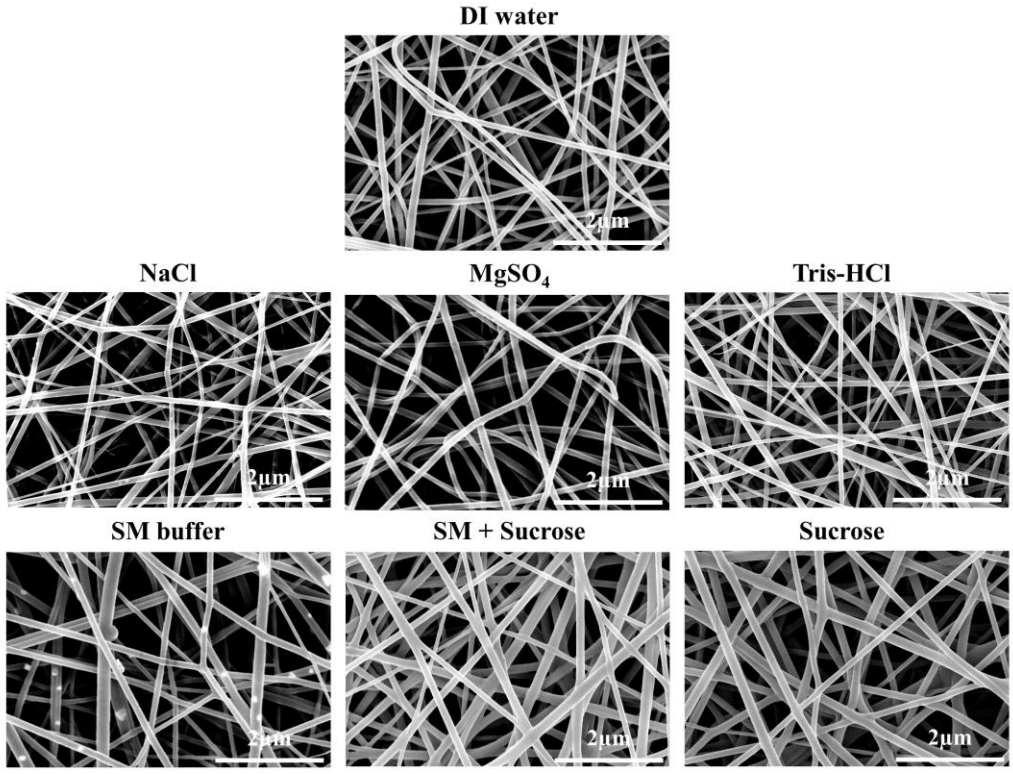

Fig. 6.3. Scanning electron micrographs (25k x magnification) of electrospun bacteriophage nanofibers formulated with salts and/or sugar protectants in PVP polymer solutions at Week 0.

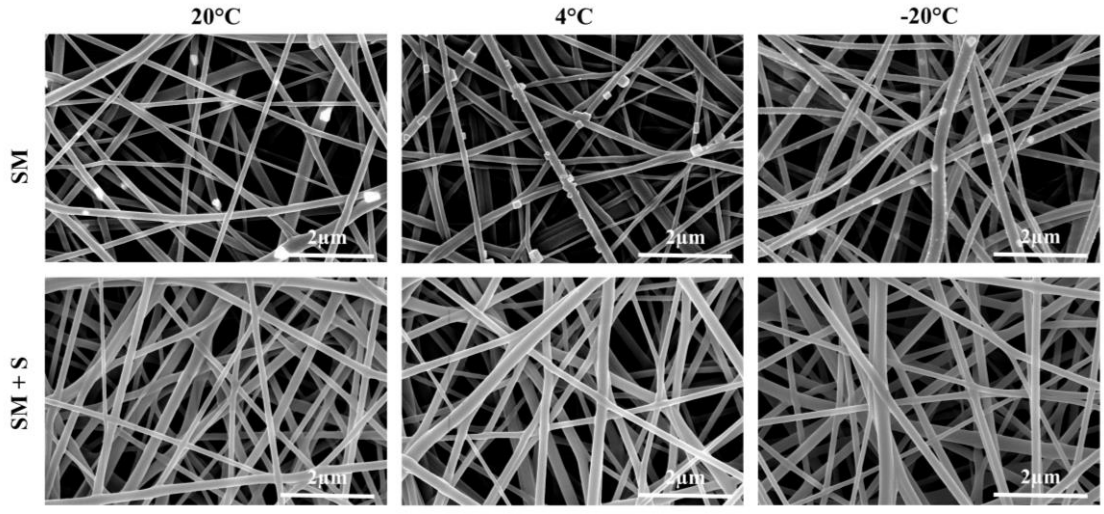

Fig. 6.4. Scanning electron micrographs (25k x magnification) of electrospun bacteriophage nanofibers (SM buffer, SM buffer/sucrose) stored at different temperatures (20°C, 4°C, -20°C) after eight weeks.

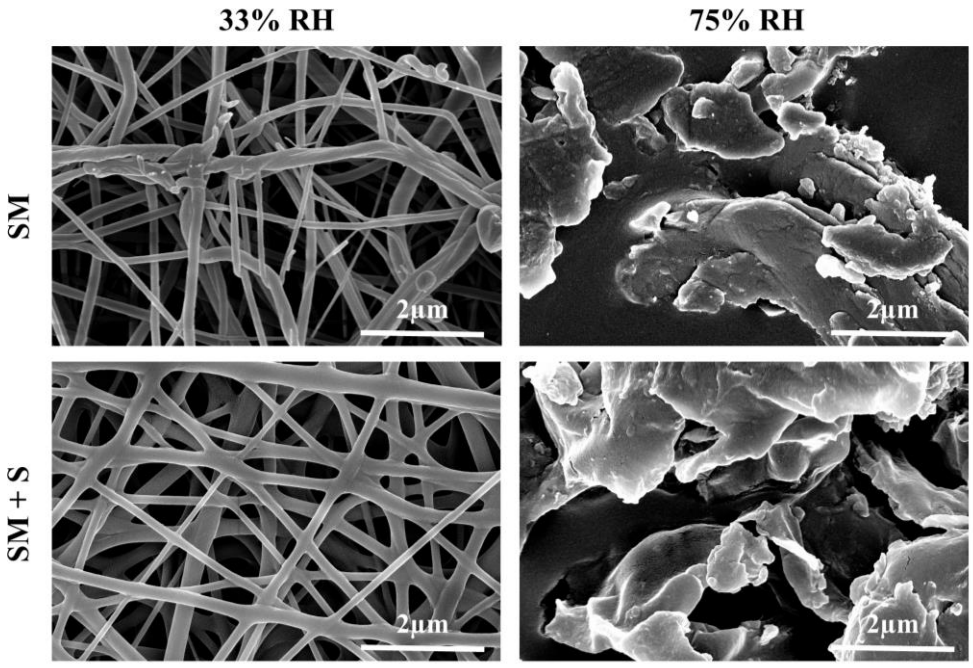

Fig. 6.5. Scanning electron micrographs (25k x magnification) of electrospun bacteriophage nanofibers (SM buffer, SM buffer/sucrose) stored at different humidity (33%, 75% RH) after eight weeks.

6.3.2 Effect of dehydration methods on bacteriophage viability

The effects of dehydration of polymeric solutions on the viability of bacteriophages, by electrospinning and freeze drying, were determined with a plaque assay before and immediately after drying. With freeze drying being the conventional method of drying, we compared the viability of phage in electrospun nanofiber mats to freeze dried polymeric powder. The overall assay results showed that both dehydration methods resulted in reduction of phage viability (Fig. 6.6). The phage activity of nanofiber mats indicated that formulations with DI water, NaCl, $MgSO_4$ and Tris-HCl (single salts) had log reductions ranging from 2.5 to 3, while formulations of SM buffer and/or sucrose (multiple components) had reductions less than 2 logs. The rapid dehydration process of electrospinning was detrimental to the viability of phage due to the high voltage and

mechanical shear stress of spinning[133] inflicted on the fragile tail structure of bacteriophage T7. Previous studies have shown that without protection of polymers, salts and sugars in the electrospinning solution, large decreases of viability of the phage were observed immediately after dehydration[137], which was also observed in our DI water systems (Fig. 6.6).

The smaller reduction of viability in SM buffer fiber mats suggests that the combination of salts in SM buffer may have provided a synergistic effect in protecting phage from sudden osmotic changes. In the single salt systems, Tris-HCl conferred higher protective effect on the phages than NaCl and $MgSO_4$, which may be due to decreased free water molecules via hydrogen bonding and trapping of water molecules around the Tris salts. As for systems containing sucrose, there seems to be a protective effect against the rapid dehydration of electrospinning compared to DI water. It is well known that disaccharides, such as sucrose and trehalose, improves protein stability during freezing and dehydration as they are lyoprotectants[144-145]. During the rapid dehydration of electrospinning, sucrose may form hydrogen bonds with polar sites on the protein coat of the phage, which will stabilize and immobilize the native structure of the protein[146]. This phenomenon is called the "water substitute hypothesis" and is used to rationalize the role of solutes in stabilizing proteins during dehydration and storage[147-149].

All freeze dried systems had less than one log reduction of phage viability, except for magnesium sulfate formulation, where more than 2.5 log reduction was observed (Fig. 6.6). In comparison to electrospinning, all of the corresponding freeze dried powders had significantly less reduction of phage activity after drying. This is because freeze drying has a milder dehydration process as it does not involve high potentials and extreme shear

stress on the solution. Furthermore, freeze dried powders have less surface area exposed than electrospun nanofiber mats, which decreases the exposure of bacteriophage to the environment. We also observed that magnesium sulfate had a significant decrease in viability compared to all of the other formulations. Mg^{2+}, a divalent cation, is known to coagulate and denature proteins by binding with the hydrophobic sites and disrupting the native conformation of the protein. Thus, it is possible that the protein coat of bacteriophage could be disrupted by the magnesium ions and was further exacerbated by the removal of water (H-bonds) during dehydration.

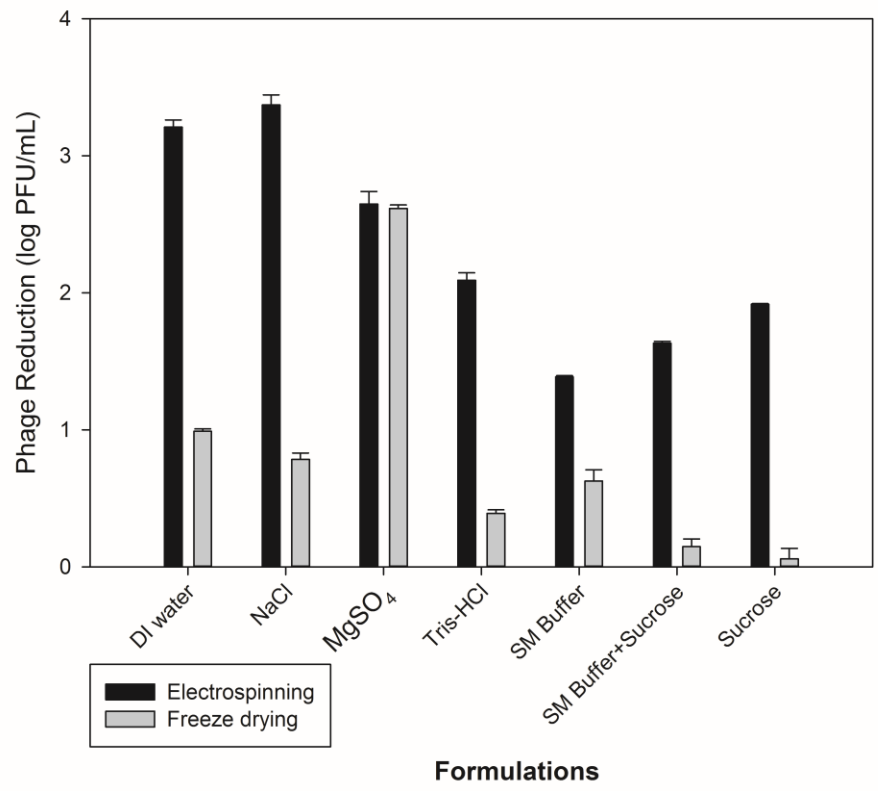

Fig. 6.6. Comparison of dehydration methods – electrospinning vs. freeze drying on the effect of bacteriophage viability in different formulations. All data points are calculated mean values (n=6) with error bars representing the standard deviations.

6.3.3 Effect of storage on bacteriophage viability

In the next part, we examined the effect of eight weeks of storage (20°C/1% relative humidity) on the viability of electrospun and freeze dried bacteriophages. Overall, there was a decreasing trend in phage activity over 8 weeks of storage for both electrospun and freeze dried phage. With the nanofiber mats, most of the activity loss was seen in the first two weeks of storage (Fig. 6.7.a, 6.7.b). Overall, SM buffer with sucrose had the smallest decrease, with less than one log reduction of activity at the end of 8 weeks. In this case, the combination of salts and the "glassy dynamics" hypothesis of sucrose provided the best protection of the electrospun bacteriophage. Studies have shown that addition of sugar during dehydration results in the formation of a rigid glassy matrix (amorphous state), which forces proteins in the system to be molecularly dispersed and separated[146]. The limited mobility in the rigid glassy matrix also reduces the motion of protein that is necessary for degradation. Consequently, this resulted in better stability of the phage protein coat during storage, as the proteins are held in its native conformation. Furthermore, the salts in SM buffer may have formed hydrogen bonds with free water molecules and acted as substitutes/fillers when the water was removed. In single salt systems, magnesium sulfate performed the worst, with more than 4 logs of activity reduction at the end of 8 weeks. This could be because the disruption of the protein coat by magnesium ions was further exacerbated over time.

For the freeze dried powder, there was less than one log of reduction of activity over 8 weeks for all formulations (Fig. 6.7.c, 6.7.d). This again shows that freeze drying retained more phage activity than electrospinning for both storage and dehydration. However, when comparing SM buffer with sucrose for both nanofiber mats and freeze

dried powders, the reduction over storage time was within the same order of magnitude (one log). This suggests that SM buffer and sucrose would provide adequate protection for the bacteriophage upon dehydration by electrospinning.

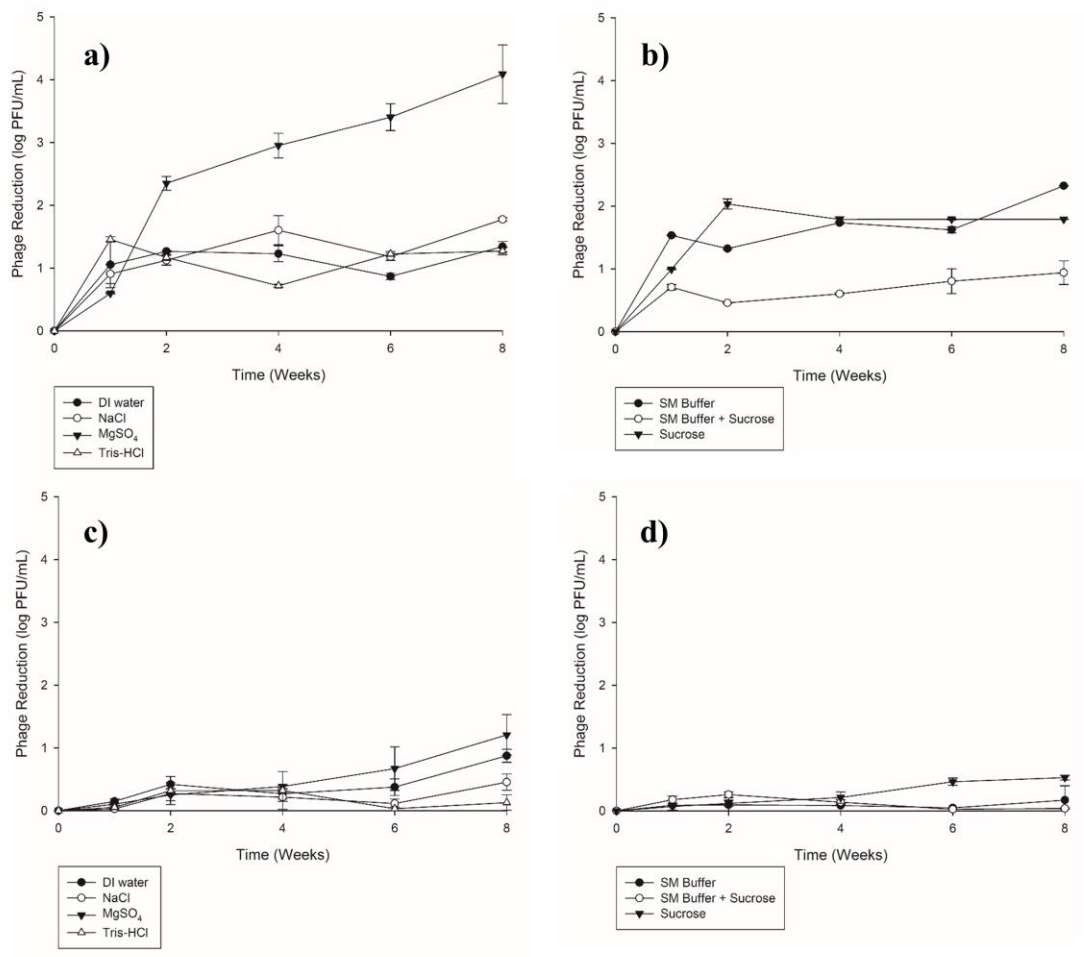

Fig. 6.7. Effect of storage (at 20°C, 1% RH) on bacteriophage viability over 8 weeks between a-b) electrospinning and c-d) freeze drying. All data points are calculated mean values (n=6) with error bars representing the standard deviations.

6.3.4 Effect of storage temperature on bacteriophage viability

We also determined the effect of storage temperatures (20°C, 4°C,-20°C) on the viability of electrospun bacteriophage over 8 weeks at 1% RH (lowest possible humidity). In Figure 6.8, we observed that as the storage temperature decreases, more phage activity was retained. This is related to the decrease in molecular mobility of solutes at lower temperatures[150], thus stabilizing the protein coat and tail fibers of bacteriophage by its restricting motion. This is apparent especially at subzero temperatures (-20°C), where all formulations resulted in less than one log reduction of activity (except sucrose). Studies have shown that using bulky polymers, such as PVP, can decrease freezing stress exhibited on proteins[145]. This is evident with polymeric solutions using DI water and 0.1 M NaCl as solvents, where they retained the most activity with no significant difference over eight weeks of storage stored at -20°C. Furthermore, the systems containing sucrose had more than one log reduction in activity (Fig. 6.8). This may be because addition of sucrose to PVP had been proven to decrease the glass transition temperature, which may have reduced the glassy state of the polymer[151], and hence rendering it less protective on the bacteriophage.

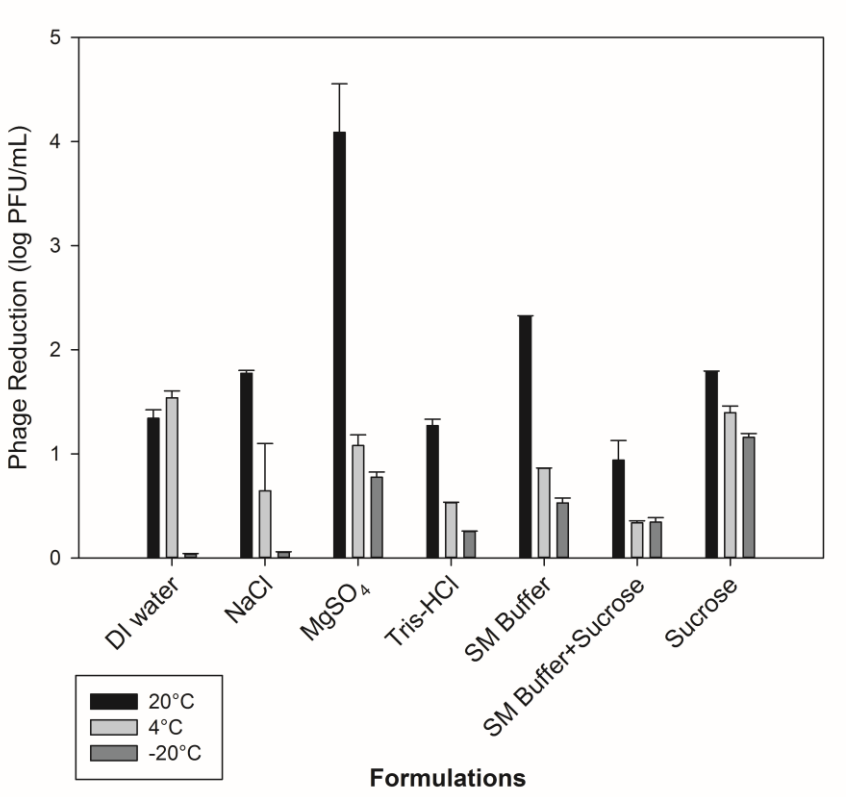

Fig. 6.8. Effect of temperature (20°C, 4°C,-20°C) on bacteriophage viability after 8 weeks of storage at 1% RH. All data points are calculated mean values (n=6) with error bars representing the standard deviations.

6.3.5 Effect of storage humidity on bacteriophage viability

Study on the effect of storage humidity (1%, 33% and 75% RH; at 20°C) on phage viability of electrospun nanofiber mats was also conducted. According to the previous sections, SM buffer/sucrose nanofiber mats retained the highest activity out of all the formulations. Therefore, this formulation and SM buffer, as a control, were selected for humidity studies. The results showed that the largest significant drop in phage activity occurred in the first week of storage in all three humidity conditions (Fig. 6.9). The activity also decreased with increasing relative humidity. When the water soluble nanofibers were placed in a high moisture environment, the nanofibers were partially re-solubilized, causing

the dried polymers and sugars to be plasticized[144]. The change from glassy state to a rubbery state may have led to increased mobility within the fibers that resulted in the destabilization and reduced activity of the bacteriophage[145, 151]. Among the two formulations, the SM buffer/sucrose mats out performed SM buffer mats for all relative humidity, with approximately less than one log reduction for 1% and 33% RH by the end of Week 8 (Fig. 6.9). This could be because the addition of sucrose to the fibers during electrospinning produced a glassy outer crust (Fig. 6.5), which served as protection against moisture and other environmental factors, such as changes in temperature. However at 75% RH, both formulations had more than five log reduction in phage activity with only one week of storage. At this humidity, the nanofibers in both formulations were completely re-solubilized and were no longer intact (Fig. 6.5), which caused the bacteriophages to be exposed.

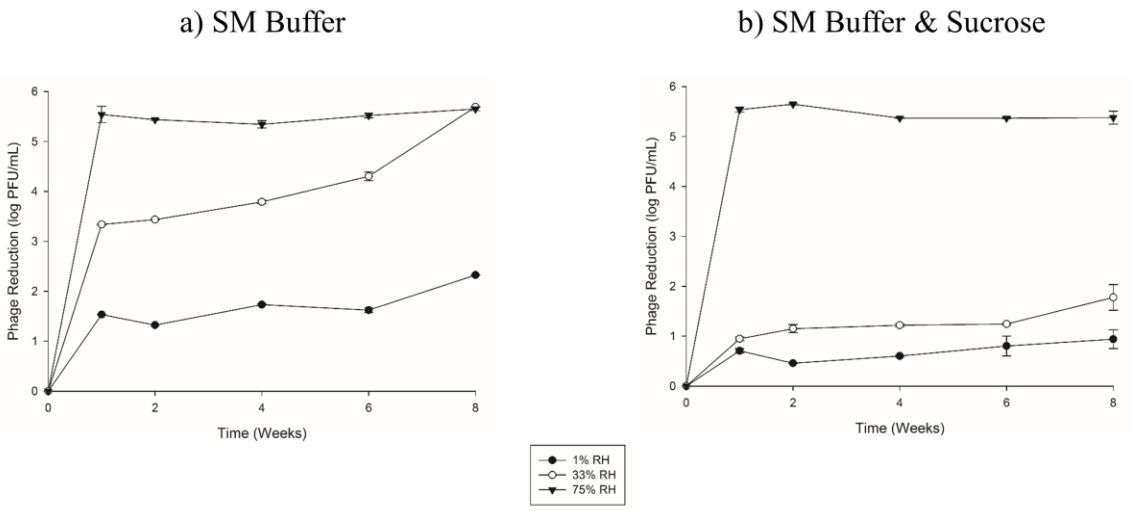

Fig. 6.9. Effect of relative humidity (1%, 33%, 75% RH) on bacteriophage viability over 8 weeks of storage at 20°C. All data points are calculated mean values (n=6) with error bars representing the standard deviations.

6.3.6 Potential application of electrospun bacteriophage nanofiber mats

Dehydrating bacteriophage for transportation and storage improves portability and convenience for the user when compared to storing phage in liquid solutions. It is especially important that dehydrated phage can be stored at ambient temperatures (e.g. 20°C) over an extended period of time (e.g. 8 weeks) and yet retain adequate viability for infection. In Figure 6.10, the effect of ambient storage (20°C, 1% RH) over eight weeks on bacteriophage viability of electrospun nanofiber mats and freeze dried powders were compared to phage stored in polymeric solutions. Overall, freeze dried powders retained highest activity during storage compared to both electrospun nanofibers and polymeric solutions. The results further suggest that the bulk of phage viability is lost during dehydration processes, which is most pronounced with electrospinning. Viability loss could be overcome by experimenting with mixtures of different polymers and excipients in future studies. Furthermore, all three storage methods with SM buffer/sucrose retained the most viability over eight weeks - all with less than one log reduction in activity. Although there is a significant difference between the three systems, there is still sufficient bacteriophage viability retained in the electrospun nanofiber mats for infection. With high activity retained (10^6-10^7 PFU/mL) after 8 weeks storage at ambient temperature in nanofiber mats, the study shows that there is potential for bacteriophage fiber mats to be mass produced and commercialized into the more convenient and cost effective dried form.

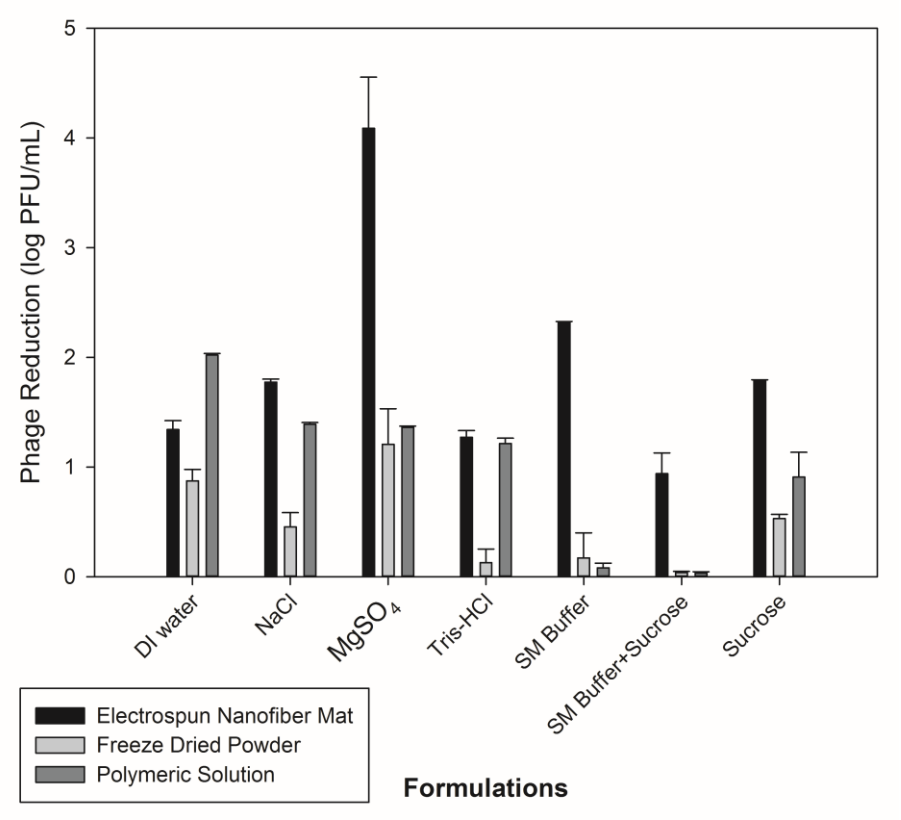

Fig. 6.10. Effect of ambient storage (20°C, 1% RH) on bacteriophage viability over eight weeks in three different storage systems (electrospun nanofiber mat, freeze dried powder and polymeric solution). All data points are calculated mean values (n=6) with error bars representing the standard deviations.

6.4 Conclusion

Preservation of bacteriophage in dried form can reduce the inconvenience and cost of transportation and storage. Freeze-drying is a commonly used method for drying, but is time and energy-consuming and requires large machinery, which makes the process expensive. Hence, in this study, we examined the potential benefits of electrospinning bacteriophage in polyvinylpyrrolidone (PVP) polymer solution. Bacteriophage nanofibers with diameter of approximately 100 to 200 nm were produced rapidly by electrospinning. However, the use of high voltage for rapid dehydration reduced the viability of bacteriophages. This detrimental effect was effectively reduced with the addition of SM

buffer and sucrose in the PVP polymer solution due to the protective effect provided by the salts and the glassy sugar layer formed when spinning. This formulation also provided best protective effect over extended storage time by lessening extreme environment fluctuation on the dried phages. Storage temperature had minimal effect on the viability of bacteriophages while relative humidity had a greater effect - with high relative humidity (33% and 75%) causing absorbance of water and swelling of the fibers, resulting in viability reduction. The overall study demonstrated the potential use of electrospinning in rapid dehydration of bacteriophages. The information obtained may provide insights on preservation of dried bacteriophage, which may have applications in decontamination of agricultural rinse water.

APPENDICES

APPENDIX A

SUPPLEMENTARY INFORMATION FOR CHAPTER 3

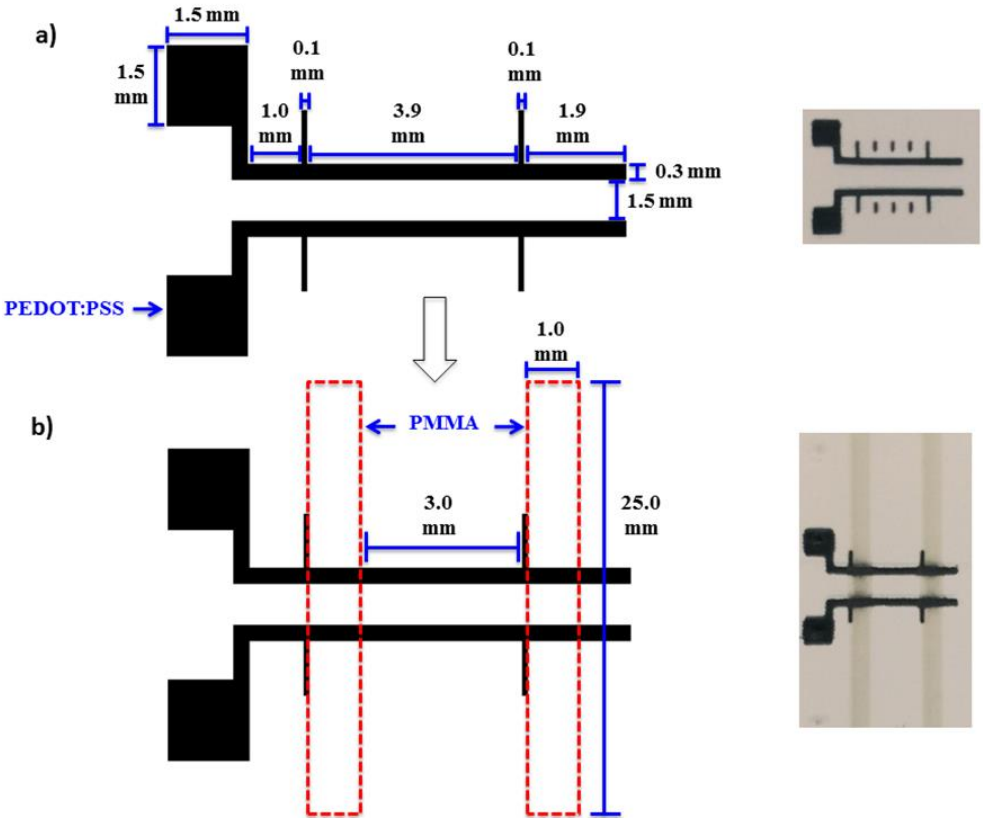

Fig. A.1. Schematic diagram and images of a) PEDOT:PSS test strips b) PEDOT:PSS test strips with printed PMMA barriers.

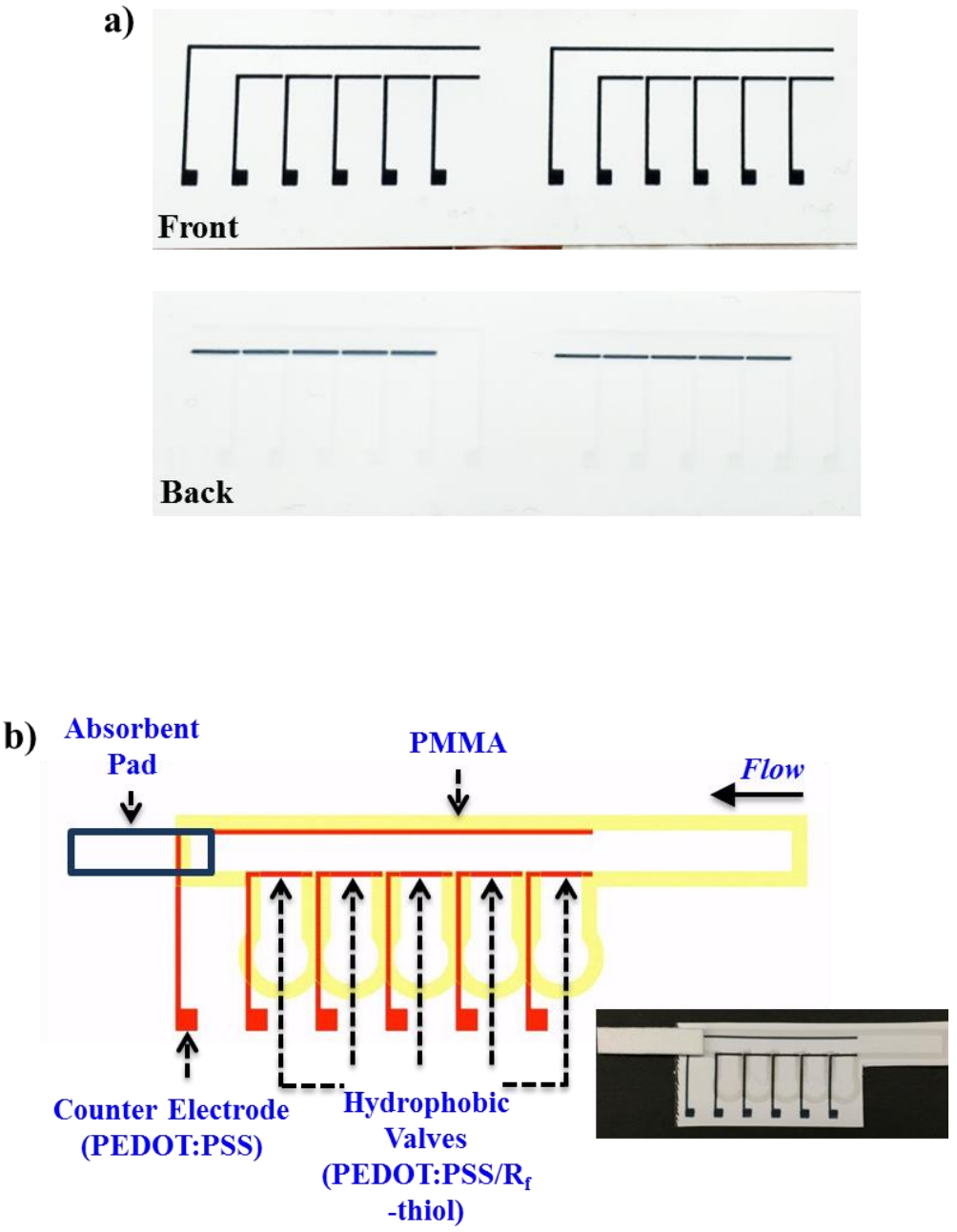

Fig. A.2. a) Inkjet-printed PEDOT:PSS electrodes on the front and back side of nitrocellulose. b) Schematic diagram of multi-valve paper-fluidic device.

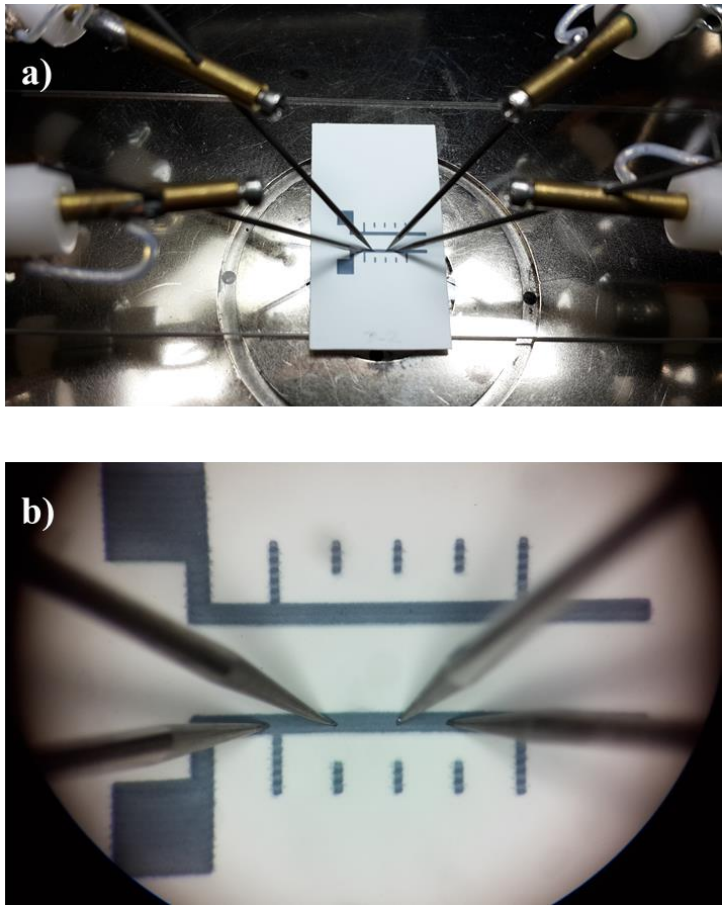

Fig. A.3. a) Setup of the four-point probe sheet resistance measurements. b) Fiducial lines spaced 1 mm apart ensures that the four probes are equidistant. Magnification from the light microscope aids with the placement of the probes on the surface of the nitrocellulose.

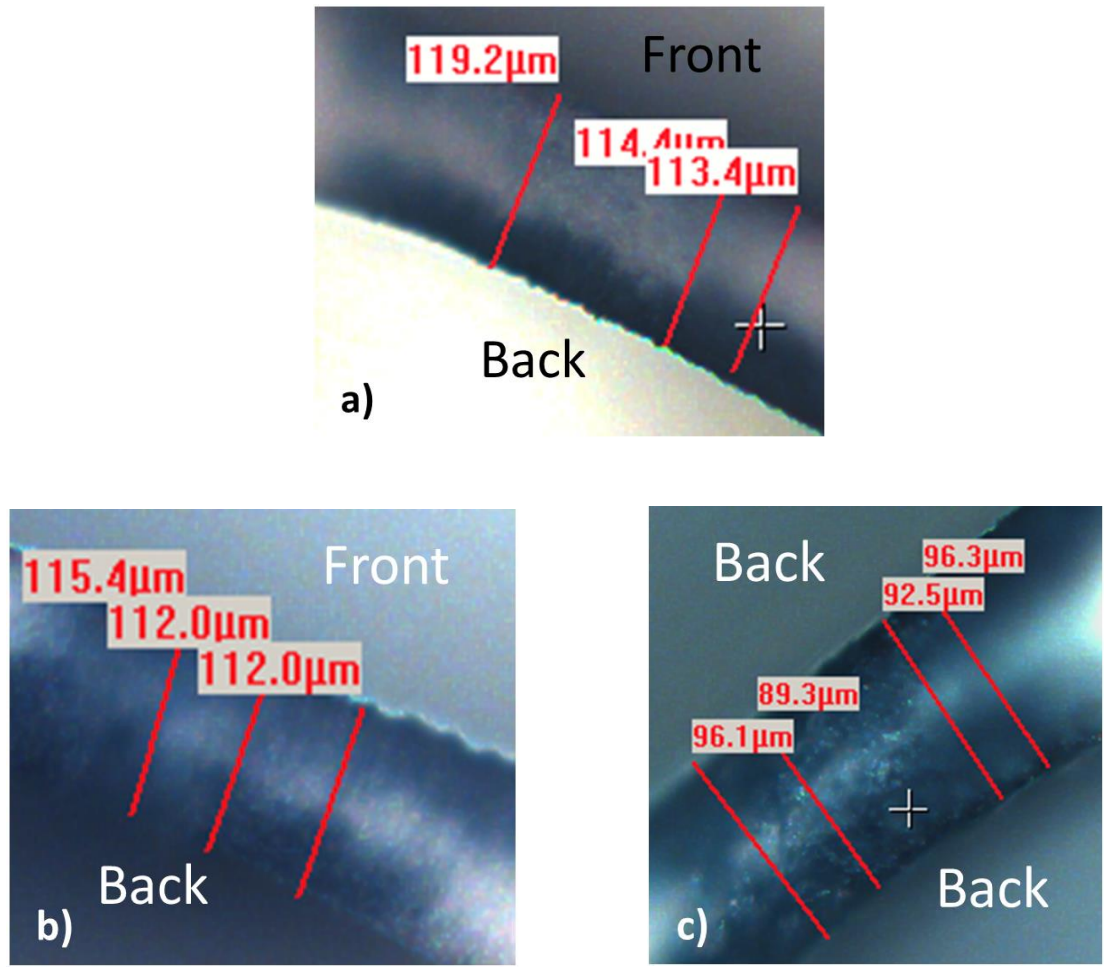

Fig. A.4. Optical micrographs of inkjet-printed PEDOT:PSS electrode cross sections. Fifteen layers were printed on the front and a) 4 layers, b) 6 layers, and c) 10 layers on the back.

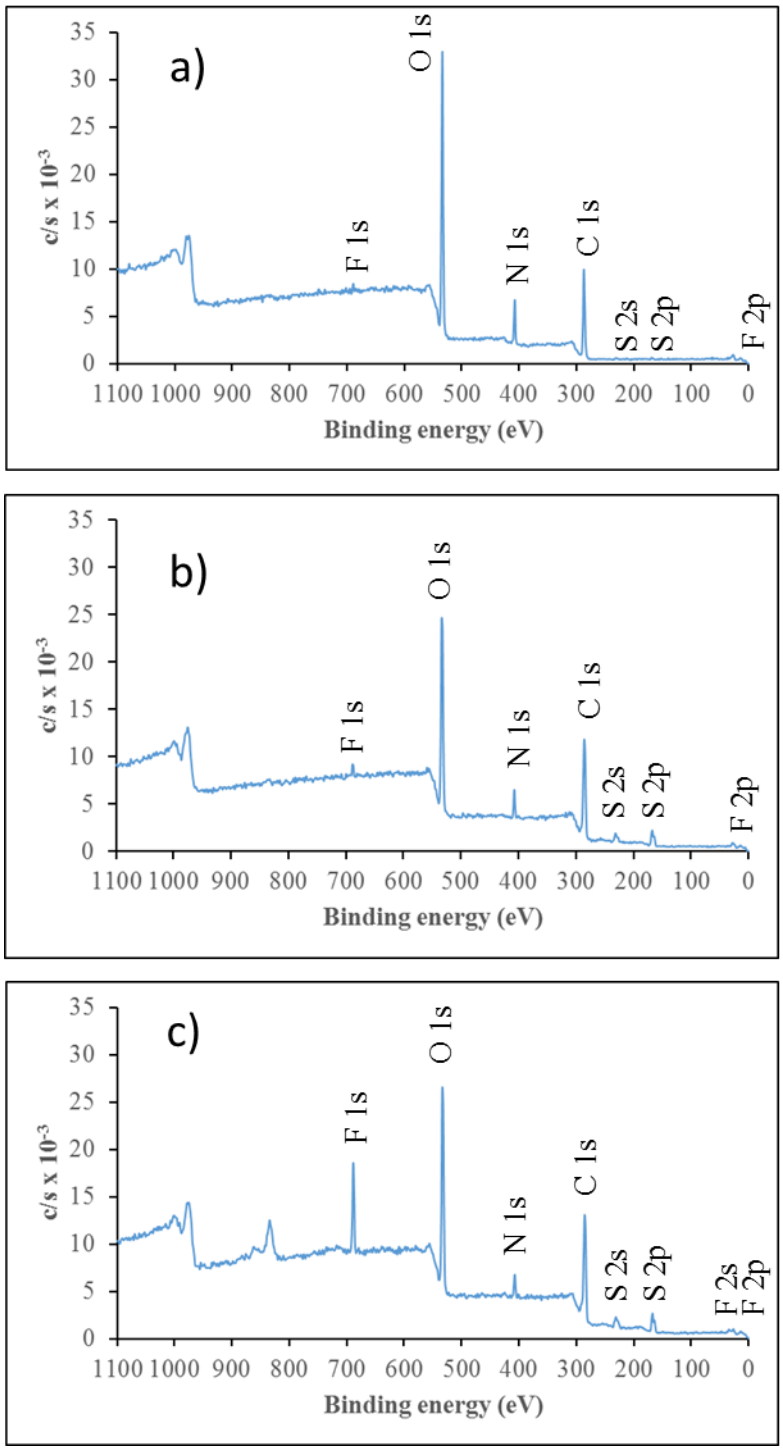

Fig. A.5. XPS survey spectra of a) nitrocellulose membrane, b) PEDOT:PSS on nitrocellulose, c) PEDOT:PSS with R_f-thiol.

APPENDIX B

FUNCTIONALIZATION OF INKJET-PRINTED PEDOT:PSS ELECTRODES WITH ELECTRODEPOSITED GOLD NANOPARTICLES

B.1 Introduction

Gold was electrodeposited on inkjet patterned PEDOT:PSS to show its potential use in an electrochemical detection. The main advantages with gold electroplating are that high sintering temperatures are not needed and gold nanoparticles attach to the surface of the electrode throughout the pores of the paper. This allows for more surface area for binding to analytes. Surface chemistry of the electrodes were determined and quantified by X-ray photoelectron spectroscopy (XPS). With the many advantages of inkjet printing PEDOT:PSS over inkjet printing metal-based inks, we believe that it is possible to fabricate more stable and effective paper-fluidic devices.

B.2 Materials and Methods

B.2.1 Fabrication and characterization of PEDOT:PSS electrodes

Materials and methods used for the fabrication and characterization of PEDOT:PSS electrodes are described in Chapter 3 (Section 3.2).

B.2.2 Electrodeposition of gold on PEDOT:PSS electrodes

In order to deposit gold on the PEDOT:PSS electrodes, 200 μL of chloroauric acid (3 mM $HAuCl_4$ and 0.1 M KCl in deionized water) was deposited on the conductive polymer (Fig. B.1). The PEDOT:PSS electrodes (cathode) and a platinum wire (0.25mm, 9.997%, Premion) (anode) were connected to a multimeter and an applied potential of

200mV was passed through the solution for a varied amount of time. The electrodes were then washed with copious amounts of deionized water and allowed to dry in a desiccated container.

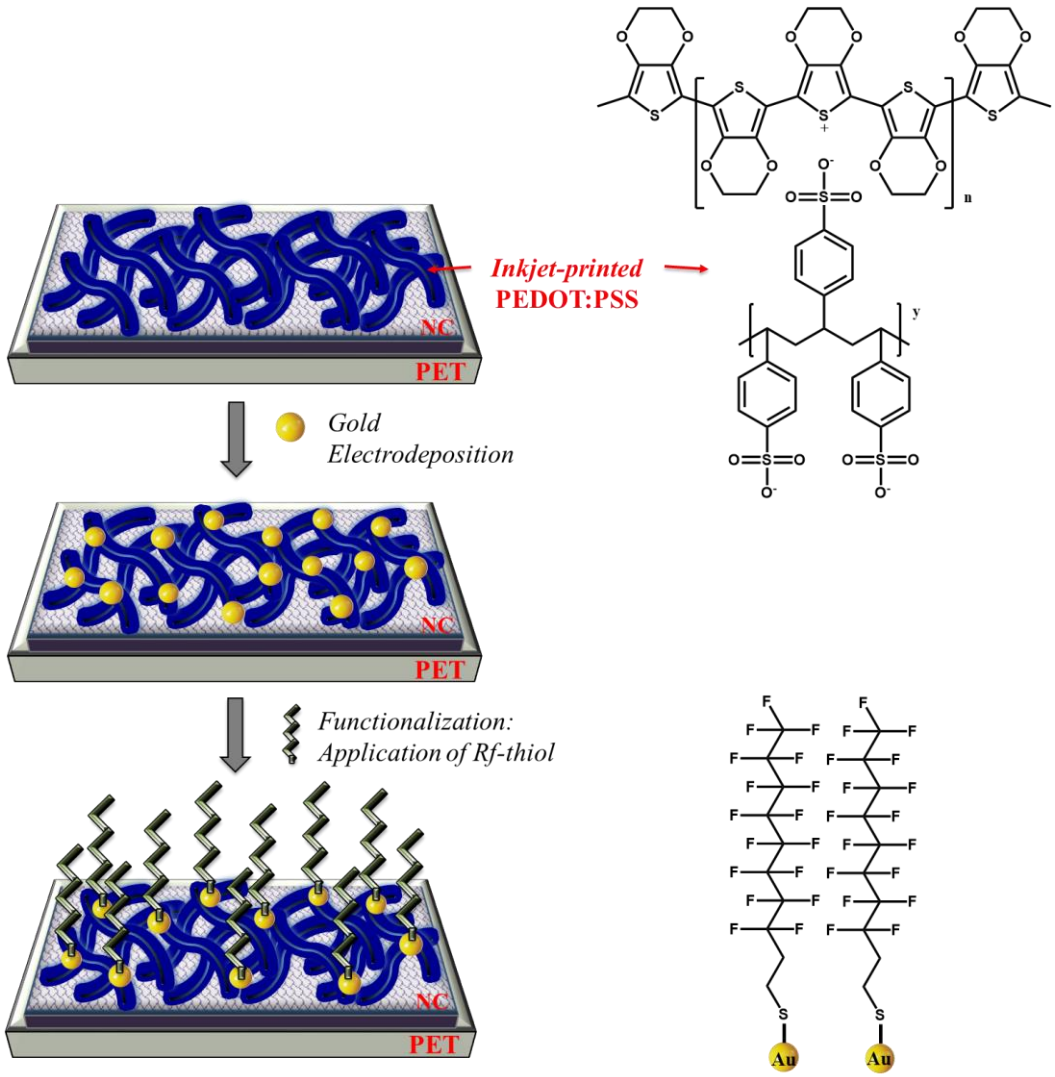

Fig. B.1. Schematic diagram of electrodeposition of gold on inkjet-printed PEDOT:PSS and the chemisorption of R_f-thiol on the Au nanoparticles.

B.3 Results and Discussion

B.3.1 Functionalization of electrodes with gold nanoparticles

As aforementioned, conducting polymers can be functionalized with noble metals (*e.g.,* gold, platinum or silver) due to their favorable electron transfer kinetics and chemical stability for molecular recognition or electrocatalytic reactions[89, 152]. In this part of work, we examined the feasibility of functionalizing the electrodes with gold by electrodeposition prior to thiolation. The deposition of gold nanoparticles (without high annealing temperature) onto the PEDOT:PSS surface not only increased the conductivity of the electrode (Fig. B.2), but it also created a higher surface area for binding sites. The SEM micrographs show that the gold nanoparticles on the surface of the coated electrodes had average diameters of about 101 nm (Fig. B.2). The gold nanoparticles were formed with a mixture of individual particles and agglomerates on the electrode surface. The micrographs also show that increasing electrodeposition time increases the amount of gold deposited on the surface. Electrodeposition of gold nanoparticles on the three-dimensional porous structure nitrocellulose may further enhance the electrochemical signal on the electrode surface compared to electrodes with lower surface area or without gold deposition.

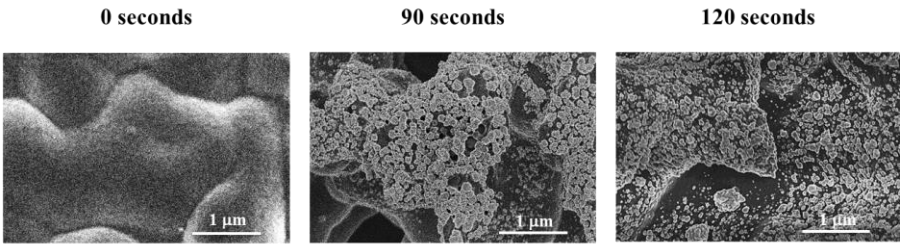

	0 seconds	90 seconds	120 seconds
Conductivity (S/m):	31.60 ± 0.9031	37.91 ± 1.445	41.03 ± 2.502
Mean Diameter (nm):	N/A	101.1 ± 14.13	106.6 ± 13.25

Fig. B.2. SEM micrographs of electrodeposited gold on PEDOT:PSS electrodes with conductivity (S/m) and average Au nanoparticle diameter (nm) in relation to amount of electrodeposition time (seconds).

After gold deposition, the Au-coated electrodes were also thiolated on the surface to form a self-assembled thiol layer. It is well known that thiol headgroups readily adsorb to the surface of gold, forming a well ordered and stable layer[153-154]. It is also proven that gold is a stable metal that has a high affinity for thiols and is compatible with cells[155]. Researchers have used this phenomenon to their advantage by using SAMs to interact with biological nanostructures such as proteins[155]. Contact angle was measured to determine the effects of the thiolated layer on wettability (Table B.1). The data suggests that gold electroplated electrodes were more hydrophobic than bare PEDOT:PSS electrodes, which is expected as pure gold is reported to exhibit a water contact angle of 55° to 85°[156]. After the addition of R_f-thiol, both electroplated electrodes (90 and 120 seconds) had contact angles greater than 90°, which suggest that the surfaces were hydrophobic. When more gold (increase in reaction time) was deposited, it created more surface area on the electrodes for thiol to bind to the nanoparticles. As a result, this creates a more densely packed fluorocarbon layer and increases the hydrophobicity of the surface.

Table B.1. Advancing water contact angle of gold electroplated PEDOT:PSS electrodes and gold electroplated with R_f-thiol applied on PEDOT:PSS electrodes.

Treatment	Electrodeposition Time (seconds)	Advancing contact angle (degrees)
Control (PEDOT:PSS)	0	26.1 ± 9.59
Electroplated Au	90	86.7 ± 8.24
Electroplated Au (R_f-thiol)	90	94.5 ± 4.90
Electroplated Au	120	88.8 ± 9.52
Electroplated Au (R_f-thiol)	120	127.7 ± 9.75

The surface chemistry of the Au-coated electrodes were quantified by X-ray photoelectron spectroscopy (XPS). Both survey scans and high resolution scans for C 1s, N 1s, O 1s, F 1s, S 2p and Au 4f were performed to quantify the change in surface atomic composition and specific bond formation after electrodeposition of gold and the subsequent thiolation. Table B.2 shows the distribution of the atomic concentrations of the gold electrodeposited PEDOT:PSS electrodes with the application of R_f-thiol, while S5 shows the intensity of each of the atomic peaks. 7.2% of Au was detected on the Au-coated PEDOT:PSS. However, after application of R_f-thiol no gold was detected but an increase of fluorine was measured due to addition of fluorinated thiol. When a take-off angle of 45° was used, the applied beam has an analysis depth of approximately 2.5 nm. This suggests that the thickness of the fluorocarbon layer is greater than 2.5 nm, which coincides with the absence of Au in the sample.

Table B.2. Atomic concentrations of gold electrodeposited PEDOT:PSS electrodes with R_f-thiol obtained from XPS (%).

Treatment	C	O	N	S	F	Au
PEDOT:PSS	53.2	37.6	4.7	3.9	0.6	--
Au/PEDOT:PSS	48.9	39.9	1.7	--	2.4	7.2
Au/PEDOT:PSS/R_f-thiol	40.8	40.8	9.2	0.7	8.6	--

To further confirm that the thiolated fluorocarbon was bound onto the electrodeposited Au, high resolution XPS scans for sulfur (S_{2p}) and fluorine (F_{1s}) were performed. The analysis of sulfur showed that the intensity of the peaks at binding energies, 162.2 eV and 163.0 eV (Fig. B.3.a) suggest that there was sulfide linkage with gold as $S_{2p3/2}$ and $S_{2p1/2}$ peaks for thiols bound to Au are known to be 162 eV and 163.2 eV respectively[93-94]. Conversely, the sulfur peak for unbound thiols appear at 164.2 eV (Fig. B.3.a), where $S_{2p3/2}$ and $S_{2p1/2}$ are known to be around 164 eV and 165 eV, respectively[93]. Furthermore, the analysis showed that there were distinct intensity changes in the electrodes for fluorine after the deposition of R_f-thiol, as there was an increase in fluorinated carbons, with a peak observed at 688.0 eV (Fig. B.3.b). The distinct peak of fluorine and the large background noise of the sulfur spectrum suggest that a multilayer of R_f-thiol had formed after application. The XPS beam can only penetrate 2.5 nm of a flat surface, which may be the reason that the long chained fluorocarbons were detected in greater intensity than the bound thiols on gold. Furthermore, the uneven nature of the electrodeposited gold increased the effect of multilayering of the R_f-thiol.

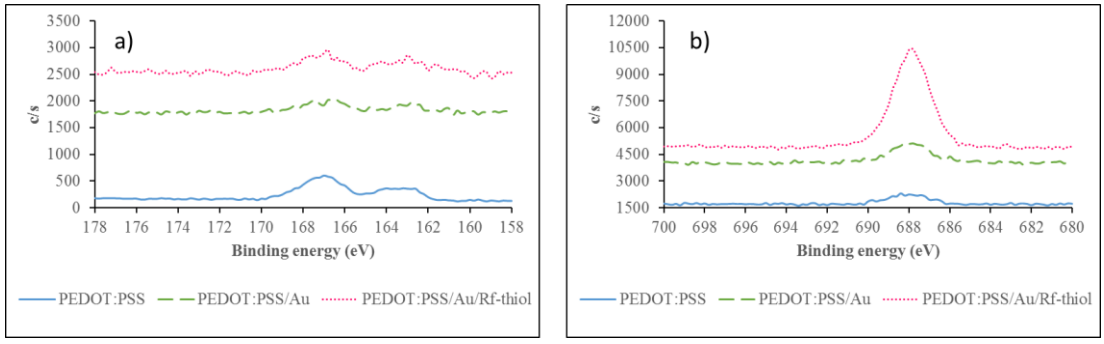

Fig. B.3 High-resolution XPS data for PEDOT:PSS, electrodeposited Au on PEDOT:PSS, and electrodeposited Au on PEDOT:PSS with R_f-thiol for a) sulfur (S_{2p}) and b) fluorine (F_{1s}).

B.4 Conclusion

With the need of more portable, inexpensive, easy to use and rapid diagnostics, many approaches have been used to produce paper fluidic devices, with inkjet printing being a popular method due to its low cost fabrication and effective patterning in recent years. This project revolves around the characterization and application of inkjet printable PEDOT:PSS on paper. In this study, we were able to electrodeposit gold onto inkjet-printed PEDOT:PSS, then effectively bind a thin film of alkanethiol onto the gold nanoparticles. Furthermore, XPS analysis, sheet resistance measurements, SEM microscopy, contact angle measurements were used to characterize the functionalized electrodes. We showed that these electrodes had the potential to be used in an electrochemical setup on paper. Therefore, future studies will be focused on the detection and diagnostics of diseases commonly found in low resource settings.

BIBLIOGRAPHY

1. Sabour, P. M.; Griffiths, M. W., *Bacteriophages in the Control of Food- and Waterborne Pathogens*. ASM Press: **2010**.

2. Alocilja, E. C.; Radke, S. M., Market analysis of biosensors for food safety. *Biosensors and Bioelectronics* **2003,** *18* (5–6), 841-846.

3. Martinez, A. W.; Phillips, S. T.; Whitesides, G. M.; Carrilho, E., Diagnostics for the Developing World: Microfluidic Paper-Based Analytical Devices. *Analytical chemistry* **2009,** *82* (1), 3-10.

4. Rivet, C.; Lee, H.; Hirsch, A.; Hamilton, S.; Lu, H., Microfluidics for medical diagnostics and biosensors. *Chemical Engineering Science* **2011,** *66* (7), 1490-1507.

5. Martinez, A. W.; Phillips, S. T.; Carrilho, E.; Thomas, S. W.; Sindi, H.; Whitesides, G. M., Simple Telemedicine for Developing Regions: Camera Phones and Paper-Based Microfluidic Devices for Real-Time, Off-Site Diagnosis. *Analytical chemistry* **2008,** *80* (10), 3699-3707.

6. Weibel, D. B.; Whitesides, G. M., Applications of microfluidics in chemical biology. *Current opinion in chemical biology* **2006,** *10* (6), 584-91.

7. Nie, Z.; Deiss, F.; Liu, X.; Akbulut, O.; Whitesides, G. M., Integration of paper-based microfluidic devices with commercial electrochemical readers. *Lab on a chip* **2010,** *10* (22), 3163-9.

8. Dungchai, W.; Chailapakul, O.; Henry, C. S., Electrochemical detection for paper-based microfluidics. *Analytical chemistry* **2009,** *81* (14), 5821-6.

9. Whitesides, G. M., The origins and the future of microfluidics. *Nature* **2006,** *442* (7101), 368-73.

10. Wen, Y.; Yang, S.-T., The future of microfluidic assays in drug development. **2008**.

11. Whitesides, G. M., Cool, or simple and cheap? Why not both? *Lab on a chip* **2013,** *13* (1), 11-3.

12. Rolland, J. P.; Mourey, D. A., Paper as a novel material platform for devices. *MRS Bulletin* **2013,** *38* (04), 299-305.

13. Liana, D. D.; Raguse, B.; Gooding, J. J.; Chow, E., Recent advances in paper-based sensors. *Sensors* **2012,** *12* (9), 11505-26.

14. O'Farrell, B., Evolution in Lateral Flow–Based Immunoassay Systems. **2009**, 1-33.

15. Fridley, G. E.; Holstein, C. A.; Oza, S. B.; Yager, P., The evolution of nitrocellulose as a material for bioassays. *MRS Bulletin* **2013,** *38* (04), 326-330.

16. Maxwell, E. J.; Mazzeo, A. D.; Whitesides, G. M., Paper-based electroanalytical devices for accessible diagnostic testing. *MRS Bulletin* **2013,** *38* (04), 309-314.

17. Connelly, J. T.; Rolland, J. P.; Whitesides, G. M., "Paper Machine" for Molecular Diagnostics. *Analytical chemistry* **2015,** *87* (15), 7595-7601.

18. Xu, Y.; Liu, Y.; Wu, Y.; Xia, X.; Liao, Y.; Li, Q., Fluorescent Probe-Based Lateral Flow Assay for Multiplex Nucleic Acid Detection. *Analytical chemistry* **2014,** *86* (12), 5611-5614.

19. Wang, Y.; Nugen, S., Development of fluorescent nanoparticle-labeled lateral flow assay for the detection of nucleic acids. *Biomed Microdevices* **2013,** *15* (5), 751-758.

20. Fang, C.; Chen, Z.; Li, L.; Xia, J., Barcode lateral flow immunochromatographic strip for prostate acid phosphatase determination. *Journal of Pharmaceutical and Biomedical Analysis* **2011,** *56* (5), 1035-1040.

21. Fung, K.-K.; Chan, C. P.-Y.; Renneberg, R., Development of enzyme-based bar code-style lateral-flow assay for hydrogen peroxide determination. *Analytica Chimica Acta* **2009,** *634* (1), 89-95.

22. Apilux, A.; Ukita, Y.; Chikae, M.; Chailapakul, O.; Takamura, Y., Development of automated paper-based devices for sequential multistep sandwich enzyme-linked immunosorbent assays using inkjet printing. *Lab on a chip* **2013,** *13* (1), 126-35.

23. Carrilho, E.; Martinez, A. W.; Whitesides, G. M., Understanding wax printing: a simple micropatterning process for paper-based microfluidics. *Analytical chemistry* **2009,** *81* (16), 7091-5.

24. Müller, R. H.; Clegg, D. L., Automatic Paper Chromatography. *Analytical chemistry* **1949,** *21* (9), 1123-1125.

25. Martinez, A. W.; Phillips, S. T.; Wiley, B. J.; Gupta, M.; Whitesides, G. M., FLASH: a rapid method for prototyping paper-based microfluidic devices. *Lab on a chip* **2008,** *8* (12), 2146-2150.

26. Bruzewicz, D. A.; Reches, M.; Whitesides, G. M., Low-Cost Printing of Poly(dimethylsiloxane) Barriers To Define Microchannels in Paper. *Analytical chemistry* **2008,** *80* (9), 3387-3392.

27. Dungchai, W.; Chailapakul, O.; Henry, C. S., A low-cost, simple, and rapid fabrication method for paper-based microfluidics using wax screen-printing. *The Analyst* **2011,** *136* (1), 77-82.

28. Fu, E.; Ramsey, S. A.; Kauffman, P.; Lutz, B.; Yager, P., Transport in two-dimensional paper networks. *Microfluidics and nanofluidics* **2011,** *10* (1), 29-35.

29. Osborn, J. L.; Lutz, B.; Fu, E.; Kauffman, P.; Stevens, D. Y.; Yager, P., Microfluidics without pumps: reinventing the T-sensor and H-filter in paper networks. *Lab on a chip* **2010,** *10* (20), 2659-65.

30. Spicar-Mihalic, P.; Toley, B.; Houghtaling, J.; Liang, T.; Yager, P.; Fu, E., CO2laser cutting and ablative etching for the fabrication of paper-based devices. *Journal of Micromechanics and Microengineering* **2013,** *23* (6), 067003.

31. Lu, Y.; Shi, W.; Qin, J.; Lin, B., Fabrication and Characterization of Paper-Based Microfluidics Prepared in Nitrocellulose Membrane By Wax Printing. *Analytical chemistry* **2009,** *82* (1), 329-335.

32. Noh, H.; Phillips, S. T., Fluidic Timers for Time-Dependent, Point-of-Care Assays on Paper. *Analytical chemistry* **2010,** *82* (19), 8071-8078.

33. Koo, C. K. W.; He, F.; Nugen, S. R., An inkjet-printed electrowetting valve for paper-fluidic sensors. *The Analyst* **2013,** *138* (17), 4998-5004.

34. Martinez, A. W.; Phillips, S. T.; Butte, M. J.; Whitesides, G. M., Patterned paper as a platform for inexpensive, low-volume, portable bioassays. *Angewandte Chemie-International Edition* **2007,** *46* (8), 1318-1320.

35. Liana, D. D.; Raguse, B.; Gooding, J. J.; Chow, E., Recent advances in paper-based sensors. *Sensors* **2012,** *12* (9), 11505-11526.

36. Li, X.; Ballerini, D. R.; Shen, W., A perspective on paper-based microfluidics: current status and future trends. *Biomicrofluidics* **2012,** *6* (1), 011301.

37. Monosik, R.; dos Santos, V. B.; Angnes, L., A simple paper-strip colorimetric method utilizing dehydrogenase enzymes for analysis of food components. *Analytical Methods* **2015,** *7* (19), 8177-8184.

38. Sajid, M.; Kawde, A.-N.; Daud, M., Designs, formats and applications of lateral flow assay: A literature review. *Journal of Saudi Chemical Society* **2015,** *19* (6), 689-705.

39. Adkins, J.; Boehle, K.; Henry, C., Electrochemical paper-based microfluidic devices. *Electrophoresis* **2015,** *36* (16), 1811-1824.

40. Gencoglu, A.; Minerick, A. R., Electrochemical detection techniques in micro- and nanofluidic devices. *Microfluidics and Nanofluidics* **2014,** *17* (5), 781-807.

41. Dossi, N.; Toniolo, R.; Terzi, F.; Impellizzieri, F.; Bontempelli, G., Pencil leads doped with electrochemically deposited Ag and AgCl for drawing reference electrodes on paper-based electrochemical devices. *Electrochimica Acta* **2014,** *146*, 518-524.

42. Ruecha, N.; Rodthongkum, N.; Cate, D. M.; Volckens, J.; Chailapakul, O.; Henry, C. S., Sensitive electrochemical sensor using a graphene-polyaniline nanocomposite for simultaneous detection of Zn(II), Cd(II), and Pb(II). *Analytica Chimica Acta* **2015,** *874*, 40-48.

43. Nantaphol, S.; Chailapakul, O.; Siangproh, W., A novel paper-based device coupled with a silver nanoparticle-modified boron-doped diamond electrode for cholesterol detection. *Analytica Chimica Acta* **2015,** *891*, 136-143.

44. Nie, Z. H.; Nijhuis, C. A.; Gong, J. L.; Chen, X.; Kumachev, A.; Martinez, A. W.; Narovlyansky, M.; Whitesides, G. M., Electrochemical sensing in paper-based microfluidic devices. *Lab on a Chip* **2010,** *10* (4), 477-483.

45. Dungchai, W.; Chailapakul, O.; Henry, C. S., Electrochemical Detection for Paper-Based Microfluidics. *Analytical Chemistry* **2009,** *81* (14), 5821-5826.

46. Wang, Y.; Fill, C.; Nugen, S. R., Development of Chemiluminescent Lateral Flow Assay for the Detection of Nucleic Acids. *Biosensors* **2012,** *2* (4), 32-42.

47. Ge, L.; Yu, J. H.; Ge, S. G.; Yan, M., Lab-on-paper-based devices using chemiluminescence and electrogenerated chemiluminescence detection. *Analytical and Bioanalytical Chemistry* **2014,** *406* (23), 5613-5630.

48. Cate, D. M.; Adkins, J. A.; Mettakoonpitak, J.; Henry, C. S., Recent Developments in Paper-Based Microfluidic Devices. *Analytical Chemistry* **2015,** *87* (1), 19-41.

49. Li, W.; Li, L.; Li, S.; Wang, X.; Li, M.; Wang, S.; Yu, J., 3D origami electrochemiluminescence immunodevice based on porous silver-paper electrode and nanoporous silver double-assisted signal amplification. *Sensors and Actuators B: Chemical* **2013,** *188*, 417-424.

50. Singh, A.; Arutyunov, D.; Szymanski, C. M.; Evoy, S., Bacteriophage based probes for pathogen detection. *The Analyst* **2012,** *137* (15), 3405-21.

51. Singh, A.; Poshtiban, S.; Evoy, S., Recent Advances in Bacteriophage Based Biosensors for Food-Borne Pathogen Detection. *Sensors (Basel, Switzerland)* **2013,** *13* (2), 1763-1786.

52. Sullivan, K. V.; Turner, N. N.; Roundtree, S. S.; McGowan, K. L., Rapid detection of methicillin-resistant Staphylococcus aureus (MRSA) and methicillin-susceptible Staphylococcus aureus (MSSA) using the KeyPath MRSA/MSSA blood culture test and the BacT/ALERT system in a pediatric population. *Archives of pathology & laboratory medicine* **2013,** *137* (8), 1103-5.

53. Hyman, P.; Abedon, P. H. S. T., *Bacteriophages in Health and Disease: Bacteriophages in Health and Disease*. CAB International: **2012**.

54. Cardoso, T. M. G.; Garcia, P. T.; Coltro, W. K. T., Colorimetric determination of nitrite in clinical, food and environmental samples using microfluidic devices stamped in paper platforms. *Analytical Methods* **2015,** *7* (17), 7311-7317.

55. Dou, M. W.; Sanjay, S. T.; Benhabib, M.; Xu, F.; Li, X. J., Low-cost bioanalysis on paper-based and its hybrid microfluidic platforms. *Talanta* **2015,** *145*, 43-54.

56. Jokerst, J. C.; Adkins, J. A.; Bisha, B.; Mentele, M. M.; Goodridge, L. D.; Henry, C. S., Development of a paper-based analytical device for colorimetric detection of select foodborne pathogens. *Analytical chemistry* **2012,** *84* (6), 2900-2907.

57. Bisha, B.; Adkins, J. A.; Jokerst, J. C.; Chandler, J. C.; Perez-Mendez, A.; Coleman, S. M.; Sbodio, A. O.; Suslow, T. V.; Danyluk, M. D.; Henry, C. S.; Goodridge, L. D., Colorimetric Paper-based Detection of Escherichia coli, Salmonella spp., and Listeria monocytogenes from Large Volumes of Agricultural Water. *Jove-Journal of Visualized Experiments* **2014,** (88).

58. Choleva, T. G.; Kappi, F. A.; Giokas, D. L.; Vlessidis, A. G., Paper-based assay of antioxidant activity using analyte-mediated on-paper nucleation of gold nanoparticles as colorimetric probes. *Analytica Chimica Acta* **2015,** *860*, 61-69.

59. Tee-ngam, P.; Nunant, N.; Rattanarat, P.; Siangproh, W.; Chailapakul, O., Simple and Rapid Determination of Ferulic Acid Levels in Food and Cosmetic Samples Using Paper-Based Platforms. *Sensors* **2013,** *13* (10), 13039-13053.

60. Mu, X.; Zhang, L.; Chang, S. Y.; Cui, W.; Zheng, Z., Multiplex Microfluidic Paper-based Immunoassay for the Diagnosis of Hepatitis C Virus Infection. *Analytical Chemistry* **2014,** *86* (11), 5338-5344.

61. Wang, H. K.; Tsai, C. H.; Chen, K. H.; Tang, C. T.; Leou, J. S.; Li, P. C.; Tang, Y. L.; Hsieh, H. J.; Wu, H. C.; Cheng, C. M., Cellulose- Based Diagnostic Devices for Diagnosing Serotype-2 Dengue Fever in Human Serum. *Advanced Healthcare Materials* **2014,** *3* (2), 187-196.

62. Lei, K. F.; Huang, C. H.; Kuo, R. L.; Chang, C. K.; Chen, K. F.; Tsao, K. C.; Tsang, N. M., Paper-based enzyme-free immunoassay for rapid detection and subtyping of influenza A H1N1 and H3N2 viruses. *Analytica Chimica Acta* **2015,** *883*, 37-44.

63. Sechi, D.; Greer, B.; Johnson, J.; Hashemi, N., Three-Dimensional Paper-Based Microfluidic Device for Assays of Protein and Glucose in Urine. *Analytical Chemistry* **2013,** *85* (22), 10733-10737.

64. Jagirdar, A.; Shetty, P.; Satti, S.; Garg, S.; Paul, D., A paperfluidic device for dental applications using a novel patterning technique. *Analytical Methods* **2015,** *7* (4), 1293-1299.

65. Cate, D. M.; Noblitt, S. D.; Volckens, J.; Henry, C. S., Multiplexed paper analytical device for quantification of metals using distance-based detection. *Lab on a Chip* **2015,** *15* (13), 2808-2818.

66. Cheung, S. F.; Cheng, S. K. L.; Kamei, D. T., Paper-Based Systems for Point-of-Care Biosensing. *Jala* **2015,** *20* (4), 316-333.

67. Mahadeva, S. K.; Walus, K.; Stoeber, B., Paper as a Platform for Sensing Applications and Other Devices: A Review. *Acs Applied Materials & Interfaces* **2015,** *7* (16), 8345-8362.

68. Li, L.; Zhang, L. N.; Yu, J. H.; Ge, S. G.; Song, X. R., All-graphene composite materials for signal amplification toward ultrasensitive electrochemical immunosensing of tumor marker. *Biosensors & Bioelectronics* **2015,** *71*, 108-114.

69. Quesada-Gonzalez, D.; Merkoci, A., Nanoparticle-based lateral flow biosensors. *Biosensors & Bioelectronics* **2015,** *73*, 47-63.

70. Ge, L.; Yan, J. X.; Song, X. R.; Yan, M.; Ge, S. G.; Yu, J. H., Three-dimensional paper-based electrochemiluminescence immunodevice for multiplexed measurement of biomarkers and point-of-care testing. *Biomaterials* **2012,** *33* (4), 1024-1031.

71. Wang, P. P.; Ge, L.; Yan, M.; Song, X. R.; Ge, S. G.; Yu, J. H., Paper-based three-dimensional electrochemical immunodevice based on multi-walled carbon nanotubes functionalized paper for sensitive point-of-care testing. *Biosensors & Bioelectronics* **2012,** *32* (1), 238-243.

72. Nugen, S. R.; Baeumner, A. J., Trends and opportunities in food pathogen detection. *Analytical and bioanalytical chemistry* **2008,** *391* (2), 451-4.

73. Li, X.; Ballerini, D. R.; Shen, W., A perspective on paper-based microfluidics: Current status and future trends. *Biomicrofluidics* **2012,** *6* (1), 11301-1130113.

74. Yu, C.; Mutlu, S.; Selvaganapathy, P.; Mastrangelo, C. H.; Svec, F.; Fréchet, J. M. J., Flow Control Valves for Analytical Microfluidic Chips without Mechanical Parts Based on Thermally Responsive Monolithic Polymers. *Analytical chemistry* **2003,** *75* (8), 1958-1961.

75. Li, X.; Tian, J.; Shen, W., Progress in patterned paper sizing for fabrication of paper-based microfluidic sensors. *Cellulose* **2010,** *17* (3), 649-659.

76. Feng, Y.; Zhou, Z.; Ye, X.; Xiong, J., Passive valves based on hydrophobic microfluidics. *Sensors and Actuators A: Physical* **2003,** *108* (1-3), 138-143.

77. Chen, H.; Cogswell, J.; Anagnostopoulos, C.; Faghri, M., A fluidic diode, valves, and a sequential-loading circuit fabricated on layered paper. *Lab on a chip* **2012,** *12* (16), 2909-13.

78. Mérian, T.; He, F.; Yan, H.; Chu, D.; Talbert, J. N.; Goddard, J. M.; Nugen, S. R., Development and surface characterization of an electrowetting valve for capillary-driven microfluidics. *Colloids and Surfaces A: Physicochemical and Engineering Aspects* **2012,** *414*, 251-258.

79. Walker, S. B.; Lewis, J. A., Reactive Silver Inks for Patterning High-Conductivity Features at Mild Temperatures. *Journal of the American Chemical Society* **2012,** *134* (3), 1419-1421.

80. Liu, H.; Dharmatilleke, S.; Maurya, D. K.; Tay, A. A. O., Dielectric materials for electrowetting-on-dielectric actuation. *Microsystem Technologies* **2009,** *16* (3), 449-460.

81. Saeki, F.; Baum, J.; Moon, H.; Yoon, J.-Y.; Kim, C.; Garrell, R., Electrowetting on dielectrics (EWOD): reducing voltage requirements for microfluidics. *Polym. Mater. Sci. Eng* **2001,** *85*, 12-13.

82. He, F.; Grimes, J.; Alcaine, S. D.; Nugen, S. R., A hybrid paper and microfluidic chip with electrowetting valves and colorimetric detection. *The Analyst* **2014,** *139* (12), 3002-8.

83. Maattanen, A.; Ihalainen, P.; Pulkkinen, P.; Wang, S.; Tenhu, H.; Peltonen, J., Inkjet-printed gold electrodes on paper: characterization and functionalization. *ACS applied materials & interfaces* **2012,** *4* (2), 955-64.

84. Wilson, P.; Lekakou, C.; Watts, J. F., A comparative assessment of surface microstructure and electrical conductivity dependence on co-solvent addition in spin coated and inkjet printed poly(3,4-ethylenedioxythiophene):polystyrene sulphonate (PEDOT:PSS). *Organic Electronics* **2012,** *13* (3), 409-418.

85. Takamatsu, S.; Kurihara, K.; Imai, T.; Yamashita, T.; Itoh, T. In *High conductive organic conjugated polymer patterning with UV-nanoimprint-based surface modification and second doping*, Micro Electro Mechanical Systems (MEMS), 2012 IEEE 25th International Conference on, IEEE: **2012**; pp 255-258.

86. Weng, B.; Shepherd, R. L.; Crowley, K.; Killard, A. J.; Wallace, G. G., Printing conducting polymers. *The Analyst* **2010,** *135* (11), 2779-89.

87. Perinka, N.; Kim, C. H.; Kaplanova, M.; Bonnassieux, Y., Preparation and Characterization of Thin Conductive Polymer Films on the base of PEDOT:PSS by Ink-Jet Printing. *Physics Procedia* **2013,** *44*, 120-129.

88. Basiricò, L.; Cosseddu, P.; Fraboni, B.; Bonfiglio, A., Inkjet printing of transparent, flexible, organic transistors. *Thin Solid Films* **2011,** *520* (4), 1291-1294.

89. Dang, A., Towards Ink-Jet Fabricated PEDOT: PSS Organic Electrochemical Transistors with Embedded Enzymes.

90. Shin, N.-R.; Choi, S.-H.; Kim, J.-Y., Highly conductive PEDOT:PSS electrode films hybridized with gold-nanoparticle-doped-carbon nanotubes. *Synthetic Metals* **2014,** *192*, 23-28.

91. Denneulin, A.; Blayo, A.; Bras, J.; Neuman, C., PEDOT:PSS coating on specialty papers: Process optimization and effects of surface properties on electrical performances. *Progress in Organic Coatings* **2008,** *63* (1), 87-91.

92. Angelo, P. D.; Cole, G. B.; Sodhi, R. N.; Farnood, R. R., Conductivity of inkjet-printed PEDOT: PSS-SWCNTs on uncoated papers. *Nordic Pulp and Paper Research Journal* **2012,** *27* (2), 486.

93. Singhana, B.; Rittikulsittichai, S.; Lee, T. R., Tridentate adsorbates with cyclohexyl headgroups assembled on gold. *Langmuir : the ACS journal of surfaces and colloids* **2013,** *29* (2), 561-569.

94. Cavalleri, O.; Oliveri, L.; Dacca, A.; Parodi, R.; Rolandi, R., XPS measurements on L-cysteine and 1-octadecanethiol self-assembled films: a comparative study. *Applied surface science* **2001,** *175*, 357-362.

95. Molino, P. J.; Wallace, G. G.; Hanks, T. W., Hydrophobic conducting polymer films from post deposition thiol exposure. *Synthetic Metals* **2012,** *162* (15–16), 1464-1470.

96. Bergman, B.; Hanks, T., Spectroscopic, microscopic, and surface analysis of alkanethiol-and fluoroalkanethiol-modified conducting polymer thin films. *Macromolecules* **2000,** *33* (21), 8035-8042.

97. Fu, E.; Kauffman, P.; Lutz, B.; Yager, P., Chemical signal amplification in two-dimensional paper networks. *Sensors and actuators. B, Chemical* **2010,** *149* (1), 325-328.

98. Miller-Chou, B. A.; Koenig, J. L., A review of polymer dissolution. *Progress in Polymer Science* **2003,** *28* (8), 1223-1270.

99. Lewis, S.; Haynes, V.; Wheeler-Jones, R.; Sly, J.; Perks, R. M.; Piccirillo, L., Surface characterization of poly(methylmethacrylate) based nanocomposite thin films containing Al2O3 and TiO2 nanoparticles. *Thin Solid Films* **2010,** *518* (10), 2683-2687.

100. Larsson, R.; Selén, G.; Björklund, H.; Fagerholm, P., Intraocular PMMA lenses modified with surface-immobilized heparin: evaluation of biocompatibility in vitro and in vivo. *Biomaterials* **1989,** *10* (8), 511-516.

101. Lutz, B.; Liang, T.; Fu, E.; Ramachandran, S.; Kauffman, P.; Yager, P., Dissolvable fluidic time delays for programming multi-step assays in instrument-free paper diagnostics. *Lab on a chip* **2013,** *13* (14), 2840-7.

102. <Two-dimensional paper network format for amplified lateral flow assays.pdf>.

103. Heineman, R. H.; Bull, J. J.; Hansen, T., Testing optimality with experimental evolution: Lysis time in a bacteriophage. *Evolution; International Journal of Organic Evolution* **2007,** *61* (7), 1695-1709.

104. Alcaine, S. D.; Pacitto, D.; Sela, D. A.; Nugen, S. R., Phage & phosphatase: a novel phage-based probe for rapid, multi-platform detection of bacteria. *The Analyst* **2015,** *140* (22), 7629-7636.

105. Cho, J. H.; Paek, S. H., Semiquantitative, bar code version of immunochromatographic assay system for human serum albumin as model analyte. *Biotechnology and bioengineering* **2001,** *75* (6), 725-732.

106. Klumpp, J.; Loessner, M. J., New research on bacteriophages and food safety. In *Advances in Microbial Food Safety, Vol 1*, Sofos, J., Ed. **2013**, pp 321-339.

107. Monk, A. B.; Rees, C. D.; Barrow, P.; Hagens, S.; Harper, D. R., UNDER THE MICROSCOPE Bacteriophage applications: where are we now? *Letters in Applied Microbiology* **2010,** *51* (4), 363-369.

108. WHO, Antimicrobial resistance: global report on surveillance. Organization, W. H., Ed. **2014**.

109. Jagusztyn-Krynicka, E. K.; Wyszynska, A., The decline of antibiotic era - New approaches for antibacterial drug discovery. *Polish Journal of Microbiology* **2008,** *57* (2), 91-98.

110. McEwen, S. A.; Fedorka-Cray, P. J., Antimicrobial use and resistance in animals. *Clinical Infectious Diseases* **2002,** *34* (Supplement 3), S93-S106.

111. Akwar, H. T.; Poppe, C.; Wilson, J.; Reid-Smith, R. J.; Dyck, M.; Waddington, J.; Shang, D.; McEwen, S. A., Associations of antimicrobial uses with antimicrobial resistance of fecal Escherichia coli from pigs on 47 farrow-to-finish farms in Ontario and British Columbia. *Canadian Journal of Veterinary Research* **2008,** *72* (2), 202.

112. Gillings, M.; Boucher, Y.; Labbate, M.; Holmes, A.; Krishnan, S.; Holley, M.; Stokes, H., The evolution of class 1 integrons and the rise of antibiotic resistance. *Journal of bacteriology* **2008,** *190* (14), 5095-5100.

113. Voss, A.; Loeffen, F.; Bakker, J.; Klaassen, C.; Wulf, M., Methicillin-resistant Staphylococcus aureus in pig farming. *Emerg Infect Dis* **2005,** *11* (12), 1965-1966.

114. Khanna, T.; Friendship, R.; Dewey, C.; Weese, J., Methicillin resistant Staphylococcus aureus colonization in pigs and pig farmers. *Veterinary microbiology* **2008,** *128* (3), 298-303.

115. Sabour, P. M.; Griffiths, M. W., *Bacteriophages in the control of food-and waterborne pathogens*. American Society for Microbiology Press: **2010**.

116. Carter, C. D.; Parks, A.; Abuladze, T.; Li, M.; Woolston, J.; Magnone, J.; Senecal, A.; Kropinski, A. M.; Sulakvelidze, A., Bacteriophage cocktail significantly reduces Escherichia coli O157: H7 contamination of lettuce and beef, but does not protect against recontamination. *Bacteriophage* **2012,** *2* (3), 178-185.

117. Dykes, G.; Moorhead, S., Combined antimicrobial effect of nisin and a listeriophage against Listeria monocytogenes in broth but not in buffer or on raw beef. *International Journal of Food Microbiology* **2002,** *73* (1), 71-81.

118. Goode, D.; Allen, V.; Barrow, P., Reduction of experimental Salmonella and Campylobacter contamination of chicken skin by application of lytic bacteriophages. *Applied and Environmental Microbiology* **2003,** *69* (8), 5032-5036.

119. O'Flynn, G.; Ross, R.; Fitzgerald, G.; Coffey, A., Evaluation of a cocktail of three bacteriophages for biocontrol of Escherichia coli O157: H7. *Applied and Environmental Microbiology* **2004,** *70* (6), 3417-3424.

120. Higgins, J. P.; Higgins, S.; Guenther, K.; Huff, W.; Donoghue, A.; Donoghue, D.; Hargis, B., Use of a specific bacteriophage treatment to reduce Salmonella in poultry products. *Poultry science* **2005,** *84* (7), 1141-1145.

121. Magnone, J. P.; Marek, P. J.; Sulakvelidze, A.; Senecal, A. G., Additive approach for inactivation of Escherichia coli O157: H7, Salmonella, and Shigella spp. on contaminated fresh fruits and vegetables using bacteriophage cocktail and produce wash. *Journal of Food Protection*® **2013,** *76* (8), 1336-1341.

122. Mullard, A., 2011 FDA drug approvals. *Nature Reviews Drug Discovery* **2012,** *11* (2), 91-94.

123. FDA, Outbreaks: Investigation, Response & Evaluation. Administration, U. S. F. a. D., Ed. **2015**.

124. Iijima, T.; Sakane, T., METHOD FOR PRESERVATION OF BACTERIA AND BACTERIOPHAGES BY DRYING IN-VACUO. *Cryobiology* **1973,** *10* (5), 379-385.

125. Miyamoto-Shinohara, Y.; Imaizumi, T.; Sukenobe, J.; Murakami, Y.; Kawamura, S.; Komatsu, Y., Survival rate of microbes after freeze-drying and long-term storage. *Cryobiology* **2000,** *41* (3), 251-255.

126. Zierdt, C. H., Stabilities of lyophilized Staphylococcus aureus typing bacteriophages. *Applied and Environmental Microbiology* **1988,** *54* (10), 2590.

127. Baji, A.; Mai, Y. W.; Wong, S. C.; Abtahi, M.; Chen, P., Electrospinning of polymer nanofibers: Effects on oriented morphology, structures and tensile properties. *Composites Science and Technology* **2010,** *70* (5), 703-718.

128. Raghavan, P.; Lim, D. H.; Ahn, J. H.; Nah, C.; Sherrington, D. C.; Ryu, H. S.; Ahn, H. J., Electrospun polymer nanofibers: The booming cutting edge technology. *Reactive & Functional Polymers* **2012,** *72* (12), 915-930.

129. Huang, Z. M.; Zhang, Y. Z.; Kotaki, M.; Ramakrishna, S., A review on polymer nanofibers by electrospinning and their applications in nanocomposites. *Composites Science and Technology* **2003,** *63* (15), 2223-2253.

130. Lee, S.-W.; Belcher, A. M., Virus-based fabrication of micro-and nanofibers using electrospinning. *Nano letters* **2004,** *4* (3), 387-390.

131. Salalha, W.; Kuhn, J.; Dror, Y.; Zussman, E., Encapsulation of bacteria and viruses in electrospun nanofibres. *Nanotechnology* **2006,** *17* (18), 4675.

132. Korehei, R.; Kadla, J. F., Encapsulation of T4 bacteriophage in electrospun poly (ethylene oxide)/cellulose diacetate fibers. *Carbohydrate polymers* **2014,** *100*, 150-157.

133. Dai, M. H.; Senecal, A.; Nugen, S. R., Electrospun water-soluble polymer nanofibers for the dehydration and storage of sensitive reagents. *Nanotechnology* **2014,** *25* (22).

134. Korehei, R.; Kadla, J., Incorporation of T4 bacteriophage in electrospun fibres. *Journal of Applied Microbiology* **2013,** *114* (5), 1425-1434.

135. Shin, Y. C.; Lee, J. H.; Jin, O. S.; Lee, E. J.; Jin, L. H.; Kim, C. S.; Hong, S. W.; Han, D. W.; Kim, C.; Oh, J. W., RGD peptide-displaying M13 bacteriophage/PLGA nanofibers as cell-adhesive matrices for smooth muscle cells. *Journal of the Korean Physical Society* **2015,** *66* (1), 12-16.

136. Tovkach, F. I.; Zhuminska, G. I.; Kushkina, A. I., Long-term preservation of unstable bacteriophages of enterobacteria. *Mikrobiolohichnyi zhurnal (Kiev, Ukraine : 1993)* **2012,** *74* (2), 60-6.

137. Dai, M.; Senecal, A.; Nugen, S. R., Electrospun water-soluble polymer nanofibers for the dehydration and storage of sensitive reagents. *Nanotechnology* **2014,** *25* (22), 225101.

138. Lu, C.; Chen, P.; Li, J.; Zhang, Y., Computer simulation of electrospinning. Part I. Effect of solvent in electrospinning. *Polymer* **2006,** *47* (3), 915-921.

139. Kim, S. J.; Lee, C. K.; Kim, S. I., Effect of ionic salts on the processing of poly(2-acrylamido-2-methyl-1-propane sulfonic acid) nanofibers. *Journal of Applied Polymer Science* **2005,** *96* (4), 1388-1393.

140. Patel, A. C.; Li, S.; Wang, C.; Zhang, W.; Wei, Y., Electrospinning of Porous Silica Nanofibers Containing Silver Nanoparticles for Catalytic Applications. *Chemistry of Materials* **2007,** *19* (6), 1231-1238.

141. Qin, X.-H.; Yang, E.-L.; Li, N.; Wang, S.-Y., Effect of different salts on electrospinning of polyacrylonitrile (PAN) polymer solution. *Journal of Applied Polymer Science* **2007,** *103* (6), 3865-3870.

142. Vega, C.; Roos, Y. H., Invited review: Spray-dried dairy and dairy-like - emulsions compositional considerations. *Journal of Dairy Science* **2006,** *89* (2), 383-401.

143. Domian, E., PROFILE OF SPRAY-DRIED EMULSIONS STABILISED BY MILK PROTEINS. *Zywnosc-Nauka Technologia Jakosc* **2011,** *18* (6), 5-23.

144. Pikal, M. J., Freeze-Drying of Proteins. In *Formulation and Delivery of Proteins and Peptides*, American Chemical Society: **1994**; Chapter 8, pp 120-133.

145. Carpenter, J. F.; Prestrelski, S. J.; Anchordoguy, T. J.; Arakawa, T., Interactions of Stabilizers with Proteins During Freezing and Drying. In *Formulation and Delivery of Proteins and Peptides*, American Chemical Society: **1994**; Chapter 9, pp 134-147.

146. Wang, B.; Tchessalov, S.; Warne, N. W.; Pikal, M. J., Impact of sucrose level on storage stability of proteins in freeze-dried solids: I. correlation of protein–sugar interaction with native structure preservation. *Journal of Pharmaceutical Sciences 98* (9), 3131-3144.

147. Allison, S. D.; Chang, B.; Randolph, T. W.; Carpenter, J. F., Hydrogen Bonding between Sugar and Protein Is Responsible for Inhibition of Dehydration-Induced Protein Unfolding. *Archives of Biochemistry and Biophysics* **1999,** *365* (2), 289-298.

148. Chang, L.; Shepherd, D.; Sun, J.; Ouellette, D.; Grant, K. L.; Tang, X.; Pikal, M. J., Mechanism of protein stabilization by sugars during freeze-drying and storage: Native structure preservation, specific interaction, and/or immobilization in a glassy matrix? *Journal of Pharmaceutical Sciences* **2005,** *94* (7), 1427-1444.

149. Prestrelski, S. J.; Arakawa, T.; Carpenter, J. F., Separation of Freezing- and Drying-Induced Denaturation of Lyophilized Proteins Using Stress-Specific Stabilization: II. Structural Studies Using Infrared Spectroscopy. *Archives of Biochemistry and Biophysics* **1993,** *303* (2), 465-473.

150. Damodaran, S.; Parkin, K. L.; Fennema, O. R., *Fennema's food chemistry*. CRC press: **2007**.

151. Zeng, X. M.; Martin, G. P.; Marriott, C., Effects of molecular weight of polyvinylpyrrolidone on the glass transition and crystallization of co-lyophilized sucrose. *International Journal of Pharmaceutics* **2001,** *218* (1–2), 63-73.

152. Spain, E.; Keyes, T. E.; Forster, R. J., DNA sensor based on vapour polymerised pedot films functionalised with gold nanoparticles. *Biosensors & bioelectronics* **2013,** *41*, 65-70.

153. Vericat, C.; Vela, M. E.; Benitez, G.; Carro, P.; Salvarezza, R. C., Self-assembled monolayers of thiols and dithiols on gold: new challenges for a well-known system. *Chemical Society reviews* **2010,** *39* (5), 1805-34.

154. Mullen, T. J.; Dameron, A. A.; Andrews, A. M.; Weiss, P. S., Selecting and driving monolayer structures through tailored intermolecular interactions. *Aldrichimica Acta* **2007,** *40* (1), 21-31.

155. Love, J. C.; Estroff, L. A.; Kriebel, J. K.; Nuzzo, R. G.; Whitesides, G. M., Self-assembled monolayers of thiolates on metals as a form of nanotechnology. *Chemical reviews* **2005,** *105* (4), 1103-1170.

156. Wu, S., *Polymer interface and adhesion*. M. Dekker: **1982**.